REVIEW

Tackling breast cancer with gold nanoparticles: twinning synthesis and particle engineering with efficacy

Suvadeep Mal, [ID] [a] Subhasis Chakraborty, [b] Monalisa Mahapatra, [ID] [a] Kakarla Pakeeraiah, [ID] [a] Suvadra Das, [c] Sudhir Kumar Paidesetty [ID] *[a] and Partha Roy [ID] *[d]

The World Health Organization identifies breast cancer as the most prevalent cancer despite predominantly affecting women. Surgery, hormonal therapy, chemotherapy, and radiation therapy are the current treatment modalities. Site-directed nanotherapeutics, engineered with multidimensional functionality are now the frontrunners in breast cancer diagnosis and treatment. Gold nanoparticles with their unique colloidal, optical, quantum, magnetic, mechanical, and electrical properties have become the most valuable weapon in this arsenal. Their advantages include facile modulation of shape and size, a high degree of reproducibility and stability, biocompatibility, and ease of particle engineering to induce multifunctionality. Additionally, the surface plasmon oscillation and high atomic number of gold provide distinct advantages for tailor-made diagnosis, therapy or theranostic applications in breast cancer such as photothermal therapy, radiotherapy, molecular labeling, imaging, and sensing. Although pre-clinical and clinical data are promising for nano-dimensional gold, their clinical translation is hampered by toxicity signs in major organs like the liver, kidneys and spleen. This has instigated global scientific brainstorming to explore feasible particle synthesis and engineering techniques to simultaneously improve the efficacy and versatility and widen the safety window of gold nanoparticles. The present work marks the first study on gold nanoparticle design and maneuvering techniques, elucidating their impact on the pharmacodynamics character and providing a clear-cut scientific roadmap for their fast-track entry into clinical practice.

1. Introduction

Cancer ranked as the leading global mortality cause in 2020, characterized by the typical presence of uncontrolled cell growth, angiogenesis and metastasis. According to the WHO factsheet, breast cancer (BC) ranks as the most commonly diagnosed with 2.26 million cases, surpassing all other cancers such as lung (2.21 million), colorectal (1.93 million), prostate (1.41 million), skin (1.20 million) and stomach (1.09 million) cancer, irrespective of gender specificity. The fatality of this variant makes it the second leading cause of cancer death (685 000 deaths globally in 2020) in women after lung cancer.[1] Most

aMedicinal Chemistry Research Laboratory, School of Pharmaceutical Sciences, Siksha 'O' Anusandhan (Deemed to be University), Campus-2, Ghatikia, Kalinga Nagar, Bhubaneswar, Odisha, 751003, India. E-mail: sairampaidesetty@gmail.com

bDmbH Institute of Medical Science, Dadpur, Hooghly, West Bengal, 712305, India

cBasic Science and Humanities Department, University of Engineering and Management, Action Area III, B/5, Newtown, Kolkata, West Bengal, 700160, India

dGITAM School of Pharmacy, GITAM (Deemed to be University), Vishakhapatnam, 530045, India. E-mail: partharoy2502@gmail.com

BCs originate as benign fibrocysts in different parts of the breast that become malignant and start to metastasize.[2,3]

Therapeutic nanoparticles (NPs) display unique colloidal, optical, quantum, magnetic, mechanical and electrical properties depending on their size, shape, surface area and surface charge, resulting in major breakthroughs in therapeutic interventions.[4] The spotlight on cancer management reveals the advantages of NPs, including transporting and shielding high drug payloads, ease of engineering with various targeting ligands, a facile route to induce multi-functionality, accommodation of drug cocktails, tuning drug release to map the intended mechanism or pharmacodynamics and their unique ability to evade clinical challenges like multidrug resistance.[5,6] Based on dimensions, NPs can be divided into zero, one, two or three dimensional frameworks. Based on their morphology and chemical properties, NPs are classified as metal nanoparticles, bio-nanoparticles, organic nanoparticles, polymeric nanoparticles, solid lipid NPs, ceramic NPs, carbon-base NPs, quantum dots *etc.*[7] (Fig. 1).

Granulations of gold or gold nuggets can be traced back to as early as 3000 BC and thereafter its increasing applications led to its reputation as the "elixir of life," believed to bestow eternal
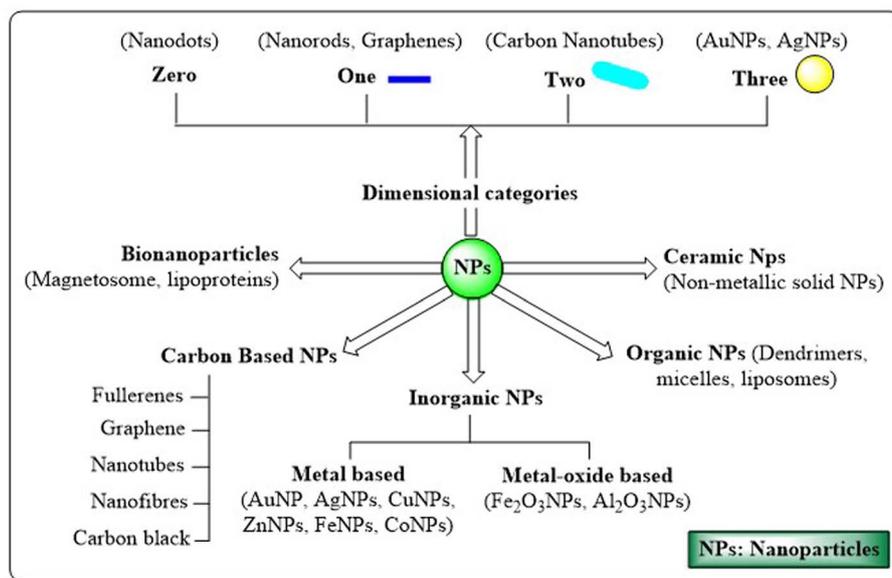
Fig. 1   Classification of nanoparticles. Based on their dimension, NPs are classified mainly into 4 types, *viz.* zero, one, two and three dimensional. Based on their chemical properties, they are classified as inorganic NPs, bio-nanoparticles, organic NPs, ceramic NPs, and carbon-based NPs.

life. In ancient times, gold was the remedy for a myriad of clinical dysfunctions. Later, in the year 1848, the "California Gold Rush" began when James W. Marshall reported the discovery of gold and its true value at Colona, California.[8] Gold nanoparticles (AuNPs) in clinical applications can be traced back over 150 years with similar increasing trends of scientific focus (Fig. 2) due to its inertness along with facile fabrication and functionalization and specific optical or physico-chemical attributes like localized surface plasmon resonance.[9] However, tackling breast cancer with AuNPs captured scientific curiosity

a little later compared to their intervention in other cancer variants.

AuNPs consist of a gold atom (Au) in the inner core decorated by a negative charge at the surface. Particle engineering of AuNPs with different biomolecules (proteins, enzymes or DNA) assures the site-specific localization of NPs with programmed delivery of drug cargo.[10] AuNPs exist in diverse morphologies *viz.* nanospheres, nanoclusters, nanorods, nanocubes, nanocages, nanostars or nanoshells (Fig. 3).[11] Some morphologies are more prominent in a specific pharmacological response such as
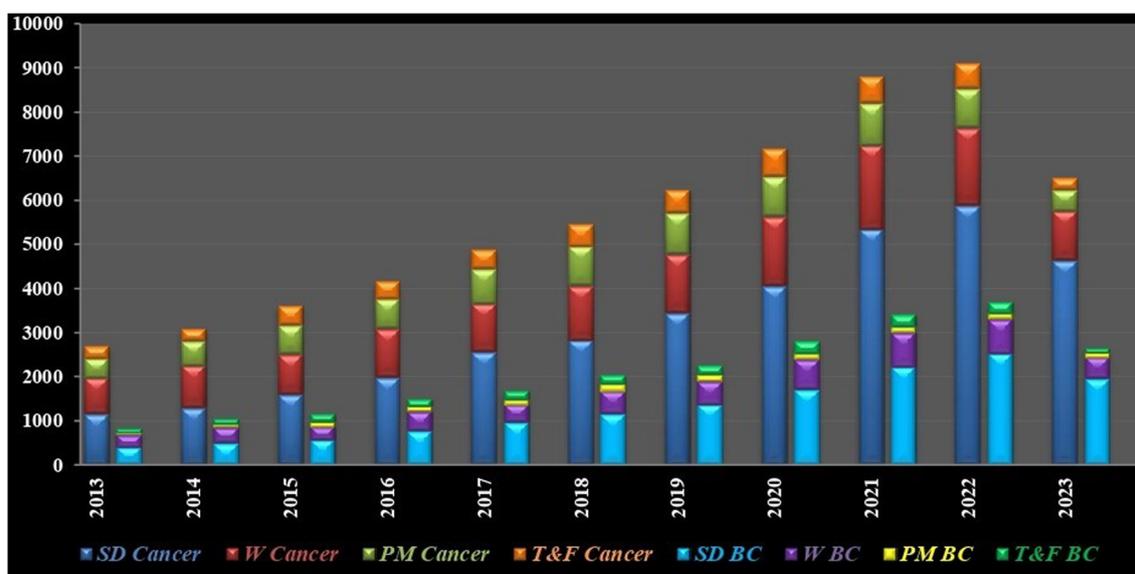

Fig. 2   Publication trends based on search terms "gold nanoparticles in cancer treatment" and "gold nanoparticles in breast cancer treatment" in different scientific repositories (SD-T&F Cancer/BC). SD: ScienceDirect; W: Wiley; PM: PubMed; T&F: Taylor and Francis; BC: *Breast Cancer*; period of interest: January 2013–July 2023.
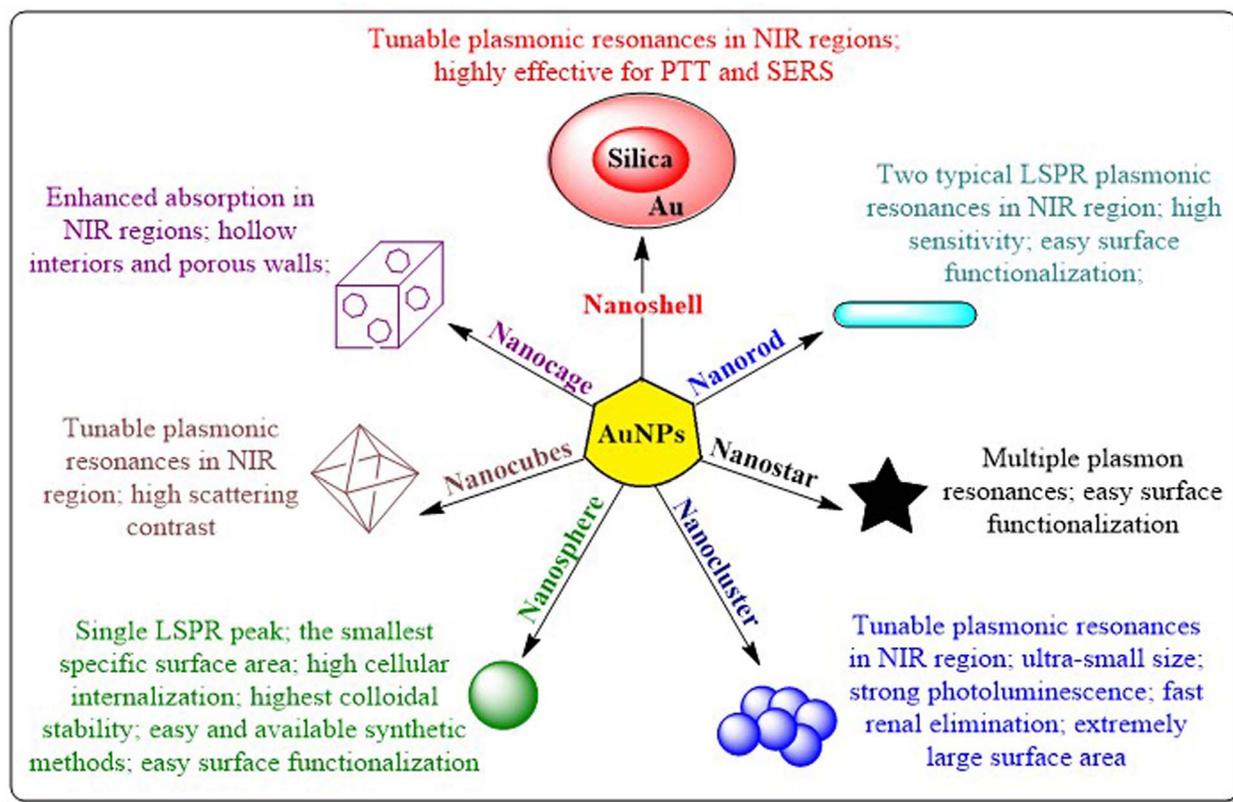
Fig. 3 Different shapes of gold nanoparticles and their significant characteristics. AuNPs can exist as nanoshells, nanorods, nanostars, nano-clusters, nanospheres, nanocubes, and nanocages. Each category possesses unique features which contribute to their physico-chemical characteristics and subsequently in their applications.

targeted delivery,[10] photodermal and photothermal therapy,[12] SERS based imaging,[13] photo-electronics, clinical management of cancer,[14] microbial infections,[15] contrast agents and field enhancers,[16] chemical and biochemical sensors[17] and as radiosensitizers.[18]

AuNPs allow easy association of site-directed ligands, imaging probes, therapeutic bioactive materials and other functional moieties to facilitate diagnostic, therapeutic or theranostic applications in cancer at the molecular level.[19] Engineering of AuNPs has become a mandatory art to favor the intended clinical application. Various mechanisms for the synthesis of AuNPs containing functional moieties are being explored either to increase their bonding with biological molecules or to make them better drug-carriers with improved specificity. Modern trends in the tuning of AuNPs involve the use of one or a combination of the functional moieties like polyethylene glycol (PEG), bovine serum albumin (BSA), amino acids and polypeptides, oligonucleotides, antibodies or biomarkers, which are discussed in this review for management of BC.

AuNPs have distinct advantages depending on their properties and intended use. The most important property of AuNPs in clinical translation is biocompatibility as they are less likely to induce immune responses or toxicity as compared to other nanoparticles *viz.* copper oxide, zinc or cobalt NPs. The facile feasibility of AuNPs for convenient surface modification is another major advantage in applications like targeted drug delivery and molecular sensing. While other nanomaterials such as silver, copper, or iron oxide nanoparticles also have surface modification capabilities, they typically require additional ligands or modifiers for surface applications. Without the need for surface engineering, AuNPs also possess distinctive optical characteristics, notably localized surface plasmon resonance (LSPR), which can be explored for diverse applications including biosensing, imaging, and photothermal therapy, making AuNPs superior to other nanoparticles.[20] With their higher atomic number and robust scattering and absorption properties, AuNPs offer various bioimaging modalities such as optical, photoacoustic, and computed tomography (CT) imaging which adds to their clinical value.

Beside all these, AuNPs have excellent chemical and thermal stability, making them suitable for applications requiring high temperatures (photothermal or radiotherapy) with high drug loading capacity. AuNPs offer similar electrical conductivity to metal oxide nanoparticles (NPs), while possessing the additional advantage of being resistant to oxidation.[21] This property ensures their efficacy and performance in harsh environments, contrasting with iron oxide or copper oxide NPs which are prone to oxidation, potentially compromising their effectiveness and durability over time.[22]

Diverse strategies exist in combating BC using AuNPs. AuNPs can be engineered to act as targeted drug delivery vehicles to deliver therapeutics to BC cells safeguarding the healthy cells. AuNPs can be used as sensors for probing and imaging BC cells using surface enhanced Raman spectroscopy (SERS). AuNPs can tackle BC through plasmonic photothermal therapy (PPTT), radiotherapy or by preventing angiogenesis and metastasis.[23] AuNPs have proved effective in critical clinical challenges like triple negative breast cancer (TNBC) by interacting with over-expressed cell-surface receptors which are not connected with cell proliferation or survival.[24] Engineered AuNPs successfully delivered drugs and induced apoptosis even in multi-drug resistant BC cells.[25] The acceptance of AuNPs in clinical applications is further intensified due to their safety towards normal cells.[26]

However, although bulk gold acts as a noble metal, AuNPs do exhibit toxicities in different systems depending on their size and shape, particle engineering, dosage, route of administration, exposure time *etc.* Increased cellular uptake and low bio-distribution often lead to long term toxicity, which is considered to be a major hurdle for nano-gold formulations. Although several AuNPs have translated into pre-clinical and clinical stages, none of them have yet progressed to the point of entering the market. As such, researchers are coming up with newer strategic manoeuvres to address their drawbacks. This review summarizes the entire portfolio of nano-scale gold, covering synthesis routes, stabilization techniques, particle engineering, toxicity, and pre-clinical and clinical developments to establish their role in BC management either as therapeutics, diagnostics or theranostics. Although numerous reports have successfully confirmed the clinical backdrop of exploring gold nanoparticles in BC, scientific insights into their formulation perspectives to arrive at tailor-made solutions remain unexplored. The present work addresses this niche area to provide a comprehensive scientific databank to assist fast-track clinical translation of nano-scale gold.

2. AuNP synthesis and stabilization

Basic strategies for nanoparticles synthesis revolve around two pivotal pillars: the "top-down" method and the "bottom-up" method. Top-down methods involve destruction, in which bulk materials are broken into smaller particles to produce nanoparticles by thermal decomposition,[27] ball milling,[28] laser ablation,[29] sputtering,[30] UV and IR irradiation[31] and aerosol technology.[32] On the contrary, bottom-up synthesis is constructive *i.e.* nanoparticles are synthesised starting from the atomic level using different techniques such as the sol–gel approach,[33] spinning,[34] chemical vapour deposition[35] and green biological synthesis using plant materials, extracts, and microorganisms.[36,37] The formation of AuNPs generally follows a bottom-up synthesis route consisting of two steps: first the reduction of bulk gold precursor (Au^{3+}) is carried out with the help of reducing agents, followed by stabilization of the AuNPs formed with specified capping agents, which helps in restricting further agglomeration of the nanoparticles. Several synthetic approaches are available to synthesize AuNPs, which are discussed as follows.

2.1. AuNP synthesis *via* chemical methods

Chemical synthesis of AuNPs involves reduction as well as stabilization with different chemicals using different techniques. The Turkevich method, Fren's method of modified synthesis, and the Brust–Schiffrin method are generally applied for the synthesis of AuNPs.

2.1.1. Turkevich method. The Turkevich method, also known as the citrate reduction method, is the most common method for the synthesis of spherical AuNPs with size ranging from 2 to 150 nm and was first reported by Turkevich in the year of 1951.[38] According to this method, the addition of citrate (trisodium citrate dehydrate) to a boiling solution of hydrogen tetrachloroaurate ($HAuCl_4 \cdot 3H_2O$) results in a colour change of the solution from light yellow to wine red after stirring for few minutes, which denotes the reduction of Au^{3+} to Au^0 and the completion of AuNP synthesis. Citrate plays a dual role as reducing agent and stabilizing agent.[38,39]

The modification of the Turkevich method by Frens modified synthesis in 1973 successfully produced the narrow size range of AuNPs by tuning the molar ratio of citrate to Au salt.[40] Several modifications were applied to the technique with different pH values to control the size and mechanism of AuNPs (Fig. 4).[41] The Turkevich method generally forms spherical to quasi-spherical nanoparticles but when the particle dimension exceeds 30 nm, it tends to exert a broader size distribution pattern with considerably low yield.[42]

2.1.2. Brust–Schiffrin method. The drawbacks of the Turkevich method have been addressed by forming less dispersed nanoparticles through the Brust–Schiffrin method. In 1994, Brust and Schiffrin successfully synthesised AuNPs of 1–5 nm with increased thermal and air stability by using a phase transfer agent *i.e.* tetraoctyl ammonium bromide (TOAB). In this method, TOAB primarily acts as a transferring agent which pushes out the gold salt from the aqueous phase to an organic phase (like pyridine). In the second stage, gold (Au^{3+}) is reduced to Au^0 using reducing agents like sodium borohydride ($NaBH_4$). The stabilization of synthesised AuNPs is achieved by capping AuNPs by alkane thiols.[43,44] In this technique, the colour change from orange to brown marks the formation of AuNPs.[45] The reaction procedure is illustrated in Fig. 5. Although the Brust–Schiffrin method is extensively utilised in the development of AuNPs, the biological activity of the synthesised nanoparticles following this route is somehow curtailed as they expressed preferential solubility in organic medium compared to aqueous.

2.2. AuNP synthesis *via* a physical method

The physical method for AuNP synthesis involves different physical or physicochemical or electrical or photochemical approaches.

2.2.1. Electrochemical method. The size of AuNPs can be electrochemically controlled using a two-electrode cell, *i.e.* an anode and cathode. This approach was first coined by Reetz
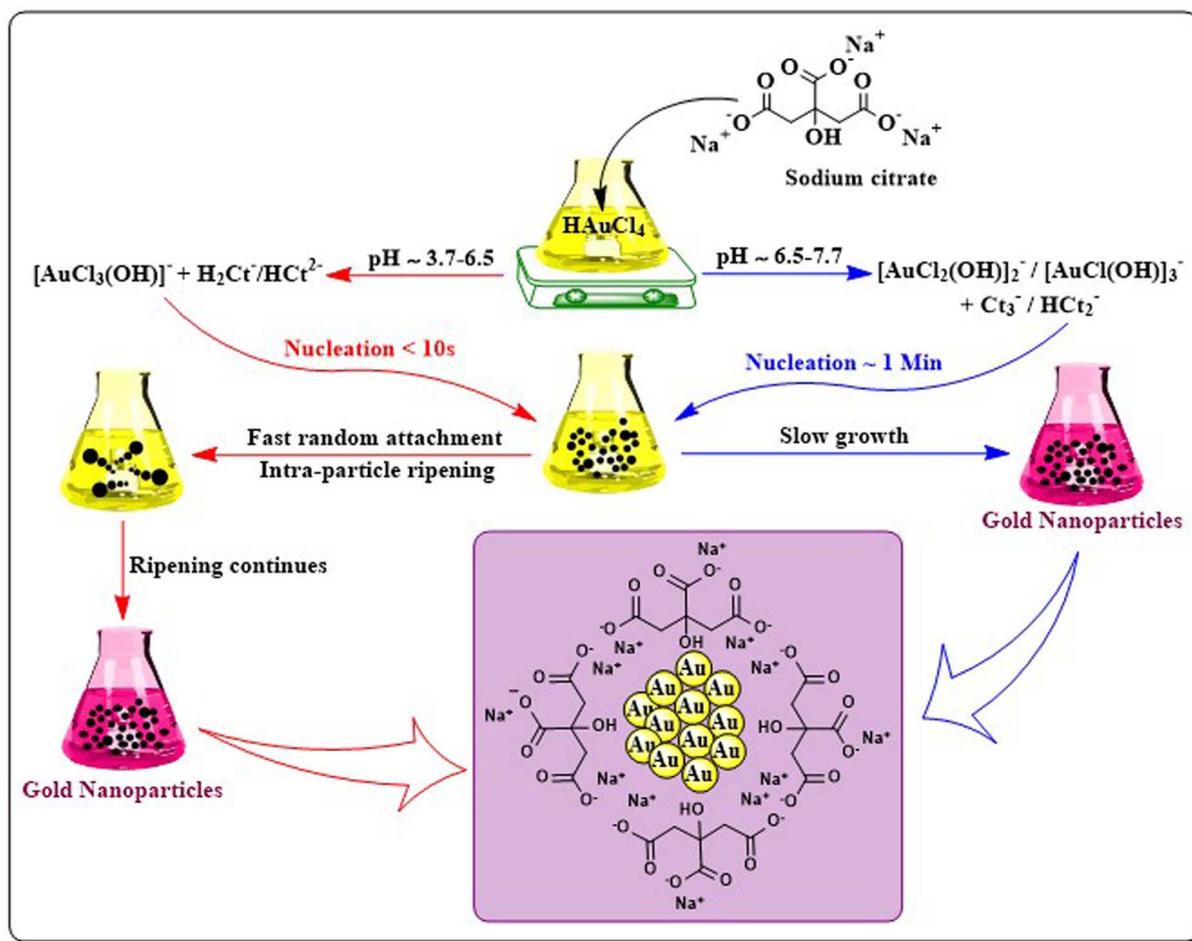
Fig. 4 Turkevich's method for AuNP synthesis and the reaction route according to different pH systems. In acidic pH conditions, nucleation is fast (<10 s) with random particle attachment followed by ripening, whereas a slightly basic pH directs slow nucleation (~1 min), followed by slow growth of intermediate particles to synthesise gold nanoparticles.
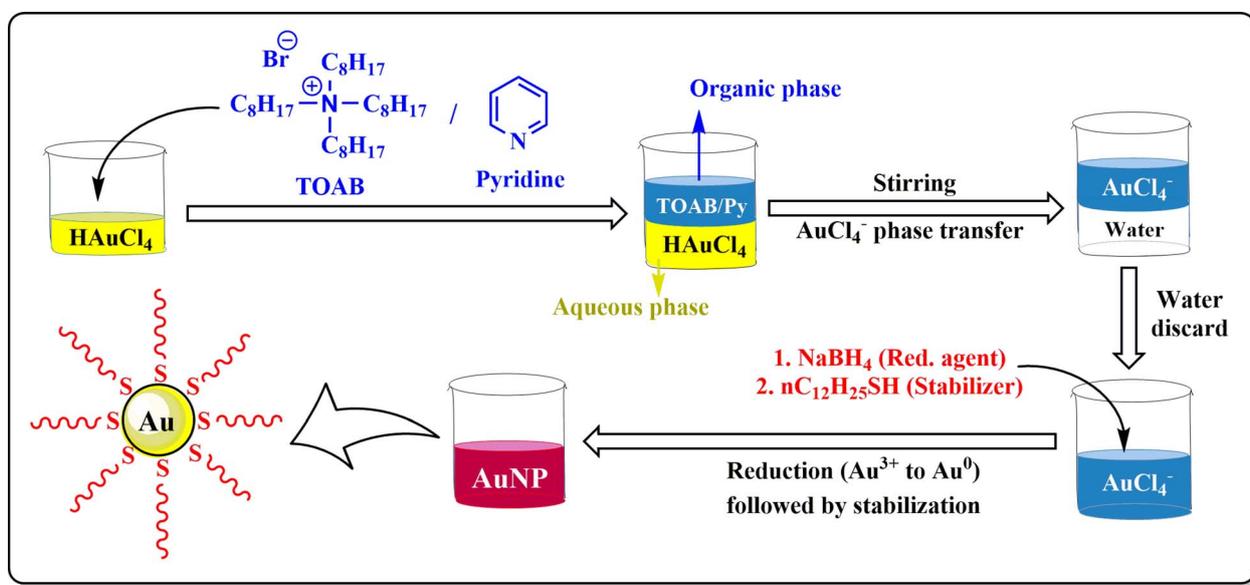

Fig. 5 Brust–Schiffrin's method for AuNP synthesis. In this two-phase synthesis method, TOAB transfers the gold salt to an organic phase (pyridine/Py) from the aqueous medium. In the second step, sodium borohydride ($NaBH_4$) reduces Au^{3+} ions to nano-gold followed by stabilization by dodecanethiol ($^nC_{12}H_{25}SH$).
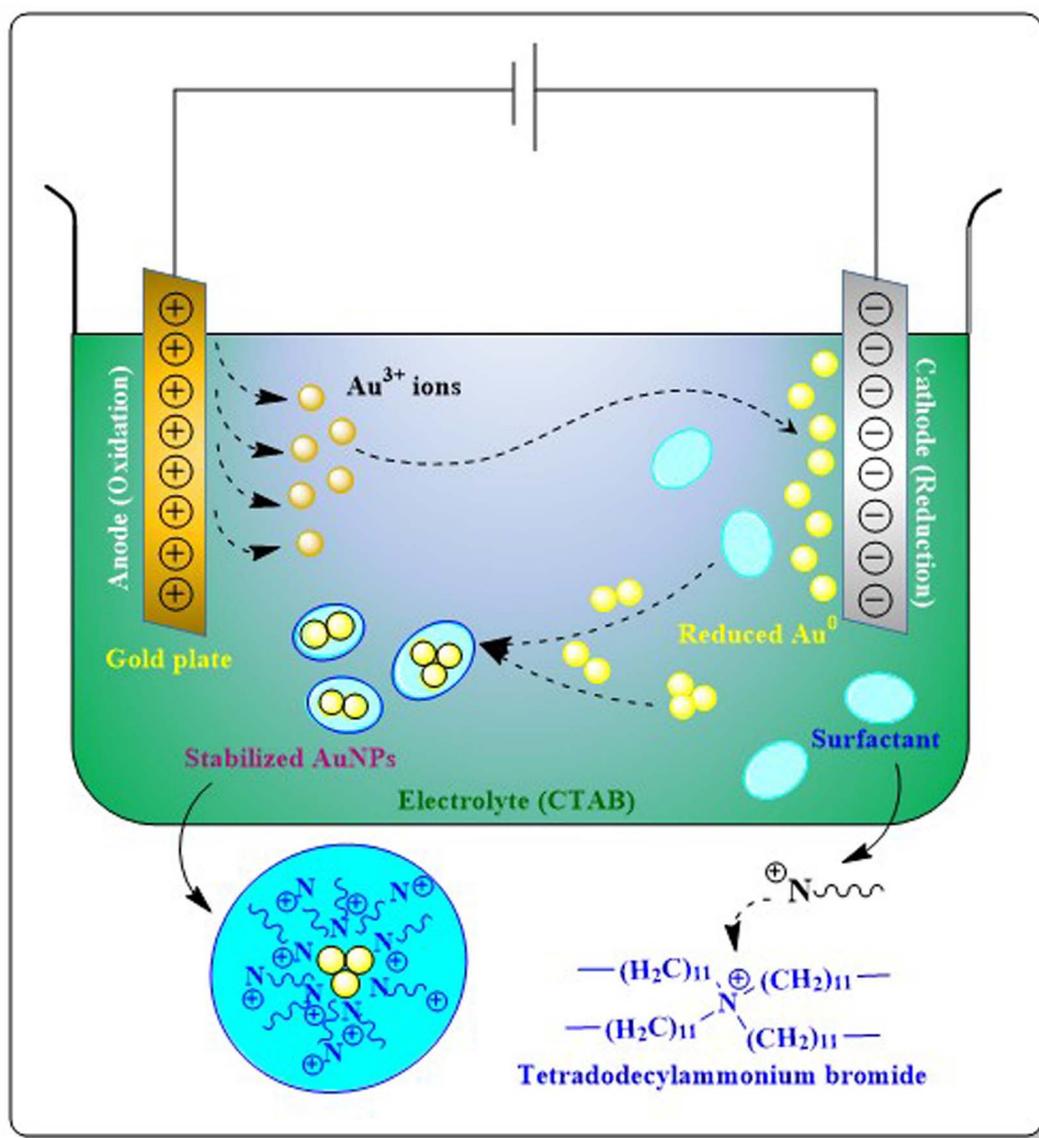
Fig. 6 Electrochemical method for AuNP synthesis. During electrolysis, a gold plate used as an anode generates Au^{3+} ions, which are attracted towards the oppositely charged cathode and reduction takes place. After reduction, the random attachment of Au^0 ions forms nanogold stabilized by surfactants like TAAB (in the figure tetradodecylammonium bromide).

et al. (1994).[46] In this method, when the oxidised metal ions in the bulk solution get trapped by surfactants like alkyl ammonium bromide, they develop a positive surface charge, which results in their attraction to the negatively charged cathode. Tetra-alkyl ammonium bromide (TAAB) also acts as stabilizer which stops the agglomeration of AuNPs in the cathode wall[47] (Fig. 6).

2.2.2. Seed growth method. Turkevich or Brust methods mostly form nanoparticles with spherical to quasi-spherical geometry, the seed growth allows tailor-made formation of different shapes of AuNPs like nanorods, nanocubes, nanowires, nanotubes *etc.* involving anisotropic growth on gold nanospheres related to the specific application desired.[48,49] This two-step procedure is initiated with the reduction of gold salts to uniform seeds with the help of a strong reducing agent like

sodium borohydride ($NaBH_4$). The seed particles in the next step act as a template in which newly reduced AuNPs are deposited to ensure several variations in size as well as shape (Fig. 7).[50] AuNP deposition or anisotropic growth is a slow process which involves the reduction of more or bulk salts using weak reducing agents like ascorbic acid. The second step comprising anisotropic growth can be regulated by adjusting parameters such as seed to metal ratio, catalyst (as a strong reducing agent) to stabilizer (weak reducing agent) ratio or pH/temperature.[49]

2.2.3. Digestive ripening. Digestive ripening is the method in which the preparation of AuNP is processed using ripening agents or ligands like alkanethiols, amines, phosphenes or silanes at a specific high temperature.[51] This method is well known for generating nano-dispersed AuNP from AuNPs with
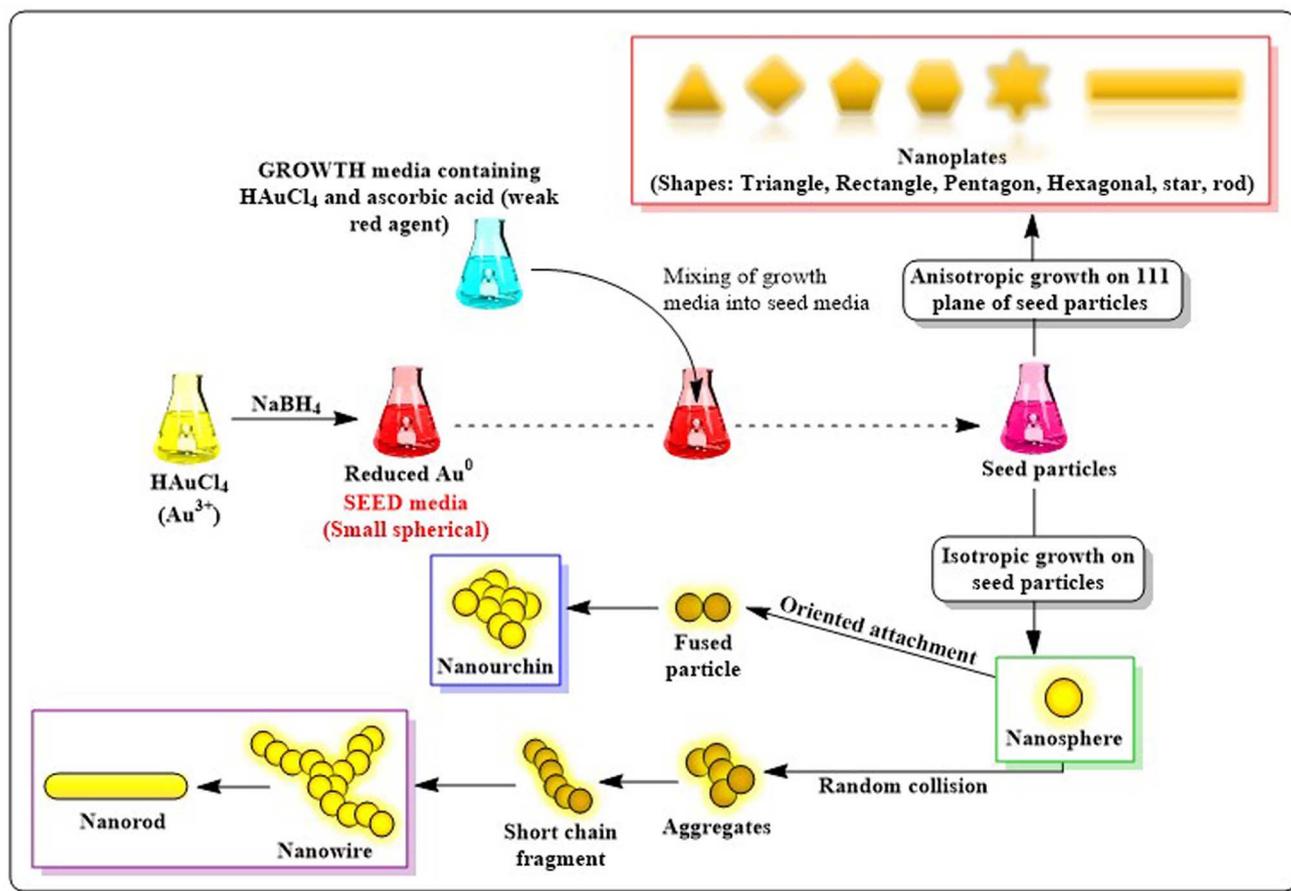
Fig. 7 Seed-mediated growth for AuNP synthesis. This two-step procedure is initiated with the reduction of gold salts to uniform seeds (seed media) with the help of the strong reducing agent $NaBH_4$. The seed media in the next step acts as a template in which growth media containing gold precursor and a weak reducing agent (ascorbic acid) is mixed. Deposition of growth particles on seed particles leads to anisotropic growth on different planes and different shapes of nano gold is achieved.
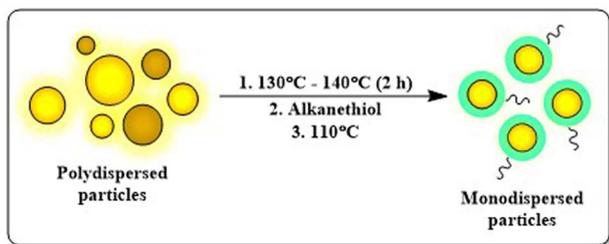

Fig. 8 Digestive ripening in AuNP synthesis. This method is well known for making monodispersed particles using alkanethiols at an elevated temperature.

a high polydispersity index (PDI). At first, gold colloidal dilution is heated for 140 °C for 2 min and the ripening occurs at 110 °C when ligands are charged into the solution (Fig. 8).[52]

Apart from all the physical methods discussed above, ultrasound mediated synthesis,[26] UV-induced photochemical reduction[31] or laser ablation techniques[29] are also employed for the synthesis of AuNPs. Microwave[53] and solvothermal

reduction of $HAuCl_4$ (ref. 54) are also considered as physicochemical approaches in synthesising AuNPs.

2.3. AuNP synthesis *via* a biological method

The chemical and physical methods applied for the synthesis of AuNPs are associated with expensive and toxic substances, which limit their biological applications. Biological methods on the other hand provide eco-friendly green approaches and have recently gained much more importance because of easy availability, biocompatibility, induced bio-applications, and easy and ready synthesis at normal suitable temperatures and pressure. Biological methods for AuNP synthesis can be achieved using different plants and their extracts, micro-organisms, biomolecules *etc.*[55]

2.3.1. AuNPs biosynthesis using microorganisms. Microorganisms like bacteria, fungi, yeast *etc.* are exciting nanofactories for synthesising AuNPs due to the presence of several reductase enzymes which convert Au^{3+} to Au^0. Microorganisms like bacteria can attract positively charged gold ions with their negatively charged cell wall and perform intracellular or extracellular reduction of gold ions. Depending on the site of

Table 1 AuNP biosynthesis using microorganisms

Genus	Microorganism	Temperature	Synthesis type	Size and shape of AuNPs	Reference
Bacteria	*Enterococcus* sp. RMAA	37 °C	Intracellular	5–10 nm; spherical	64
	Vibrio alginolyticus	40 °C	Extracellular	50–100 nm; irregular shape	65
	Lysinibacillus odysseyi	45 °C	Extracellular	12–16 nm; spherical	66
	Bacillus marisflavi	r.t.	Extracellular	14 nm; spherical	67
	Amycolatopsis sp.	30 °C	Extracellular	44 nm; spherical and irregular	68
Fungi	*Fusarium oxysporum*	30 °C	Extracellular	22–30 nm; spherical or hexagonal	69
	Agaricus bisporus	80–100 °C	Extracellular	53 nm; spherical, oval, drum-like, hexagonal, and triangular shapes	70
	Fusarium solani	28 °C	Intracellular	40–45 nm, spindle shape	71
Yeast	*Candida parapsilosis*	37 °C	Intracellular	< 30 nm, spherical	72
Algae	*Acanthophora spicifera*	60 °C	Extracellular	< 20 nm, spherical and oval	73
	Gracilaria crassa	r.t.	Extracellular	28–36 nm; spherical	60
	Halymenia dilatata	60 °C	Extracellular	16 nm, triangular and spherical	74
	Chondrus crispus, *Gelidium corneum* and *Porphyra linearis*	30 °C	Extracellular	16.9–44.2 nm, spherical and polyhedral	75
Bread mold	*Neurospora crassa*	28 °C	Intracellular	32 nm; spherical	76

reduction, bacterial synthesis of AuNPs can be classified into two processes-extracellular and intracellular. During intracellular synthesis, gold ions become electrostatically attached with the carboxyl groups present in the cell wall of microbes, followed by transportation of gold ions inside microbial cells where enzymes or intracellular co-factors finally reduce Au^{3+} to form AuNPs. On the other hand, extracellular synthesis is quite easy and devoid of critical separation processes like intracellular ones as reduction of gold ions occurs outside the microbial cells after getting trapped on the cell surface by different extracellular enzymes.[56,57] Microbes sometimes go through biosorption, metal complexation, extracellular precipitation, or induce toxicity *via* oxidation–reduction during the biosynthesis of metallic NPs.[58]

Nowadays, biosynthesis of AuNPs using fungi rather than using bacteria is becoming a more popular approach due to more frequent and less tedious work plans with successful outcomes. Fungi produce more enzymes than bacteria which make them more suitable for the faster conversion of metallic salts to NPs. Using fungi for the microbial synthesis of metallic nanoparticles is more advantageous than that with bacteria due to the presence of mycelia, a thread-like hyphae which causes greater surface for interaction with metallic salts.[59] Yeasts and algae can also perform biological synthesis of AuNPs. Several studies have suggested that the hydroxyl and carbonyl groups present in algal biomass are responsible for the reduction as well as stabilization of AuNPs.[60]

Extracellular microbial or fungal enzymes like nicotinamide adenine dinucleotide (NADH) and nicotinamide adenine dinucleotide phosphate (NADPH)-reliant enzymes *viz.* nitrate reductase act as electron carriers essential for the conversion of Au^{3+} to Au^{0}.[61] Fungi also produce enzymes like acetyl xylan esterase, cellobiohydrolase D, glucosidase and β-glucosidase, hemicellulose, 3-glucanase, cell wall lytic enzyme β-1 *etc.* for extracellular mycosynthesis of AuNPs.[62] *Rhodococcus* or *Thermomonospora* sp. (actinomycetes) and *Verticillium* sp. (fungi) are involved in the intracellular synthesis of AuNPs. *Phanerochaete chrysosporium*, a fungi producing laccase enzyme, acts as an extracellular reducing agent, whereas ligninase from the same sp. helps in intracellular bioreduction of gold ions.[63] Recent developments in biosynthesis of AuNPs using microorganism are summarized in Table 1.

2.3.2. AuNP biosynthesis using plant-derived materials. Plant-derived materials consisting thousands of active metabolites like alkaloids, polyphenols, glycosides, tannins, pigments *etc.* have emerged as greener, cleaner, and reliable tools in biosynthesis of NPs. Numerous reports exist related to the biosynthesis of AuNPs using different plant-derived materials, plant extracts, and isolated plant bioactives where they effectuate the formation and stability of NPs. Using plant products in AuNP synthesis also limits the waste formation and tedious purification steps after synthesis.[77] Among the different plant parts used, plant leaf extracts are mostly reported to initiate faster Au^{3+} reduction to form AuNPs with higher yields as leaves are richer in polyphenolic contents. The leaf extract of *Capsicum chinense* was found to synthesise stable AuNPs easily with a faster rate than the root or stem extract.[78] Uzma *et al.* (2020) have synthesised AuNPs of 20 nm size within 5 min using leaf extracts of *Commiphora wightii* and evaluated it against MCF-7 BC cells where they find remarkable anti-cancer activity exhibited by the nanosystem. The authors concluded that several secondary metabolites *i.e.* alkaloids, flavonoids, saponins, steroids, glycosides, tannins, amino acids and phenolic groups present in the leaf were responsible for the bioreduction of Au ions.[79] Another study by Akhtar *et al.* (2022) reported the formation of AuNPs within <20 s using microwave heating, the flower extract of *Hibiscus rosa sinensis* (AuNP-Hibiscus) and turmeric powder (AuNP-Curcumin). Their study revealed better anti-proliferative activity of AuNP-Hibiscus than of AuNP-Curcumin against colon (HCT-116) and breast (MCF-7) cancer with no significant toxicity in non-malignant embryonic kidney cells (HEK-293) ensuring its biocompatibility.[80] Seeds of *Foeniculum vulgare* were used by Chen *et al.* (2022) to prepare 17–20 nm AuNPs which exhibited dose-dependent cytotoxicity against ZR 75-30, T47D, and HCC1187 BC cell lines without producing any cytotoxicity on the normal cell (HUVEC).[81] Root

Table 2 AuNP biosynthesis using plant-derived materials

Part of plant used	Plant	Active components	Size of AuNPs	Shape of particles	Reference
Seed	*Mangifera indica*	Hydroxyl and carboxyl groups in flavanoids, terpenoids, tannins	50 nm	Spherical	85
	Garcinia kola	OH (polyphenolic compounds) and NH (proteins) of phytates, tannin, oxalate, cyanate, saponins and anthraquinones	2–17 nm	Spherical	86
	Citrus reticulata	Vitamins, citric acid, amino acids, proteins, terpenes, ascorbic acid	11.14–32.76 nm	Spherical	87
	Parkia speciosa Hassk	OH, C=C, C–H, and C–N functional groups of polyphenol, phytosterol, and flavonoids	5–20 nm	Spherical	88
Leaves	*Terminalia arjuna*	Arjunetin, leucoanthoc-yanidins, hydrolyzable tannins	15–30 nm	Spherical	89
	Saturejarechingeri	Geraniol, geranyl acetate, geranial and neral	15.1 ± 3.7 nm	Spherical	90
	Cyanthillium cinereum	Phenols, flavonoids, steroids, tannins, saponins and phlobatannins	14.90 nm	Spherical	91
	Jasminum auriculatum	Amine, hydroxyl and amide present in flavonoids, polyalcohols and terpenoids	8–37 nm	Spherical	92
	Combretum erythrophyllum	Flavonoids, alkaloids, terpenoids, proteins, and water-soluble biomolecules	13.20 nm	Spherical	93
Flower	*Clitoriaternatea*	Flavonol and anthocyanin	18–50 nm	Spherical	94
	Jatropha integerrima	Anthocyanin, carbohydrate, coumarin, glycoside, phenol, protein, saponin, and tannin	28–43 nm	Spherical	95
	Polianthes tuberosa L.	Amines, phenol, alcohol, ester linkages, and carboxylic acid	38.76 nm	Spheres, triangles, pentagons, hexagons, and rods	96
Stigma	*Crocus sativus*	NH or OH groups for reduction, COOH for stabilization	25–35 nm	Spherical, rod and triangle	97
Fruit	*Rosa canina*	Polyphenols, flavanols, carboxylic acid, alkenes	20 nm	Pseudo-spherical	98
	Carica papaya	Flavonoids, tannins, alkaloids, polyphenols, carotenoids, papain and chymopapain	12 ± 2.31 nm	Spherical	99
	Piper nigrum	NH or OH groups for reduction, COOH for stabilization	40–60 nm	Spherical and oval	100
Peel	*Spondias dulcis*	Carboxyl, hydroxyl, and amide groups	36.75 ± 11.36 nm	Spherical	101
	Ananas comosus and *Passiflora edulis*	Proteins, minerals, lipids, vitamin, phenolic compounds, flavonoids and carotenoid	20.71 ± 7.44 nm and 18.68 ± 5.55 nm	Spherical	102
Plant	*Physalis minima*	OH or NH groups found in carbohydrates or proteins	36 nm	Cubical	103
	Turnera diffusa	Hydroquinone-β-D-glucoside (arbutin)	24 nm	Spherical	104
Stem	*Brassica oleracea* var. *acephala*	OH and NH groups of proteins, polysaccharides or polyphenols, sulphoraphane and glucosinolates	25.08 ± 3.73 nm	Spherical	105
	Euphorbia neriifolia L.	Sugar, tannins, flavonoids, alkaloids, 24-methylene cycloartenol, triterpennoidal saponins	23–25 nm	Spherical	106
Root	*Glycyrrhiza glabra*	NH, OH and CH groups present in flavonoids, phenolics, glycosides, organic acid, proteins, amino acids and fatty acid	2.6–16.25 nm	Spherical	107
	Hemidesmus indicus L.	Proteins, lipids and polyphenols	37 nm	Hexagonal	108

Table 2 (Contd.)

Part of plant used	Plant	Active components	Size of AuNPs	Shape of particles	Reference
Rhizome	*Corallocarpus epigaeus*	Hydroxylamine and proteins	30 nm	Spherical	109
	Kaempferia parviflora	Polymethoxy flavanones, hydroxyl and carbonyl groups	44 ± 3 nm	Spherical	110
Bark	*Cinnamomum cassia*	Terpenoids, carbohydrates, flavones, and proteins	35 nm	Spherical	111
	Salix alba L.	Hexose (fructose, glucose, mannose and xylose), tannins and mineral substances	8–25 nm	Spherical	112
Nut shells	*Juglans regia*	Reducing sugars, alkaloid, tannins, phenols and saponins	10–50 nm	Spherical and triangular	113

extracts of *Terminalia mantaly* were used to prepare AuNPs which were found to be cytotoxic against colon (Caco-2), MCF-7 and hepatocarcinoma (HepG2) cell lines.[82] Apart from leaves, flowers, and roots, other plant parts like stems, bark, fruit, peel, seeds, and nutshells or sometimes whole plant extracts have been used to synthesise AuNPs.[83] Santhoshkumar *et al.* (2017) and Bharadwaj *et al.* (2021) comprehensively reviewed plant-derived product assisted synthesis of AuNPs.[77,84] Table 2 lists

Table 3 Plant-metabolites explored in AuNP synthesis

Phytometabolite	Class	Size of AuNPs	Shape of AuNPs	Activity	Reference
Epigallocatechin-3-gallate (EGCG)	Catechin	135 and 39 nm	Sea-urchin (135 nm) and spherical (39 nm)	Uptake increases on HeLa (135 nm AuNPs) and MDA-MB-231 cells (with 39 nm AuNPs)	119
Kaempferol 3-O-β-D-apiofuranosyl-7-O-α-L-rhamnopyranoside	Flavonol linked with sugar	37 ± 11 nm	Spherical	Catalytic, antioxidant and anticancer activities	120
Arbutin	Glycoside	10.30–17.13 nm	Spherical	Enhanced anti-inflammatory activity and whitening capabilities	121
Apigenin	Flavonoid (tri-hydroxy flavone)	21.4 ± 11.6 nm	Not mentioned	Cardioprotective activity against Dox-induced cardiotoxicity. Boost myocardial performance	122
Chrysin	Dihydroxy flavone	32–38 nm	Spherical	Anti-cancer, antioxidant and anti-microbial	123
Quercetin	Flavonoid (flavonol)	20–50 nm	Spherical	Anticancer activities against A549 and HeLa	124
Curcumin	Phenolic pigments (diarylheptanoid)	18 ± 3.3 nm	Spherical	ROS mediated apoptosis in MCF-7 cancer cells	125
Resveratrol	Polyphenolic phytoalexin (stilbenoid)	11.9 ± 3.1 nm	Spherical	Caspase mediated apoptosis in pancreatic cancer cells BxPC-3	126
Baicalein	Trihydroxyflavone	20–40 nm	Spherical	Anti-cancer, antioxidant and anti-microbial	127
Genistein	7-Hydroxyisoflavone	10–23 nm	Spherical	Anti-oxidative and anti-proliferative activity in prostate cancer cell lines	128
Luteolin	Tetrahydroxyflavone	25–30 nm	Spherical	Anti-cancer activity against TNBC cell line	26
Naringenin	Flavanone	12.53 nm	Spherical	Anti-cancer activity against prostate cancer	129
Anthracene	Alkaloid	76 nm (DLS)	Not mentioned	$^1O_2$ generation and local X-ray dose enhancement efficacy	130
Phenylalanine conjugated cholic acid	Protein	21.4 nm	Spherical	Colorimetric probe for the detection of Hg^{2+}, Pb^{2+} and Cr^{6+} ions	31

Table 3 (*Contd.*)

| Phytometabolite	Class	Size of AuNPs	Shape of AuNPs	Activity	Reference
Methionine	Protein	13 nm	Spherical	Tumor targeting efficacy and SPECT-based imaging capacity	131
Cysteine, tyrosine, tryptophan	Protein	8–27 nm	Spherical	Increased cellular uptake by HeLa cancer cells	132
Histidine	Protein	3 ± 0.3 nm	Spherical	Novel detection platform for barbaloin and temperature sensor	133
Calix[4] resorcinarene	Cyclic oligomer	20 nm	Spherical, hexagonal, rods	Selective and sensitive fluorescent probe for copper and leucine	134
Thymol	Terpenoid	10 nm	Granular	Reduce toxicity of bacteria resistant last-resort antibiotics	135
Cinnamic acid	Organic acid	89 nm	Spherical	Anti-amoebic activity against *Naegleria fowleri*	136
Ferulic acid	Hydroxycinnamic acid	34.2 ± 1.3 nm	Spherical	Inducing ROS mediated apoptosis on skin cancer cells (A431) by increasing MMP	137
Chlorogenic acid	Hydroxycinnamic acid	35–40 nm	Flower-shaped	Antioxidant activity	138
Gallic acid	Phenolic acid	14.1 ± 2.2 nm	Spherical	Multifunctional theranostic agent with Doxorubicin loading capacity	139
Rosmarinic acid	Polyphenolic ester	100 nm	Spherical or quasi-spherical shape	NIR-mediated PTT system for the treatment of breast cancer	140
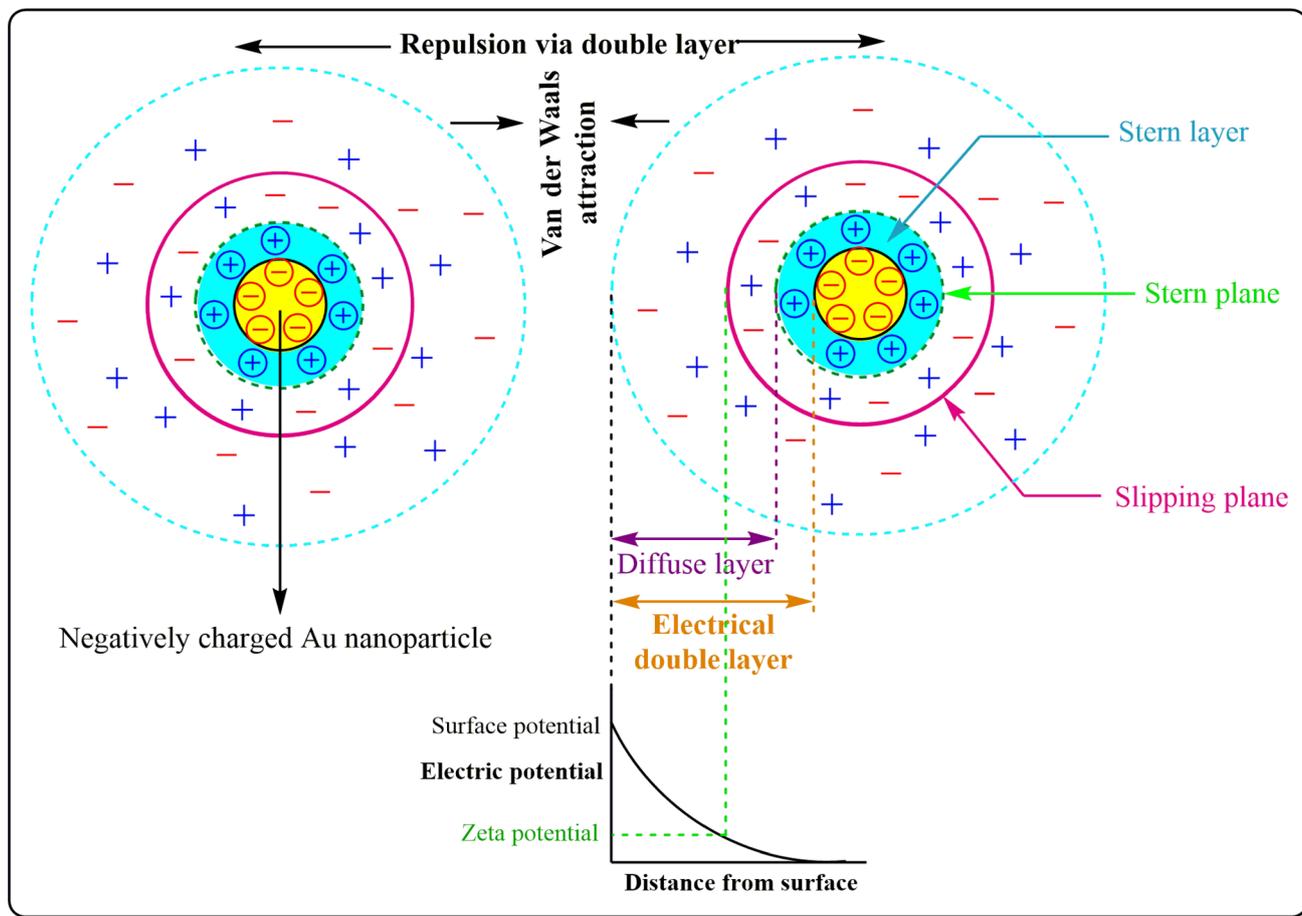
Fig. 9 Electrostatic stabilization through the electrical double layer. Positive and negative ions present in the dispersion media involved in surrounding the negatively charged NPs give rise to form an electrical double layer which mainly contributes to repulsive forces between two double layer forming particles. Stability of colloidal particle is achieved by the interplay between van der Waals's attraction and electrical double layer repulsion.

diverse plant-derived materials and their active constituents explored for AuNP synthesis.

2.3.3. Synthesis of AuNPs using phytometabolites. Secondary metabolites produced in plants mainly contribute to the defense mechanism owing to the presence of phenolic or reducing groups that act as anti-oxidants to protect plants from harmful biological or environmental factors.[114] Plant derived metabolites like polyphenols (phenolic acids, flavonoids, lignans, and tannins), alkaloids, terpenoids, reducing sugars, glycosides, saponins, proteins and organic acids are of interest in the synthesis of AuNPs [Table 3]. Among the metabolites, particularly flavonoids are widely used due to their high reducing efficacy as well as stabilizing property. The phenolic hydroxyl (–OH) groups present in the catechol moiety of flavonoid participates in keto–enol tautomerism and provide the electrons needed for the reduction of gold. The oxidized keto form of the flavonoid further attaches on the surface of the nanoparticles providing stability.[115] During the synthesis, the –OH groups initially capture metal ions via chelation and in the next step oxidation-reduction simultaneously occur viz. –OH oxidizes to carbonyl (C=O) and Au^{3+} reduces to Au^0. Generally, for flavonoids, the preferred chelating site is found to be at the 3rd or 5th positioned –OH or the 4th positional carbonyl group possibly due to the comparatively lower bond dissociation energy than that of the –OH at other positions.[116] In the case of reducing sugars, the electron is transferred when oxidation of aldehyde (–CHO) groups takes place to produce corresponding carboxylic acids (–COOH) in the synthesis of nanoparticles.[117]

While synthesizing nano-gold, determining the optimized conditions i.e. optimal concentration, temperature, reaction time or pH should be done very carefully as these factors significantly affect the physical, morphological and even chemical characteristics of the synthesized particles. In our previous study with luteolin engineered AuNPs, we found that even with a small change in optimized concentration (molar ratio), temperature or reaction time, particle size and zeta potential values change drastically.[26] The reason behind the controlled NP properties with respect to these factors are well explained by Zuhrotun et al. (2023).[116] Kuppusamy et al. (2016) reported that the number of hydrogen ions in the hydroxyl group possessed by a phytochemical could affect the size and shape of synthesized NPs.[118]

2.4 Stabilization of the synthesised AuNPs

After synthesis, metallic NPs possess high surface energy (up to 2000 mJ m^{-2}) due to their surface area enhancement resulting in thermodynamic instability.[141] By their nature, NPs undergo aggregation which reduces the interfacial tension of nano-conjugates via decreased surface area and effective volume fraction, thus compensating for the disordered circumstances of NPs in a colloidal state. Despite the relative high surface area and high energy, van der Waals forces serve as the main attractive force which leads to nanoparticle aggregation, with co-ordination unsaturation and unstable atomic environment as other proven contributors. To perform the stabilization of colloidal NPs, stabilizing agents, capping agents come into play which mainly work via creating repulsive barrier between the particles to overcome the influence of van der Waals forces among the particles.[142] The stabilization process of NPs can be achieved by three different stabilization phenomena i.e. electrostatic, steric and electrosteric techniques.

2.4.1. Electrostatic stabilization. The mainstay of electrostatic stabilization (ES) is the fact that particles with equal or the same charge experience repulsive forces between each other. After synthesis, different ions present in the dispersion media surround the NP surface which results in a charged layer. The
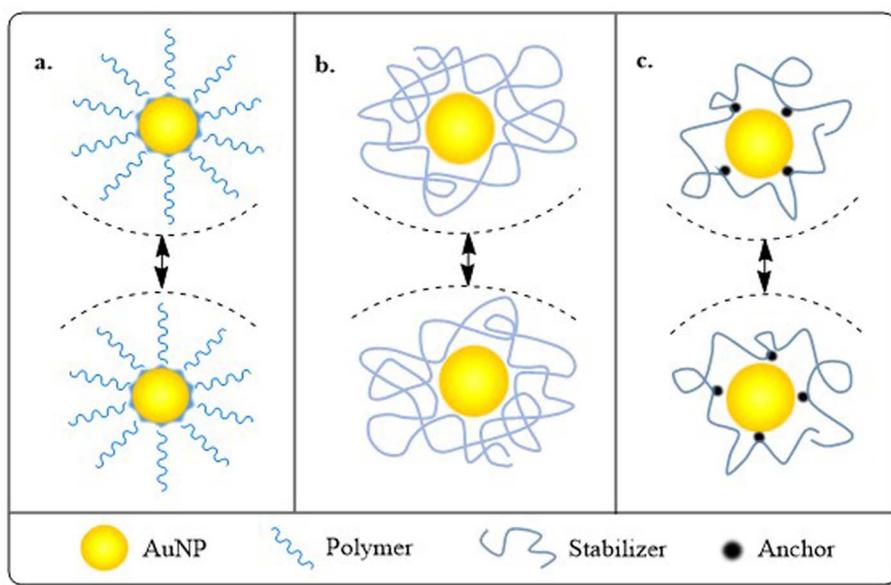

Fig. 10 Steric stabilization through (a) elongated bulky molecules, (b) polymers or (c) chelating agents. These bulky molecules/polymers/chelating agents create steric hindrance which forms the basis of the NPs stability in dispersed media.
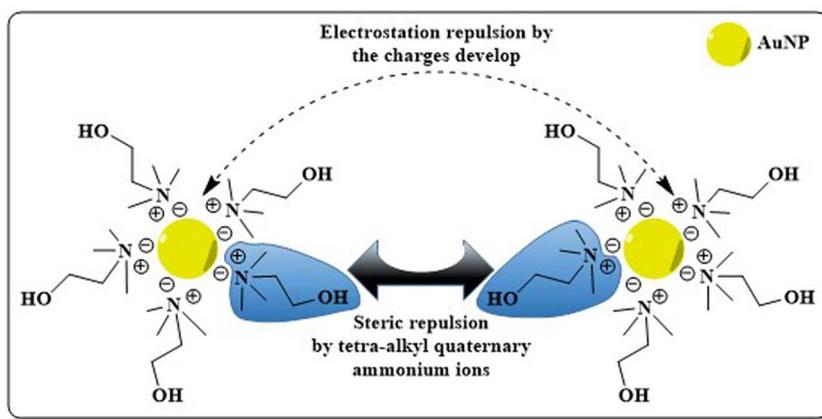
Fig. 11 Electrosteric stabilization obtained using quaternary ammonium ionic liquids. Charged molecules like tetra-alkyl quaternary ammonium ions can stabilize NPs *via* electrostatic stabilization and as they are bulky, they can also induce steric stabilization. Coupling electrostatic and steric stabilization forms the basis of electrosteric stabilization.

opposite ions then become attracted and also border the first layer giving rise to electrical double layer around the NPs. The double layer is responsible for repulsion between particles and generally the basis of ES.[52] ES is well explained by the Derjaguin Landau Verwey and Overbeak (DLVO) theory, which basically suggests that the stability of a colloidal particle is achieved by the interplay between the van der Waals's attraction and electrical double layer repulsion. When the overall energy potential (V_T) (sum of the van der Waals's attraction and double layer counter-ion repulsion) exceeds the kinetic energy (E_k) of the particles ($V_T > E_k$), the particles gain stability and *vice versa*.[143] In 1940, Levine and Dube *et al.* suggested that in the case of ES, not only the electric double layer, but also the induced dipole or multipoles determine the strength of interaction.[144] Depending on the dipole moments high or low, one can modulate the agglomeration or redispersion to synthesize "smart NPs".[145] However, because it is a type of kinetic stabilization, ES cannot be achieved in multiple phase systems and electrolyte sensitive media[52] (Fig. 9).

2.4.2. Steric stabilization. Steric stabilization (SS) deals with repulsive force between the steric layers formed around the NP surface. The size and chemical nature of the adsorbed molecule/ions forming the steric layer affects the degree of stabilization. Elongated bulky molecules or polymers or chelating agents can be adsorbed *via* anchoring entities or can encapsulate the NPs and curtail their coalescence[143,146] (Fig. 10).

2.4.3. Electrosteric stabilization using ionic liquids (IL). Polyelectrolytes or polymeric surfactants can combine the effects of ES and SS giving rise to electrosteric stabilization (ESS). Ionic liquids (IL) or surfactants with high positive and negative ion densities, can participate in ES and on the other hand, they also possess a bulky geometry necessary for steric repulsion. Tetra-alkyl quaternary ammonium halides or imidazolium surfactants are widely used as ILs for ESS.[147] The negatively charged halide ions are adsorbed on the surface of NPs very easily (chemisorption), while tetra-alkyl quaternary ammonium ions provide the bulky geometry. Using ILs during

synthesis can also suppress NP diffusion at elevated temperature due to high viscosity.[143] ILs also provide increased solubility for metal precursors, substrates or polymers. Different cations *viz*, tetraalkylammonium, tetra-alkylphosphonium, 1-alkyl-3-methyl imidazolium, alkylpyridinium, 1,1-dialkylpyrollidium, *N*-(2-hydroxyethyl)-*N*-methylmorpholinium and anions like trifluoromethanesulfonate (CF_3SO_3), alkylsulfonate or tetra/hexafluoroborate or phosphate (BF_4^-/PF_6^-) with their complementary counter ions form suitable electrosteric stabilizers.[143,148,149] Different capping agents used in the AuNP synthesis and stabilization are illustrated in Fig. 11.

3. Engineering AuNPs with diverse moieties for BC management

The primary limitation of AuNPs without functionalization lies in their *in vivo* drug delivery applications. AuNPs with their ease of functionalization offer remarkable clinical opportunities, which provides solution to the problems present in first generation AuNPs.[150] Engineering AuNPs with different modifiers like PEG, antibodies, proteins, oligonucleotides, sugars *etc.* ensures selective or site-specific targeting approaches and improved pharmacokinetics with the desired renal clearance.

Targeting AuNPs in cancer cells without hampering healthy cells can be achieved through two different targeting approaches *i.e.* passive and active targeting. Tumor cells possess larger vasculature gaps (100 nm–2 μm) than normal cells. Being nano-sized, AuNPs can easily penetrate through these gaps and are retained in tumor cells for a much longer time, as tumor cells possess disorganized lymphatic systems, restricting lymphatic clearance and resulting in "enhanced permeability and retention" (EPR) effects. Passive targeting of AuNPs into cancer cells exploring EPR facilitates selective targeting and improved retention assisting in enhanced therapeutic efficacy[151,152] (Fig. 12). Though passive targeting ensures preferential accumulation of AuNPs in tumors, active targeting offers an enhanced therapeutic response with maximized
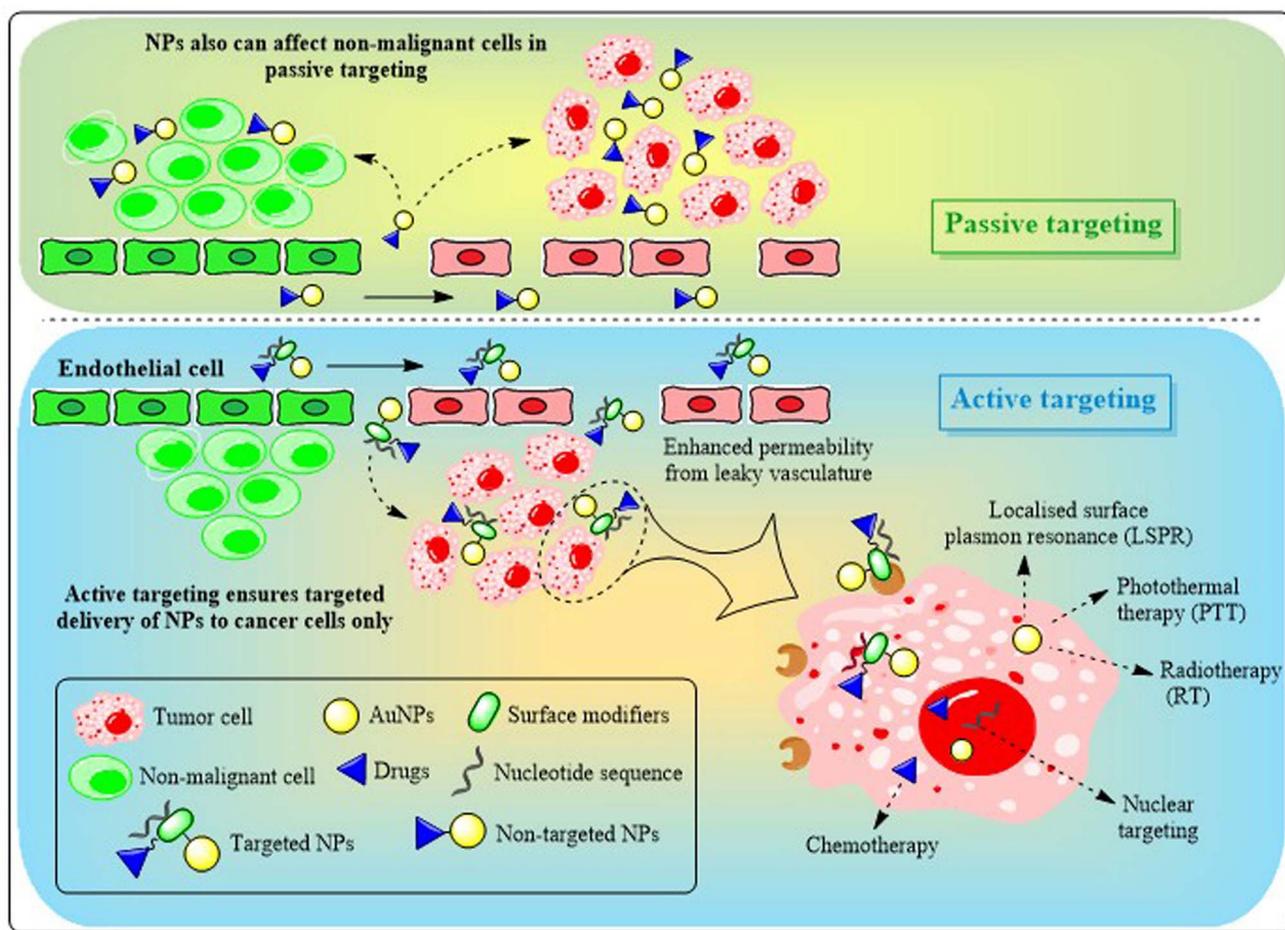
Fig. 12 Active and passive targeting approach with AuNPs in cancer treatment. Passive targeting depends on the EPR effect of AuNPs and drug delivery in passive targeting can work on cancer as well as non-malignant cells creating a loophole for the strategist treatment of cancer. On the other hand, attaching specific surface modifiers or biomarkers to AuNPs viz. peptides, nucleotide sequences, or antibodies ensures active targeting. In active targeting, drugs can be targeted to the overexpressed biomarkers or cancer related receptors on the surface of the cancer cells facilitating biosafety.

chances of protecting healthy tissues compared to the passive approach. Attaching different targeting ligands like antibodies, cell surface markers, oligonucleotide sequences, or proteins with AuNPs helps with targeting and interacting with specific receptors over-expressed on the BC cell surface[152] (Fig. 12). Thus, the active targeting technique follows a dual approach, one through EPR and the other through ligand–receptor interactions.

Modification of AuNPs with different ligands requires suitable attachment either by covalent or by non-covalent interaction between the particle and the ligands. Gold has a strong gold–thiol (Au–S) bond. Love et al. (2005) calculated Au–S bond energies between Au–thiol and Au–disulfide, in which they reported Au–S (disulfide) to be stronger ($\sim$60 kcal mol^{-1}) than Au–S (thiol) ($\sim$45 kcal mol^{-1}).[153] On the other hand, non-covalent interaction can be classified as two types-electrostatic attachment or by layer-by-layer (LbL) assembly. Electrostatic attachment/adsorption generally involves attachment of antibodies, DNAs or proteins. Proteins being zwitterionic biomolecules, possess charge when a suitable pH system with a similar isoelectric point is applied. The developed charged molecules are absorbed on the charged surface of AuNPs easily.[154] Electrostatic adsorption can alter, weaken or even denature the protein structure, which plays a disadvantageous role along with weak interaction. LbL assembly of multiple polymers with alternative charge allows AuNPs to bear tunable surface charges or enables introduction of hydrophobic or lipophilic regions in AuNPs, thus ensuring increased solubility and clearance of drugs with low solubility.[155]

3.1. Engineering AuNPs with polymers or PEG

The main hurdle AuNPs face in biological applications is their opsonization. The reticuloendothelial system (RES) engulfs the opsonized NPs by phagocytosis which limits their targeting approach. PEG is the polymer most commonly used to functionalize AuNPs to achieve a stealth effect.[156] PEG can be attached directly with AuNPs or through a linker i.e. thiols. In a study, it was suggested that thiol-PEGylated AuNPs not only offered cargo (Tamoxifen) delivery but also increased intracellular drug import which led to 2.7 fold more potency of the drug

Table 4 Current engineering AuNPs with different surface modifiers for application in BC

Functionalization system	Coating agent or ligand	Conjugated system	Synthesis/conjugation technique	Key features of the functionalized ligand	Main outcome delivered by the conjugated system	Reference
Polymers	PEG	Triptorelin (TRP)-functionalized PEG-AuNPs	Layer by layer assembly	Adhesion with plasma membrane	Specific targeting achieved through TRP-LHRH interaction present in TNBC surface	197
		AuNPs-KT2-PEG conjugates	Covalent technique	Increases colloidal stability of KT2 peptide	Rapid internalization and increased cytotoxicity in MDA-MB-231 cell line	198
	PVP	PVP-*co*-2-dimethylaminoethyl methacrylate modified celastrol-folic acid-AuNPs	PVP capping induced acid–base reaction	High encapsulating efficiency, improves solubility and loading content	Induced cellular uptake, apoptosis with low colony-forming assay unit in 2D and 3D breast cancer models	199
	PLGA	AuNP encapsulated PLGA modified nanoclusters	Single step nano-precipitation method	Encapsulation of AuNPs into polymer nanoconstructs enhance Specific Absorption Rate (SAR) value	Photothermal ablation in SUM159 BC cells	200
	Poly(ethylimine) (PEI)	PEI–PEG-AuNPs	Layer by layer assembly	Low mol wt of PEI reduce toxicity, helps in delivering gapmers in cancer cells	Reduce TNBC cell proliferation, reduce Gemcitabin resistance in mutant p53 cancer cells (MDA-MB-231)	201
	Polylysine	Poly-L-lysine (PLL)-AuNS-miRNA	Layer by layer assembly	Deliver miR-34a to TNBC cells	Suppress proliferation	202
Peptides and proteins	Albumin (HSA or BSA)	Gd$_2$O$_3$@BSA-Au NPs	Chemical reduction	Forms metal ion complex with Au and Gd during synthesis and enhanced stability observed	Enhanced tumor suppression when exposed to X-ray radiation (5 Gy) in 4T1 bearing mice	203
		HSA-AuNPs-TMX	Chemical reduction	Template to fabricate AuNPs with better TMX delivery	Dose dependent cytotoxicity in BT-474 and MDA MB-231 BC cell line	163
	Glutamine	Glucose-BSA-AuNPs, glutamine-BSA-AuNPs, and folic acid-BSA-AuNPs	Chemical conjugation	Increase biocompatibility, better tumor targeting efficacy	Glutamine-BSA-AuNPs showed better targeting, better gold accumulation and enhanced radiosensitizing property in 4T1 bearing BALB/c mice	204
	Folate	AuNP-CS-FA-His	Carbodiimide coupling	CS induced stability, histidine enhanced endosomal escape and folic acid for targeting	Less cytotoxicity observed. Conjugation of His and FA to Au-CS produced a significant increase in the luciferase activity in SKBR-3 and MCF-7 cells, respectively	205
	RGD, TAT, NLS	DOX, RGD and nuclear localization peptides (NLS) tagged AuNPs (DRN AuNPs)	Chemical reduction	Targeting- RGD ensures cell penetration, NLS ensures cargo release inside nucleus	More efficacy observed in HeLa cells than in MCF-7	206
		RGD-Gd@Au core–shell tecto dendrimer CSTDs-PS-nanocomplex	Carbodiimide coupling	Targeting specificity to $\alpha_v\beta_3$ integrin-overexpressing tumors because of RGD	Enhanced CT/MR imaging of 4T1 BC model *in vivo* and metabolism capability with good biosafety	207
		^{111}In-Match-AuNP-Tat	Carbodiimide coupling	TAT increased nuclear localization	DNA double-strand breaks and caused a dose-dependent reduction in clonogenic survival of telomerase-positive (MDA-MB-435) cells	208

Table 4 (Contd.)

Functionalization system	Coating agent or ligand	Conjugated system	Synthesis/conjugation technique	Key features of the functionalized ligand	Main outcome delivered by the conjugated system	Reference
	EGF	EGF-luteolin tagged AuNPs	Carbodiimide coupling	Targeting and enhanced cellular uptake	Protein tagging leads to better cytotoxicity with AuNPs delivered into TNBC (MDA-MB-231) cell line in vitro	26
	Tumor-penetrating peptide (TPP)	Hsp70 (TPP)-PEG4-FeAuNP	Covalent linker coupling	Increased uptake	Induced G_2/M cell cycle arrest and ROS mediated apoptosis in MDA-MB-231 and 4T1 cell line	209
Antibodies	Trastuzumab	G5-AuNP-Gd-trastuzumab nanoconjugate	Click reaction using G5-PEG-allyne-DOTA-NHAc and trastuzumab-azide	Targeting	Enhanced MRI signal intensity by 20% and improved CT resolution and contrast by two-fold in vivo	16
	HER-2	BSA-AuNCs-FA-HER	Carbodiimide coupling	Targeting and radiosensitizing effect	Increased cellular internalization with improved radiation therapy in SK-BR3 BC cells	210
	Cetuximab	Ctxb-AuNPs	Using coupling reagent (COMU)	Targeting	Enhanced proton irradiation based cytotoxicity in A431 cells but not in MDA-MB-453 cells	211
	ER-α	Anti-ERα-AuNPs	Carbodiimide coupling	Targeting	1,2-Bis(4-pyridyl) ethylene (BPE)-ERα-AuNPs Raman nanotags highly accumulated with a strong SERS signal to ensure detection of spheroid BC cells (MCF-7)	212
	EpCAM or TARP	(Paclitaxel-thiol-AuNPs-thiol)-TARP and EpCAM	Carbodiimide coupling	Cargo loading and targeting	AuNPs-thiol-TARP/EpCAM is a non-toxic drug delivery system. Attachment of TARP antibody to paclitaxel-thiol-AuNPs showed more activity than EpCAM attached system	174
	Hsp-70	cmHsp70.1-AuNPs	Maleimide coupling reaction	In vivo tumor targeting	Accumulation in intracellular vesicles observed without any toxicity	213
	CA 15-3	CA 15-3/Au based screen printed electrode	Carbodiimide coupling	Selectivity towards CA 15-3 BC antigen	Immunosensor successfully quantified CA 15-3 BC antigen in artificial serum samples with wide linear response	214
	Affibody	Dox@affi-F/AuNPs (affibody used: ZhcHER2:342)	Covalent conjugation	Targeting for HER2	Enhanced co-delivery of 5-fluorodeoxyuridine and doxorubicin	215
Nucleotides or aptamers	DNA	Dual-miRNA activated DNA walker comprised of carboxyfluorescein (FAM) and cyanine5 (Cy5) attached Mg^{2+}-specific DNAzyme (Dz) hybridized AuNPs	Freeze mediated conjugation bypassing salt-aging technique	FAM fluorescence enhancement, recovers the Cy5 fluorescence	Depending on the expression levels of miR-21 and miR-31, DNA walker can successfully distinguish malignant (noninvasive) MCF-7, metastatic (highly invasive) MDA-MB-231, and nontumorigenic MCF-10A cell lines	216

Table 4 (Contd.)

Functionalization system	Coating agent or ligand	Conjugated system	Synthesis/conjugation technique	Key features of the functionalized ligand	Main outcome delivered by the conjugated system	Reference
	RNA	TectoRNAtrimer:AuNP	Thiolated conjugation via salt-aging technique	Targeting against the CopGFP gene	Regulates the GFP gene expression, biocompatible system	217
		Peptide–AuNR–siRNA	Thiolated conjugation	Targeting and gene silencing effect	Gene silencing, and inhibition of metastasis in TNBC MDA-MB-231	218
	Aptamer	AS1411-chitosan-AuNPs loaded with methotrexate	pH mediated conjugation	Nucleolin targeting	Chitosan gives better biocompatibility, AS1411 ensures targeting, MTX induce cytotoxicity in vitro and in vivo	219
Monosaccharides & polysaccharide	Chitosan	Janus chitosan/gold nanoparticles (J-Au-CS NP)	Nonsolvent-aided counterion complexation method	Selective surface fabrication	Enhanced cytotoxicity and intracellular localization achieved. PA imaging-guided synergistic PTT/gene therapy was achieved after CD-PGEA decoration upon J-Au-CS NP	220
	Glucose	2-Amino-2deoxy glucose (2DG) conjugated Au-loaded apoferritin nanoparticles (Au-HoSAF-2DG NP)	COOH activated EDC/NHS coupling	Cell surface glucose transport protein specific targeting	Selective targeting for MCF-7, selective cell death, enables in vitro X-ray and computed tomography (CT) imaging	221
	Cellulose	Carboxy methyl cellulose (CMC)-AuNPs	Chemical reduction	Reduction, providing chemical stability	Nanocomposite confers promising antibacterial, antifungal and anticancer activities. Induces apoptosis and necrosis by increasing caspase-8/-9 and decreasing VEGFR-2 activity	222
	Gum acacia	Gemcitabin (GEM)-GA-AuNPs	Chemical reduction	Reduction, drug loading capacity improvement	Enhanced aqueous solubility and drug release rate of GEM, enhanced cytotoxicity by the nanosystem	223
	β-Cyclodextrin	AuPEI-β-CD-Pep NPs	Microwave radiation	Decorated the carrier with targeting moieties using "host–guest" inclusion complexation	Enhanced transfection efficacy, targeted therapeutic delivery of nucleic acids to MCF-7 BC cells	224
Enzymes	Collagenase	COL-AuNPs	Carbodiimide chemistry	Improved cellular interaction/penetration of Metformin (MET)-AuNPs in mammospheres	Increased apoptosis and reduced $CD24^-/CD44^+$ CSCs by COL-AuNPs and MET-AuNPs co-treatment against JIMT-1 BC cell	225
	L-Asparaginase	AuNPs-PEG-L-asparaginase-RGD	Thiol mediated conjugation	Enhanced anti-cancer efficacy	Remarkable antioxidant effects with high tumor targeting efficacy and distribution in MCF-7 cells. Decreased cell proliferation and clonogenicity of MCF-7, apoptosis through intrinsic pathway and cell cycle arrest at the G_2/M phase	226
	Horseradish Peroxidase	HRP-AuNPs	Carbodiimide chemistry	Ensured enzyme prodrug therapy	Co-treatment with HRP-AuNCs and IAA efficiently triggers cell death induced by oxidative stress	227

in estrogen receptor positive BC cells.[157] Along with stabilization, PEG block polymer can also be used as a reducing agent to synthesize AuNPs. Sarkar *et al.* (2017) used a non-toxic, non-ionic amphiphilic tri-block copolymer made up of PEG and polypropylene glycol (PPG) (PEG–PPG–PEG) as a reducing and stabilizing agent for the synthesis of Au-nanomicelles. The nanomicelle was further conjugated with ZD6474 (a tyrosine kinase inhibitor) and the nano-conjugate was targeted to tumor cells in MDA-MB-231 xenograft mice models where the authors observed decreased tumor size with promising conclusions.[158] In a recent study, Wang *et al.* (2021) also synthesized Au-nanorods functionalized with copolymer PLGA–PEG. The biodegradable and biocompatible copolymeric system carried water insoluble Paclitaxel to the targeted vicinity.[159] Mahalunkar *et al.* (2015) used another polymer polyvinylpyrrolidone (PVP) to functionalize with curcumin–gold nanoconjugate and further tagged with folic acid (FA). FA–curcumin–PVP–AuNC exhibited promising *in vivo* anti-cancer activity without any significant toxicity.[160] Some of the recent studies of polymer functionalized Au-nanosystems for the treatment of BC are given in Table 4.

3.2. Engineering AuNPs with proteins and peptides

The most effective way to achieve targeted drug delivery using AuNPs is to conjugate different proteins or peptides *via* amino acid conjugation. Different proteins *i.e.* essential amino acids (aspartic acid, glutamic acid, phenylalanine, tryptophan, tyrosine, and L-cysteine), plasma proteins (albumins), epidermal growth factor (EGF), protein sequences *i.e.* RGD, NLS or TAT or even vitamins (folic acid) can be easily conjugated with AuNPs *via* covalent or non-covalent interactions to favour the intended application (Table 4). The amine group present in an amino acid or peptide bind with negatively charged AuNPs through ionic interaction, whereas the negatively charged carboxylic group helps in stabilizing AuNPs.

The direct conjugation or ligand exchange method, amine carboxylate coupling or carbodiimide coupling technique and click chemistry are the three main techniques are used in covalent attachment of peptides to NPs. The ligand exchange method, which is the most commonly used approach to prepare peptide engineered AuNPs, was first explored by Hostetler *et al.* (1999).[161] Due to their strong affinity to Au, sulphur containing amino acids *i.e.* cysteine, can easily undergo a ligand exchange method to substitute itself with citrate and produce stable cys-AuNPs[162] (Fig. 13). Certain basic amino acids like tyrosine or cysteine also reduce $AuCl_4^-$ to Au^0 and form peptide conjugated AuNPs through the chemical reduction method.[163] Although direct attachment is an easy technique, multivalent interactions between numerous residues of protein and the NP surface often lead to protein structure deformation, which is a major disadvantage.[164] The most important method to functionalize proteins or peptides to carboxylated AuNPs through chemical conjugation technique is using "carbodiimide coupling chemistry", where EDC (1-ethyl-3-(3-dimethylaminopropyl) carbodiimide) reacts with COOH to form an active intermediate *i.e.* O-acylisourea. The unstable O-acylisourea then gets easily displaced by nucleophilic attack from primary amine

groups present in the protein, leading to the formation of an amide bond and thus conjugates proteins with AuNPs. N-hydroxysuccinimide (NHS) or Sulfo-NHS is often used in carbodiimide coupling reaction (EDC/NHS coupling) to generate another amine-reactive ester intermediate which more efficiently conjugates with proteins (Fig. 13).[165] Raposo *et al.* (2017) conjugated BSA (bovine serum albumin) to PEG-AuNPs *via* the carbodiimide coupling reaction and then AuNPs@PEG@BSA were further functionalized with Zn(II) based complex TS262 ([Zn(1,10-phenanthroline-5,6-dione)$_2$]Cl) and Co(II) based complex TS265 ([CoCl(H$_2$O)(1,10-phenanthroline-5,6-dione)$_2$] [BF4]). BSA ensures high loading of cargo in the nanosystems (AuNPs@PEG@BSA@TS262 and AuNPs@PEG@BSA@TS265), which exhibited remarkable cytotoxicity in canine mammary FR37-CMT cell line with IC$_{50}$ values better than the standard drugs Doxorubicin and Cisplatin.[166]

Recently, click chemistry has been used by researchers for allowing site specific protein conjugation to NPs through carbon-hetero-atom bond formation giving high and selective yield. Though click chemistry generally suggests the copper-catalyzed azide–alkyne 1,3-dipolar cycloaddition reaction (CuAAC), the presence of copper is detrimental to living cells. Keeping this in mind, Liu *et al.* (2017) used a strain-promoted azide–alkyne cycloaddition reaction (called copper-free click chemistry or SPAAC) to synthesise folate receptor (FR)-targeted SERS active Au-nanoprobe without observable cytotoxicity. The SERS nanoprobe is created by modifying hollow AuNPs with a monolayer of a Raman-active label known as tris-aza-5,5′-dithiobis(2-nitrobenzoic acid) or N$_3$-DNBA. These labels are comprised of disulfides, enabling them to be covalently attached to the surface of AuNPs and azide groups, facilitating their connection with folate bicyclo[6.1.0]nonynes derivatives (BCN-Folate) through click chemistry. The click coupling reaction facilitated by cyclooctynes activated by ring strain proceeds rapidly under mild conditions and does not necessitate a cytotoxic copper catalyst[167] (Fig. 13). AuNPs functionalized with lysine or glycine bind to DNA efficiently and ensure efficient gene delivery without any toxicity. One of the major hurdles associated with protein engineered AuNPs is the pH dependency of the tagged protein which often lead to the aggregation of AuNPs.[168]

3.3. Engineering AuNPs with antibodies

Antigens present in cancer cells are able to assist in treating cancer *via* immunotherapy. Specific cancer cells produce their own significant antigens *i.e.* tumor-associated antigens (TAAs) by cellular gene mutation of aberrantly expressed normal genes. In BC, mutated as well as genes those are over-expressed in breast tissues produce different antigens. The antigens found in BC include human epidermal growth factor receptor 2 (HER2), carcinoembryonic antigen (CEA), mucin-1 (MUC-1), carbohydrate antigens (CA-15, Tn, TF, and STn) which are over-expressed and produced by abnormal or immature glycosylation of different amino acids *i.e.* serine and threonine, human telomerase reverse transcriptase (hTERT), and p53 – the most common tumor suppressor gene found mutated in cancers.[169]
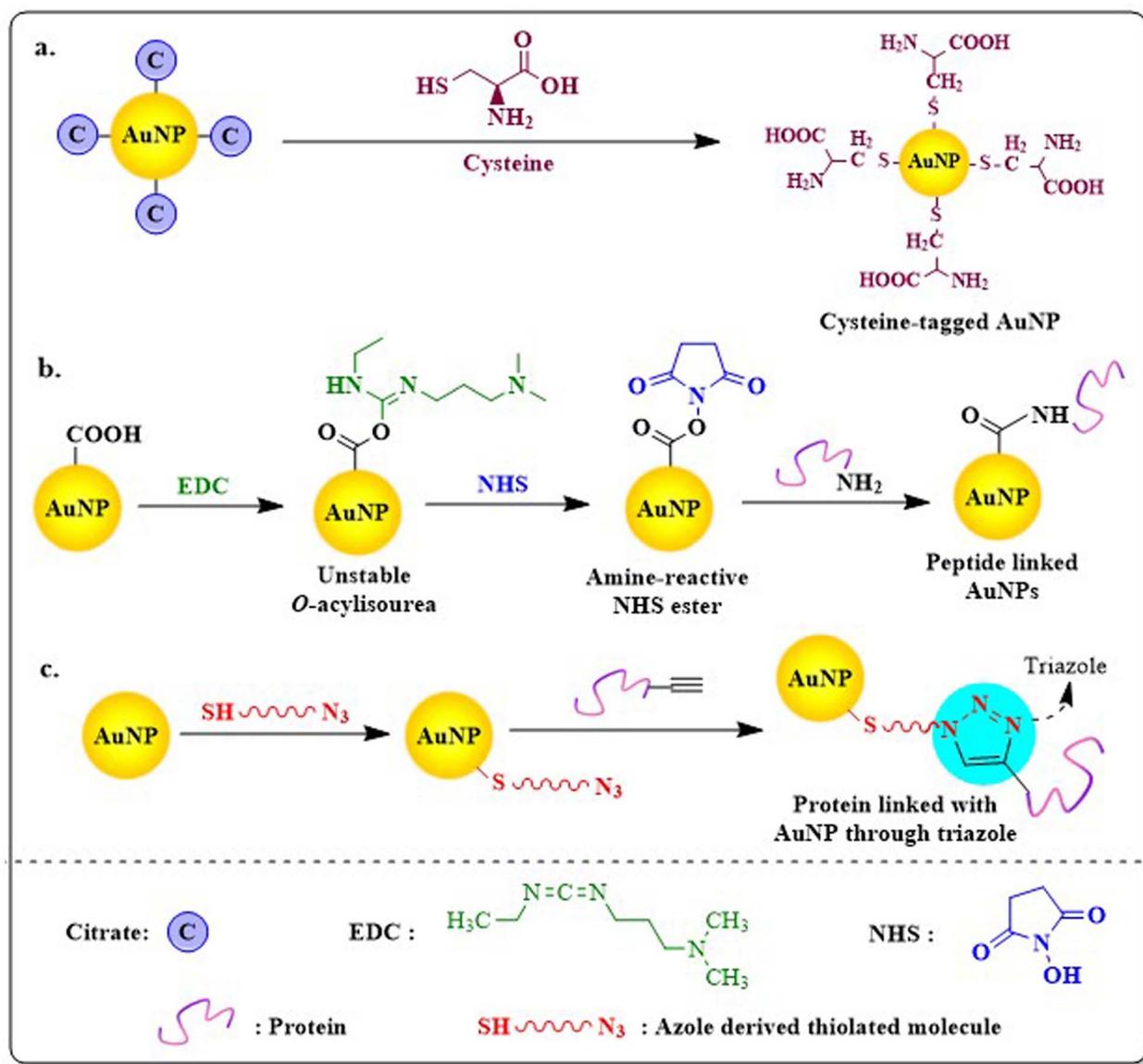
Fig. 13 Functionalization of proteins with AuNPs using (a) direct conjugation technique where sulphur containing amino acid substitute citrates take advantage of the affinity of gold for sulphur; (b) through carbodiimide chemistry where carboxylic AuNPs react with EDC and NHS to form an amine reactive ester which easily reacts with amino groups present in the protein; and (c) through click chemistry using azide derived thiolated polymer, alkyne terminated proteins. Proteins are attached with newly formed high-strained triazole rings bridging between thiolated polymers and proteins.

AuNPs engineered with specific antibodies bind to definite antigens present in adenocarcinoma cells and induce an antigen–antibody reaction, thus improving biosensing efficacy and site-specificity of nanoparticles.

Antibodies can be coupled with AuNPs through covalent, non-covalent or coordinate (dative) interactions (Fig. 14). Generally, the EDC/NHS coupling reaction involved in covalent bonding between antibodies and the COOH/NH$_2$ group activates AuNPs but often leads to aggregation and polymerization. Another problem arises from disordered orientation or wrapping of antibodies on the surface of nanoparticles blocking free antigen binding sites.[170] The problem can be solved by incorporating external pH near the isoelectric point of antibody which favors ionic or electrostatic adsorption of antibodies to the surface of nanoparticles. In ionic interaction, although the net charge distribution and the asymmetry of the antibody allows the antigen binding sites to be free for binding, it has certain limitations like a high antibody requirement to conjugate with non-magnetic nanoparticles, instability in different pH conditions and replacement of antibody with other biomolecules by electrostatic interactions.[171] Another non-covalent attachment is the hydrophobic interaction often formed when the hydrophobic area of the antibody interacts with the metal surface. Dative binding or coordinate bonding is one type of physical interaction that occurs between the antibody and AuNP surface, when only the free sulfhydryl group
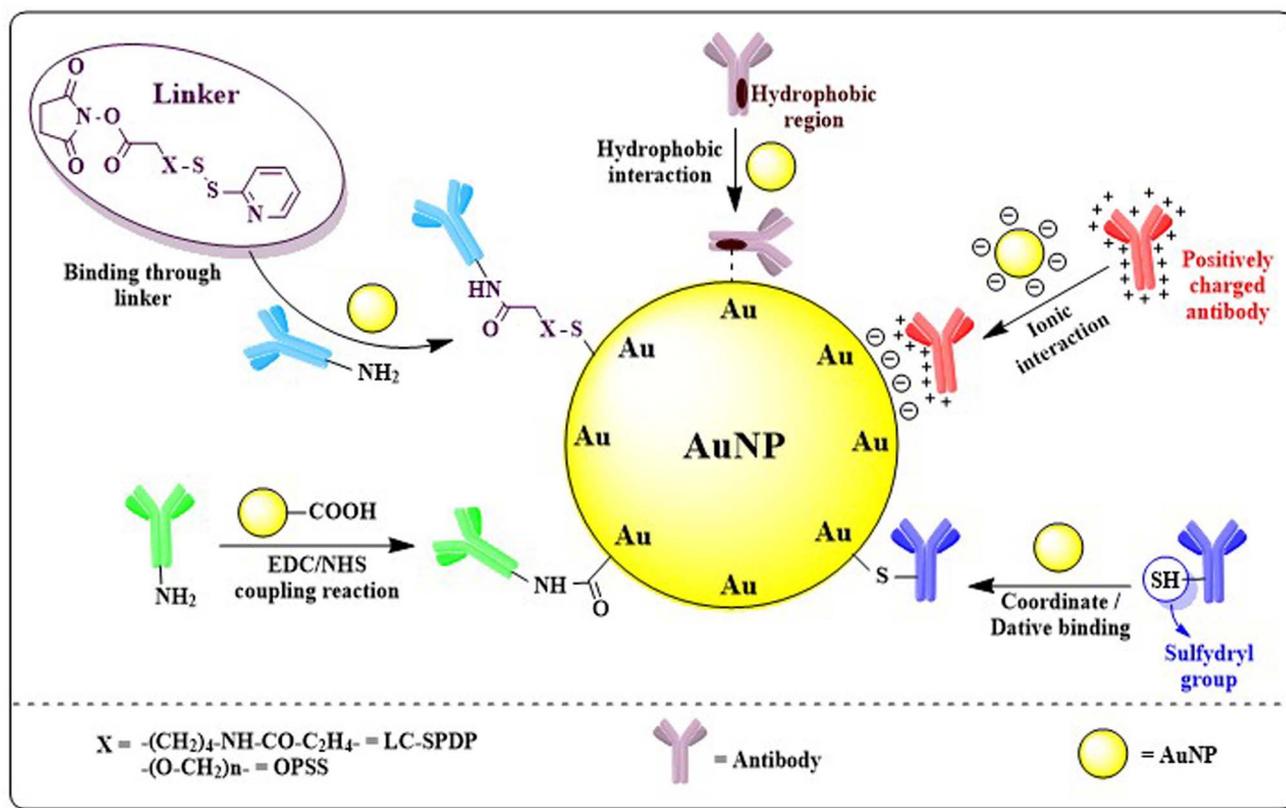
Fig. 14 Different interactions favouring functionalization of antibodies with AuNPs. Hydrophobic interaction, ionic interaction, dative interaction with sulfydryl groups, carbodiimide coupling through EDC/NHS and linker facilitated binding are generally utilized to conjugate specific antibodies to the surface of the nano gold.

present in the antibody shares its outermost electron and both of them use it covalently.[170] Antibodies can also be attached to AuNPs through a linker. Liao *et al.* (2005) and Loo *et al.* (2005) used pyridyl cross-linkers *i.e.* long chain succinimidyl 6-[3(2-pyridyldithio)propionamido]hexanoate (LC-SPDP) or orthopyridyl disulfide (OPSS)–PEG–NHS to conjugate antibodies with Au-nanosystems.[172,173]

Protein EpCAM over-expression in BC was targeted by antibody engineered AuNPs with paclitaxel payload. They exhibited significant diminution of BC cell viability compared to AuNPs designed without antibodies.[174] In another comparative study report it was observed that lectin jacalin or anti HER-2 antibody conjugated AuNPs exhibited a similar localisation pattern in the acidic compartments of both human colorectal adenocarcinoma (HT-29) and HER2+ BC cells (SK-BR-3).[175] Penon *et al.* (2017) reported that engineered gold nanoparticles with a porphyrin derivative ligand, a PEG derivative ligand and an anti-erbB2 antibody resulted in a site-directed photodynamic response against SK-BR-3 human breast cancer cells.[176] Recent advancement of antibody linked AuNPs in BC treatment is disclosed in Table 4.

3.4. Engineering AuNPs with oligonucleotides

Oligonucleotide (DNA or RNA) or aptamer functionalized AuNPs find use in a wide range of applications, with the most common being as probes in DNA-based biosensing assays, or in therapy for nucleic acid delivery including cell-related applications.[177] DNA hybridized AuNPs have become a fascinating area of research because of the attachment of a definite and sequential probe which possesses a programmable assembly process followed by a specific action. Functionalization of AuNPs with DNA is easy because of the tendency of DNA bases to form coordinate bonds with Au.[178] For direct conjugation or covalent conjugation, oligonucleotides are first introduced to thiol linkers at either the 5′- or 3′-end of the aptamer to form thiol-modified oligonucleotide. Since both oligonucleotides and AuNPs are negatively charged, this conventional technique needs to follow "salt-aging" and delicate control of the ionic strength to compensate for the charge repulsion between the nanoparticles surface and the DNA strands with a longer incubation period (usually overnight).[179] DNA absorption onto the AuNP surface also depends on pH, a freezing environment, presence of anions like arsenates, or small molecules.[180] The study by Shin *et al.* (2012) suggested DNA-functionalized AuNPs were very stable in buffer but they lost stability in PEG and became easily aggregated.[181] Dougan *et al.* (2009) used disulphide-(thioctic acid) modified oligonucleotide probes which suggested significant improvements in the stability of oligo-Au/Ag nanoparticles.[182] Apart from the conventional technique, non-thiolated DNA functionalized AuNPs have also been

reported.[183] Some recent studies with oligo-AuNPs in breast cancer treatment are given in Table 4.

PEGylated AuNPs engineered with the mucin1 (MUC1) aptamer loaded with Paclitaxel resulted in synergised photothermal therapy and targeted drug delivery leading enhanced cytotoxicity compared to photothermal therapy or chemotherapy alone.[184] Nano-complex designed with AS1411 aptamers, melittin and AuNPs produced significant selective cytotoxicity to MCF-7 BC cells compared to L929 cells ensuring site-directed delivery of melittin.[185] AuNP modified with polyA sequences, AS1411 aptamer and antagomir-155 influences targeted delivery and promotes apoptosis by enhancing the expression of Tp53INP1 in MCF-7 cells.[186]

3.5. Engineering AuNPs with saccharides

Apart from proteins, carbohydrates gained much popularity in nano-based treatment as they possess specific but complex structural features, which affect different physiological and pathological circumstances in living systems. Carbohydrate based nanosystems or simply glycol-nanosystems possess the capability to restrict first pass metabolism, counteract p-glycoprotein mediated efflux, improve intestinal lymphatic transport, enhance absorption, facilitate chemical modification, and exhibit mucoadhesive properties make them an excellent solution for drug delivery associated problems in BC treatment. According to the Warburg effect, cancer cells need glucose far more than healthy cells as they reproduce quickly and at a greater rate. Substitution of this energy source with other monosaccharides could retard tumor progression and hence such carbohydrate tagged AuNPs could play an important strategic role in cancer treatment.[187] AuNPs attached to the second carbon of glucose propound special features like targeting, the ability to differentiate between cancer and inflammatory cells, enabling contrast ability and triggering clathrin-mediated cellular uptake of NPs inside cancer cells depending on GLUT-1 expression.[188]

Fabrication of different carbohydrate polymers into nanosystems can be achieved via the in situ copolymerization technique, solvent casting method or by the electrospinning technique.[189] Glyco-AuNPs can be synthesized through a one, two or three step reaction (Fig. 15). Single step functionalization or direct conjugation simply refers to the reduction of Au^{3+} to Au^0 with sugar itself being a reducing agent as well as a stabilizer. Two steps synthesis consists of synthesis of citrate-capped AuNPs commonly via the Turkevich method and then ligand exchange of citrates with thiol ending sugars. Mannose, galactose and glucosamine functionalized Au-nanosystems were synthesized using this approach; however, a longer synthesis time, lower glycan loading, and difficulty in controlling the size and shape of the nanosystem are the main drawbacks associated with the method.[190–192] Three step reactions enable synthesis of AuNPs via traditional methods, attachment of linkers through the ligand exchange method followed by functionalization of sugar moieties using different reactions between ligands and carbohydrates i.e. oxime formation, reductive amination, alkyne–azide cycloaddition, perfluorophenylazide (PFPA) photochemistry, amidation etc.[193] Katti et al. (2009) functionalized glucose (monosaccharide); sucrose, maltose, or lactose (disaccharides); raffinose (trisaccharide); and starch (polysaccharide) with AuNPs using the nontoxic, water-soluble reducing agent tris(hydroxymethyl) phosphine-alanine (THPAL).[194]

AuNPs with glycoamino acids ligands bearing the Thomsen–Friedenreich antigen linked to isolipoic acid had a profound influence on stability enhancement of AuNPs without hindering their biological action.[195] Phthalocyanine-AuNPs engineered with lactose were reported to produce singlet oxygen and effect cell death upon irradiation as well as be associated with the galectin-1 receptor on the surface of BC cells.[196] Carbohydrates as glycolipids or glycoproteins serve as important signalling moieties of our bodies. Among them monosaccharides and oligosaccharides have binding selectivity to protein receptors

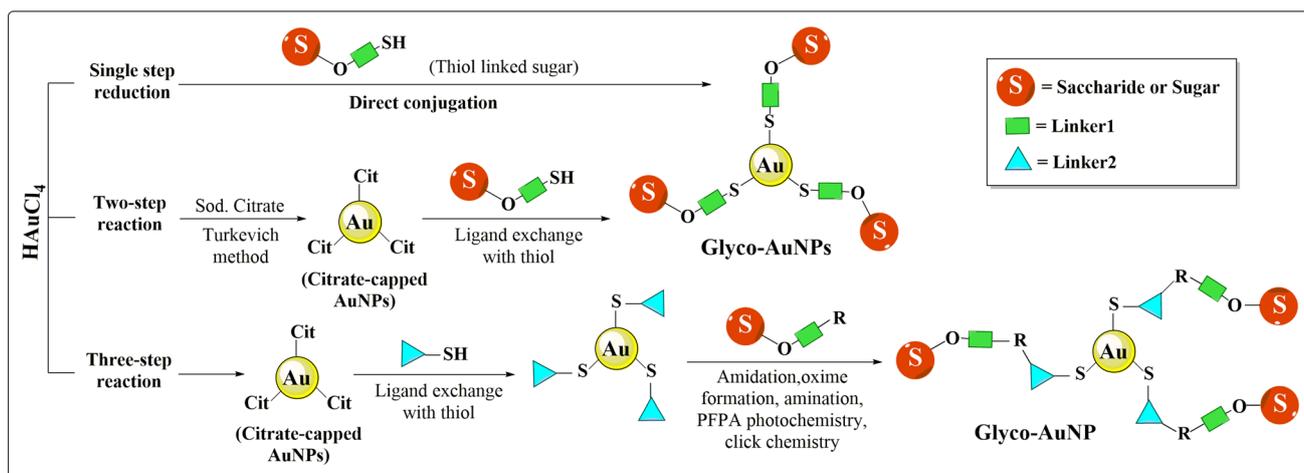Fig. 15 Synthetic procedure of glyco-AuNPs through one, two and three step reactions. In a single step reaction, sugar itself acts as a reducing and stabilizing agent. Two-step synthesis consists of synthesis of citrate-capped AuNPs followed by ligand exchange of citrates with thiol ending sugars. Three-step reactions involve reduction, ligand exchange and conjugation via amidation, amination, oxime formation etc.

overexpressed on cancer cells. So, these variants can be engineered with AuNPs to get a favourable clinical outcome as therapeutic, diagnostic or theranostic agents.

4. Theranostic effects of AuNPs

Conventional therapy for heterogeneous diseases lacks specificity towards particular cell types or tissues, often resulting in suboptimal outcomes. Theranostics, a concept combining "therapy" and "diagnostic" into a single approach, was coined in 1998 by US consultant John Funkhouser, aiming for personalized medicine offering improved prognoses.[228] By integrating nanotechnology, specifically nanotheranostics, targeted early disease detection, treatment, and monitoring becomes feasible. AuNPs serve as effective carriers for both imaging and therapeutic agents, enabling precise delivery to target sites while minimizing systemic toxicity. Moreover, AuNPs can be loaded with multiple contrast agents *viz.* fluorophores, MRI agents, photoacoustic agents, and surface-enhanced Raman spectroscopy (SERS) reporters for multimodal imaging with real-time monitoring of their effects, enhancing disease characterization without overwhelming the patient's immune system.[229] Nanoplatforms leverage particle size for enhanced tumor targeting *via* the EPR effect, exploiting differences in the tumor microenvironment (TME) such as vascular abnormalities, hypoxia, and pH. TME-triggered theranostic gold nanoparticles hold promise for tumor-specific detection and therapy by capitalizing on these unique features.[230]

AuNRs with varying aspect ratios were coated with folic acid (FA)-PEG block copolymer (FAP) and pheophorbide a (Pheo) for tumor targeting and photodynamic therapy (PDT). AuNRs with an aspect ratio of 3.84 and longitudinal plasmon resonance at 873 nm (Pheo-conjugated AuNR100) demonstrated enhanced singlet oxygen generation, photothermal conversion, GSH-mediated Pheo release, tumor targeting, and a synergistic PDT–PTT effect.[231] An amphiphilic AuNP was coated with a Raman reporter (BGLA) and made stealthy with PEG, while pH sensitivity was achieved *via* PMMAVP grafts. DOX was incorporated as cargo, and HER2 antibody enabled specific targeting. The system's cellular binding, uptake, and intracellular disruption were evaluated, highlighting its potential for targeted theranostic applications of AuNPs.[232] Nanoparticles face a highly intricate *in vivo* environment, which differs significantly from *in vitro* settings. This leads to notable disparities attributed to (i) a limited understanding of how NP properties influence biointeractions and (ii) variations in experimental parameters.[233] For instance, Zhang *et al.* (2020) observed discrepancies where PEG-AuNPs were swiftly cleared from mouse circulation despite *in vitro* studies showing reduced uptake by RAW 264.7 macrophages.[234] Similarly, J. Cancino-Bernardi *et al.* (2018) found no significant differences in shape or protein coating *in vitro*, yet AuNP-HSA triggered a myeloperoxidase mediated inflammatory response when orally administered to Wistar rats.[235] Citrate-capped AuNPs showed no impact on cytokine secretion *in vivo* but caused DNA damage *in vitro*.[236] Wang *et al.* compared the *in vitro* and *in vivo*

performances of Au-nanohexapods for theranostic applications, revealing discrepancies in tumor accumulation and cytotoxicity.[237] Moreover, Dubaj *et al.* (2022) noted significant variations in the internalized gold concentrations between cell lines and corresponding tissues *in vivo*, emphasizing the absence of natural barriers in *in vitro* setting as the primary cause for these inconsistencies.[238] The discrepancy of *in vitro* and *in vivo* results are well discussed in the reviews of Pavithra Natarajan *et al.*[239] and Khlebtsov *et al.*[233]

While various nanoparticles like carbon nanotubes, quantum dots, iron oxide nanoparticles, and silica nanoparticles can be utilized for theranostic applications, AuNPs hold a prominent position due to their distinct features such as strong surface plasmon absorption, stability, biosafety, and ease of modification. Unlike quantum dots, which face concerns about the fragility of disulfide binding during surface modification, stable ligand anchoring of AuNPs typically requires only a monodentate thiol. However, there is debate regarding whether residual carbon nanotubes may cause long-term damage to the host, and the absence of a standardized protocol for preparing high-purity carbon nanotubes at a large scale presents a challenge for clinical translation.[240] Despite the advantages of each nano-scale agent, they also present their own set of drawbacks, like toxicity of quantum dots, high-cost of gold nanoparticles, the limited sensitivity of iron oxide nanoparticles as MRI contrast agents, non-biodegradability of carbon nanotubes, and the size and self-destructing properties of silica NPs.[241] The study of Alexander Vasil'kov with Au and iron-oxide NPs in conjugation with Methotrexate clearly suggested the better stability of AuNPs over iron-oxide NPs as iron was involved in oxidation at higher temperature.[242] Research for improvement of these limitations is ongoing and could be an interesting brainstorming option for future endeavours. Here, in this review, we would like to address the theranostic applications of AuNPs part by part, first its diagnostic applications, then therapeutic strategies including photothermal therapy, radiotherapy and AuNPs as cargo delivery.

4.1. AuNPs in BC diagnosis

The unique optical properties of AuNPs aptly supported by sophisticated instrumentation setting facilitate BC management by exploring them in a dual platform of therapy and diagnostics.[243] Reports of AuNPs tailored with different moieties like peptides or nucleic acids, antibodies, photo-enhancers, radiolabeled agents, aptamers, oligonucleotide sensors, antigen detectors and immunosensors have assisted molecular probing or imaging of BC cells with high accuracy. AuNPs have been reported for their integration with BC surface receptors *i.e.* HER-2 (human epidermal growth factor receptor-2), integrin β, and CD-44 (cluster of differentiation 44), in detection of overexpressed intracellular receptors *i.e.* ERα (estrogen receptor α) and also in genetic alterations *i.e.* mutated *BRCA1* (breast cancer gene 1), p53 over-expression, tumor mi-RNA *etc.*[244]

4.1.1. HER-2 expression in BC. HER-2 (a BC cell surface receptor) oncogenes (*HER2*, *HER2/neu*, *and cErbB-2*) have been suggested to control growth and progression of BC. HER-2

receptor itself is overexpressed in 20–25% of total cases for BC incidences.[245] HER-2 positive BC has its own unique epidemiological and clinical attributes with poor therapeutic responses which makes it more aggressive and complex than HER-2 negative one.[246] HER-2 or anti-HER-2 antigen conjugated AuNPs are routinely used not only for diagnosis, but also for the treatment of BC after successful association of nanoconjugates with HER-2 overexpressed BC cells. Aptamers are generally single stranded short nucleotide sequence of artificial DNA and RNA which binds to specific target receptors, Wu *et al.* (2022) conjugated 3′-thiolated HER2 probe (AH′) and 5′-TAMRA tagged anti-HER2 aptamer (tAH) with AuNPs to form a dual aptamer AuNP probe (DA-AuNP). The group was able to classify BC subtypes *i.e.* SK-BR-3, MCF-7 or MDA-MB-231 based on Förster resonant energy transfer (FRET) measuring fluorescence intensity. In single and dual color mode, no fluorescence was observed in the case of MDA-MB-231 (HER2^{-ve}/ER^{-ve}) subtypes, green fluorescence related to FAM (carboxyfluorescein) was observed for MCF-7 cells (HER2^{-ve}/ER^{+ve}) and red fluorescence related to TAMRA (carboxytetramethylrhodamine) was observed for HER2^{+ve} SK-BR-3 cells.[247]

4.1.2. Expression of ERα in BC. Estrogen is a hormone that impacts in growth and development of mammary glands. ERα is the endocrinal nuclear receptor that activates several pathways upon binding with estradiol and approximately 80% of total BC possess ERα (+ve) diagnostic results, which makes ERα an abundant receptor for the most common targeted treatment in BC.[248] Ahirwar and Nahar (2015) developed salt induced aggregation resistant ERα-RNA-aptamer coated AuNPs which changes colour from wine-red to deep blue when it attaches to an ERα receptor. Based on this colorimetric ERα-aptasensor, they not only detected the ERα (+ve) MCF-7 cells, but also they were able to quantify ERα with a range of 10 ng mL^{-1} to 5 μg mL^{-1}.[249]

4.1.3. BRCA1 overexpression and mutation in BC. Breast cancer genes (*BRCA1* and *BRCA2*) produce proteins which help in repairing the damaged DNA. The most common cause of hereditary BC is represented by the mutated *BRCA* genes which account for 5–10% of total BC. *BRCA1*-related BC is indicated as the most aggressive phenotype compared to sporadic BC with a high tendency of being triple negative.[250] Depending upon the hybridization properties of DNA-AuNPs, a research team successfully detected single base BRCA1 mutation using colorimetry at an arbitrary temperature.[251]

4.1.4. miRNA overexpression in BC. Micro RNAs (miRNAs) are small non-coding RNA which interact with cyclin proteins, protein kinases and growth promoters or suppressors to regulate cell proliferation and cell cycle progression pathways in BC. miRNA family subtypes *i.e.* miR-21, miR-155, miR-10b, and miR-9 are reported to promote BC metastasis.[252] Hakimian *et al.* (2018) mixed DNA probe conjugated citrate modified AuNPs and miR-155 conjugated PEI capped AuNPs to form a hybridized biosensor which detected 3-BP mismatches in miR-155. The hybridized biosensor was suggested to detect and quantify miR-155 at very low concentrations with a linear range of detection of 100 fM where the lowest range of detection was 100 aM.[253]

4.1.5. BC antigens and overexpressed MUC1. BC antigen 15-3 (CA 15-3) is a glycoprotein encoded by plasma mucin 1 gene (*MUC1*). *MUC1* amplification accounts a significant amount (40%) of total BC and CA 15-3 serum biomarker overexpression has been found in 80% of overall metastatic BC.[254] CA 15-3, in combination with CEA (carcinoembryonic antigen), is the tumor marker most commonly used in breast cancer detection. A few-layer black phosphorus (FL-BP) conjugated AuNP hybrid was developed by Peng and co-researchers in 2017, which possessed a unique reversible switching property between inactive and active states upon antigen–antibody treatment. The FL-BP/AuNP hybrid successfully detected CEA level colorimetrically with a wide range of detection (1 pg mL^{-1}– 10 μg mL^{-1}) as well as elevated CEA levels in BC cells.[255]

4.1.6. Nucleolin overexpression in BC. Nucleolin (NCL) is a multifunctional nucleolar phosphoprotein which acts as a tumor angiogenic marker when overexpressed. Nucleolin overexpression is suggested to enhance the growth of ErbB2-positive breast cancer xenografts *in vivo*. Though 90% of nucleolin is found in the nucleolus, it is also present in the cytoplasm and on the cell surface.[256] AS1411 is a 26-BP guanine rich anti-nucleolin DNA aptamer which binds with nucleolin present in several cancer cells but absent in normal tissues. In a study, a magnetic-gold nanocomplex (Fe$_2$O$_3$-AuNPs) was hybridized with the AS1411 aptamer which successfully distinguished between nucleolin overexpressed 4T1 BC cells [darker MR intensity] and human foreskin fibroblast (HFFF-PI6) [brighter MR intensity] by T$_2$-weighted magnetic resonance signal intensities using MRI.[257] Current research inputs exploring the diagnostic attribute of AuNPs are tabulated in Table 5.

4.2. AuNPs as probing agents

The strong interactions of AuNPs with visible light (SPR properties) are often explored as labeling agents for sensing cancer cells. Site-directed AuNPs accumulated in cancer cells exhibit optical scattering properties, which helps in visualization of cancer cells which can be tracked using different sophisticated techniques *i.e.* TEM, phase contrast optical properties, dark field microscopy, photoacoustic or photothermal imaging.[276] Sensitive probing of cancer cells with the help of AuNPs also can be achieved using SERS imaging. External radiation passing through materials results in elastic and inelastic collision. In inelastic collision of photons with the matter, the molecular vibrations cause scattering of photons with a different wavelength which is known as Raman scattering. Nanoparticles like Au and Ag, can enhance the energy of scattering photons or simply amplify the Raman signals due to the spikes present on their surface acting as "SERS hot-spots" and therefore can be used as SERS sensors to detect even extremely low concentrations of biomarkers for disease quantification and identification when appropriately targeted.[277] Raman reporters (dye molecules) were usually immobilized or embedded onto plasmonic nanoparticles to produce SERS nanotags which exhibit attractive properties like generating multiple sets of narrow peaks, low spectral overlap, negligible photobleaching, high

Table 5   Recent diagnostic applications of AuNPs conjugated with different biomarkers

Nanoparticle variant	Conjugation	Target biomarker	Detection technique	Detection limit (lower)	Additional findings	Reference
GCE modified ErGO-SWCNT/AuNPs	Thiolated anti-HER2 aptamer	HER2	Cyclic voltammetry (CV), differential pulse voltammetry (DPV) and electrochemical impedance spectroscopy (EIS)	50 fg mL⁻¹; analytical range (0.1 pg mL⁻¹–1 ng mL⁻¹)	—	258
Antibody tagged AuNPs (2018)	Anti-HER2 antibody	HER2	ELISA	0.01 ng mL⁻¹	—	259
BPE-tagged AuNPs	Anti-ERα antibody	ERα	Surface enhanced Raman spectroscopy (SERS)	—	Identification and distinguishing of MCF-7 (Erα/+) and SK-BR-3 (Erα/−) BC cells	212
Graphene oxide (GO)-AuNPs and Bi₂Se₃-AuNPs	BRCA1 nonsense mutated ssDNA	BRCA1	Colorimetric analysis	1 aM (GO-AuNPs); 1 pM (Bi₂Se₃-AuNPs)	—	260
DNA-functionalized AuNPs	cfDNA probe	BRCA1	Metal-enhanced fluorescence (MEF); colorimetric analysis	0.34 fM; linear range: 1 fM–100 pM	Activated CRISPR-Cas12a cleaves ssDNA but dsDNA cannot be cleaved	261
Thiolated DNA conjugated AuNP duplex	Thiolated DNA	BRCA1	Surface plasmon coupling electrochemiluminescence (SPC-ECL)	0.83 fM; linear range: 1 fM–1 nM	Au–Au dimers with a gap distance of 2 nm is superior in enhancing ECL signal of GCN QDs	262
Tetrahedral DNA framework (TDF)-modified AuNPs	cfDNA probe	BRCA1	CV and amperometry	1 aM; linear range: 1 aM–1 pM	Biosensor with TDF-26 showed unique and best response with selective stability	263
AuNPs/Thi/MSNP-NH₂	HPR-anti-CA 15-3 antibody	CA 15-3	DPV	0.001 U mL⁻¹; range: 0.002–125 U mL⁻¹	Quantification of MCF-7 cells; range: 10 000–50,000 cells per mL	264
Polypyrrole-luminol-AuNPs	Anti-CA153 antibody	Carbohydrate antigen 153	ECL	5.8 × 10⁻⁴ U mL⁻¹; linear range: 0.001–700 U mL⁻¹	Good film-forming property, quantifies CA-153 in serum plasma	265
AuNPs@Cu₇S₄@Cu/Mn-AzoPPOP	MUC1 aptamer	MUC1	CV and CA	0.72 fg mL⁻¹ (DPV) and 0.82 fg mL⁻¹ (CA); linear concentration range: 1 fg mL⁻¹–10 pg mL⁻¹	Quantifies MUC1 in serum plasma	266
Polyethylenimine coated-gold nanoparticles AuNPs	DNA probes	CA 15-3, MUC1 and HER2 antibody	Electrochemical redox analysis	0.21 U mL⁻¹ (CA 15-3), 0.53 ng mL⁻¹ (MUC1) and 0.50 ng mL⁻¹ (HER2); range: 0.10–100 U mL⁻¹ (CA 15-3) and 0.10–100 ng mL⁻¹ (MUC1 and HER2)	Detect three tumor markers in human serum also	267
GO-IL-AuNPs	Anti-CD44 antibody	CD-44	DPV, EIS	2 fg mL⁻¹ (DPV) and 1.90 fg mL⁻¹ (EIS); linear detection range: 5.0 fg ml⁻¹–50.0 µg mL⁻¹	—	268
Diphenylalanine-AuNPs	CD44BP	CD-44	EIS	2.17 pg mL⁻¹; linear range: 0.01 ng ml⁻¹–100 ng mL⁻¹	Limit of detection: 8 cells per mL for CD44-positive BC stem cells	269
PEGylated AuNPs	Cyclic 4-aminoproline-RGD semipeptides	Integrin $\alpha_v\beta_3$	Confocal laser microscopy	—	Potent inhibitors of integrin-mediated melanoma tumor cell and are selectively internalized via receptor-mediated endocytosis	270

Table 5 (Contd.)

Nanoparticle variant	Conjugation	Target biomarker	Detection technique	Detection limit (lower)	Additional findings	Reference
Raman reporter tagged AuNPs	ssDNA probe	miR-200c	SERS	—	The expression level of miR-200c in SK-BR-3 cells was 5 times greater than that in MCF-7	271
AuNPs/GQDs/GO	Thiol-modified miRNA probes	miR-21, miR-210, miR-155	Square wave voltammetry (SWV)	0.04 fM (miRNA-21), 0.33 fM (miRNA-155), and 0.28 fM (miRNA-210); linear dynamic range: 0.001 to 1000 pM	High selectivity and applicability for the detection of miRNAs in human serum samples	272
Hydroxyapatite nanorods (HApNRs) decorated with AuNPs	Thiolated AS1411 aptamer and 1-ethyl-3-methylimidazolium alanine	Nucleolin cell surface protein	DPV	8 ± 2 cells per mL	Highly sensitive and selective detection of surface nucleolin on MCF-7	273
Graphene oxide-chitosan-gold nanoparticles	AS1411 aptamer	Nucleolin cell surface protein	CV and EIS	Linear range: $1 \times 10^1 - 1 \times 10^6$ cells per mL	MCF-7 LDQ: 4 cells per mL	274
MoS$_2$-AuNPs modified carbon paper (CP)	DNA S1 probe and biotinylated DNA S3 probe	p53	CV and EIS	68 fM	Linear ranges: $10^{-15} - 10^{-12}$ M for wild type p53 in MCF-7 and $10^{-12} - 10^{-6}$ M for mutated p53 in SK-BR-3	275

sensitivity and multiplexing ability or low background noise *etc.* making the nanotags much more efficient than conventional fluorescence probes.[278]

The major disadvantage of using plasmonic nanoparticles in Raman nanotags arises when adsorption of Raman code onto the reporter causes colloidal instability of the nanoparticles. This problem was solved by using a self-assembled monolayer (SAM) of long chain thiolated polymers but the problem with SAMs is its constant desorption and degradation upon laser excitation.[279] Keeping the several stability issues, researchers nowadays are focused on applying different chemical approaches in making synthetic compounds which can be attached to plasmonic AuNPs with strong covalent bonds. Li *et al.* (2019) developed alkyne and nitrile based background free SERS reporters also acting as anchors for citrate capped AuNPs as well as for different antibodies. Radiation of the 633 nm laser on alkyne/nitrile SERS Au-nanoprobes significantly produced sharp Raman signals in the 2000–2230 cm^{-1} region against ER, PR and EGFR over-expressed human BC cells, thus acting as biosensors for multiplex detection and imaging.[280] Song *et al.* (2012) developed a suitable plasmonic vesicle using SERS active amphiphilic AuNPs and BGLA Raman reporter, which not only amplify the Raman signal given by SERS active AuNPs, but also induce Doxorubicin loading and its release inside cancer cells. The probing of cancer cells was tracked down using Raman spectroscopy as well as by plasmonic imaging.[232]

Using SERS spectra, Zhu *et al.* (2013) in their study, reported the interaction of AuNPs with intracellular components inside cancer cells. Raman spectroscopy combined with TEM study revealed the interaction of AuNPs with the phenylalanine present in MDA-MB-231 with a sharp peak at 1030 cm^{-1} could be useful in cancer cell SERS mapping.[281] Cellular components of MDA-MB-231 TNBC cells were also well observed using Raman spectroscopy due to amplified SERS signal by rhodamine 6G reporter tagged Au-aryl nanostars.[13] Rhodamine 6G-AuNP nanotags also exerted their effectiveness in distinguishing different BC cells by altering two-photon scattering intensity. In the MDA-MB-231 cell line, the scattering intensity changed 2.2 times while in the case of the SK-BR-3 cell line, the scattering intensity differed 13 times.[282] In a recent study, Gao *et al.* (2021) successfully attached 785 porous silicon photogenic crystals which acted as a SERS substrate to distinguish the blood serum in healthy people from the serum obtained from BC patients.[283] In spite of the various advantages driven by AuNPs as biosensors, its applicability is somehow limited to cancer cells close to the skin surface.[284]

4.3. Treatment of BC using AuNPs

Due to recent availability of advanced treatment facilities like gene expression profiling and endocrine therapy, the incidences of BC and its associated lymphedema have declined, with enhancement of survival rate. However, maintaining patients' cosmetic appearance and associated challenges still remained unsolved. Chemotherapy related adverse effects, lack of targets, metastasis of tumor cells or managing TNBC are some of the major problems that continuously invite questions about

effective treatment strategies in BC. In the nanotechnology guided era, AuNPs can provide answers to those issues as they are biologically inert or non-reactive and can offer suitable drug delivery *in vivo* compared to relatively toxic (cadmium) Cd or (silver) Ag-NPs.[285] Besides, controlled synthesis for maintaining appropriate size and surface chemistry, strong optical and electrical properties due to localized surface plasmon resonance (LSPR), multifunctional domain serving ability pushes AuNPs ahead of other NPs in the road to BC management.

Once AuNPs accumulate in tumor cells with the help of EPR effect or by active targeting, they can damage cell membranes or DNA when illuminated by a NIR laser. NIR light can be transmitted through tissue components with minimal absorption. When NIR radiation is applied, AuNPs accumulated in tumor cells generate heat *via* localized surface plasmon resonance (SPR) due to AuNPs' special optical effect of light absorption and scattering in the NIR region (650–900 nm). The heat generated in cancer cells successfully ablates the tumor cells without or with minimal effects in normal tissues, thus ensuring the limitation exerted by conventional chemotherapy *i.e.* death of cancer as well as normal cells.[286] Targeted therapy in BC and the thermal ablation method achieved by AuNPs ensure increased heat distribution throughout the cancer cells as well as the surrounding perivasculature area. External heating treatments often face inappropriate ablation as the blood flow by the adjacent capillaries cool down the perivasculature area acting as a 'heat sink' but when AuNPs accumulate in tumor cells as well as in the surrounding vasculature, not only do they cause heating of the tumor upon NIR irradiation, but they also destroy the surrounding capillaries. However, certain episodes of bleeding, skin burning or inflammation, and pain induction have been claimed as side effects when this application of AuNPs has been explored.[24]

4.3.1. Plasmonic photothermal therapy (PPTT) of AuNPs. Traditional heat treatment using microwaves, radio waves or ultrasound kills cancer cells effectively but the surrounding area also gets affected. Through SPR of AuNPs, nowadays, laser therapy enables accurate tumor cell ablation with little or no significant collateral damage to the nearby cellular environment. The mechanism by which AuNPs exert photothermal energy was well explained by Link and El-Sayed *et al.* (2000) using femtosecond transient absorption spectroscopy.[287] Metal nanostructures when photo-excited by light or laser irradiation with a frequency that overlaps with AuNPs SPR absorption band, generates heated electron gas which transfers to AuNP lattices very rapidly (within 1 ps). The overheated lattice then exchanges its heat to the local surroundings.[286] It was suggested that a lower excited laser power of 100 nJ can induce the temperature of hot electrons to 1000 K. This high energetic rapid heat transfer and exchange makes AuNPs a promising treatment strategy to fight against different cancers including BC.[287]

A study by Zharov *et al.* (2005) suggested effective laser (λ = 1064 nm) induced selective cell damage to TNBC cell line (MDA-MB-231). Antigens attached to 40 nm AuNPs self-assembled to form nanoclusters on the tumor cell membrane which destroyed cancer cells through laser induced bubble formation.[288] In a similar study with Au-nanoshells and SK-BR-3 BC cells, Loo *et al.* (2005) reported that Anti-HER2 immuno-targeted Au-silica nanoshells could be used effectively for the detection as well as treatment of BC cells when NIR laser beam of 800 nm was applied.[289]

Mohammed and his group in their research study prepared multi-walled carbon nanotube (MWCNT) conjugated AuNPs and tested for anti-cancer efficacy using laser irradiation on the MCF-7 cell line. They found that the thermal ablation and cytotoxicity effect of AuNP/CNT was boosted compared to simple MWCNT alone, establishing the PPTT efficacy of nano-gold.[290] In another study by Yang *et al.* (2015), the MUC1-aptamer conjugated AuNP based graphene-oxide (GO) nano-composite exhibited specific targeting efficacy and increased bioavailability along with remarkable photo-ablation capacity by controlled heat generation under laser irradiation. In the same study, the group also suggested that fabrication of heat shock protein (HSP-70) inhibitor to aptamer-AuNPs destroyed MCF-7 cells in a synergistic manner.[291] Another study involving anti-EGFR engineered AuNPs, irradiation with NIR laser not only significantly increased different autophagy associated protein and gene expression *i.e.* light chain-3 (LC3), beclin-1 and *Atg5*, but also inhibited Akt-mTOR pathway pointing out the photothermal efficacy of AuNPs in inducing autophagy related cell death in TNBC (MDA-MB-231) cell *in vitro*. The group also performed a gene expression study with MDA-MB-231 xenograft mouse models where they found that NIR laser induced AuNP mediated PPTT also increased LC3 and beclin-1 level *in vivo*.[292] Chen *et al.* (2020) performed a similar study with folic acid (FA)-functionalized gelatin based AuNPs for TNBC management *in vitro* and *in vivo*. The study results indicated a complete photothermal ablation of MDA-MB-231 cells with NIR laser irradiation but the damage to the tumor cells depended on the shape of the NPs, irradiation time and the laser intensity applied.[293] An interesting study with AuNRs by Ali *et al.* (2019) in canines and felines suggested that PPTT treatment before tumor removal effectively decreases the risk of metastasis and blood loss during surgery due to altered blood vessels in mammary tumors.[294] In a similar study with AuNRs previously, they had successfully ablated mammary tumors in BC xenograft cat and dog models without any signs of toxicity on liver, kidney and blood profiles after NIR laser irradiation suggesting the biocompatibility achieved using AuNR-PPTT treatment.[295]

Combination of chemotherapy and photothermal therapy is one of the finest treatment strategies involved in BC prevention. In one recent study by Faid *et al.* (2022), it was suggested that combination of chemotherapy and PTT of 6-marcaptopurine (6 MP) alone or loaded in highly stable chitosan AuNPs could be effective in damaging MCF-7 BC cells *in vitro* when DPPS laser beam was irradiated.[296] Thiol modified mannoside tagged AuNP was synthesized which offered targeted delivery to human TNBC cells due to the over-expressed mannose receptor on MDA-MB-231 and resulted in laser (λ = 808 nm) ablated cell death as well as metastasis reduction by Lin *et al.* (2020).[297] Another example of combination of chemo-photothermal therapy was given by Poursalehi *et al.* (2019). According to their research, terpolymer

modified smaller AuNPs (30 nm) along with Doxorubicin showed a synergistic effect by completely abolishing MCF-7 cells that underwent PTT.[298] Similar combination treatment was performed in MCF-7 cells, in which it was observed that chemo-photothermal therapy was shape dependent as Doxorubicin-loaded polymer coated Au-nanostars showed more efficacy in thermal ablation than Au-nanocages.[299] The shape dependency of NIR laser induced thermal treatment can be quite conflicting as upon intense laser illumination, AuNRs sometimes get converted to Au-nanoshells which possess different optical properties to AuNRs, thus altering BC management efficacy.[300]

One of the major disadvantages of PPTT using AuNPs in BC management is that for effective photothermal ablation, the size of NPs should be larger (~50 nm). Xia et al. (2018) developed a suitable method to solve the above problem associated with smaller particles by inter-conversion of modifying agents to another. They synthesized 2-5-diphenyl-tetrazole modified methacrylic group linked AuNPs of smaller (23 nm) diameter. A shorter wavelength laser ($\lambda = 405$ nm) irradiation effectively converted 2,5-diphenyltetrazole to nitrile-imine dipole which covalently cross-linked with methacrylic groups present on the surface of AuNPs which resulted in particle aggregates. The resultant aggregates exhibited enhanced photothermal efficacy against 4T1-murine BC upon 808 nm laser irradiation while the cross-linked exempted particles did not.[301] To enhance the efficacy of the smaller particles, different strategies like tuning the charge shared by the surface or utilizing an internal or external stimuli also can be performed.[302–304]

4.3.2. AuNPs as radiosensitizers. The high atomic number of gold ($Z = 79$) assists AuNPs to readily interact with keV energy radiation due to the enhanced 'Compton and photoelectric effect' which allows AuNPs to emit photo/auger electrons in targeted therapy resulting an increased radiotherapy (RT) efficacy along with increased therapeutic ratio. AuNPs as 'nano-enhancers' possess higher mass-energy absorption co-efficients than the soft tissues which cements their role as both internal and external radiosensitizers.[305] Several study reports confirm that due to the LSPR effect of AuNPs and its good distribution pattern in the target vicinity, treatment time as well as the radiation dose for RT can be shortened increasing therapeutic efficacy in RT for BC treatment.[306] The radiosensitizing property of AuNP is dependent not only on the physicochemical properties i.e. size, shape, charge, surface modification etc. but also on radiation source, radiation energy, dose, dosing schedule etc. Radiosensitizing properties of AuNPs can be greatly influenced by microbeam RT, superficial X-ray, and megavoltage electron beam RT.[18] Despite all the advantages, AuNP supported RT should ensure accurate and specific targeting because non-specific radiosensitization by AuNPs often cause fatal radiational damage.

The experimental studies both in vitro and in vivo investigations suggest the plausible mechanisms by which AuNPs act as radiosensitizers. Though mainly physical enhancement was found to be the primary attribute, researchers also found chemical and biological radiosensitization of AuNPs in different studies. The physical dose enhancement effect of AuNPs as a radiosensitizer mainly involves the 'Compton and photoelectric effect' of AuNPs, responsible for absorption co-efficient differences between AuNPs and soft tissues.[307] The Compton effect relies on the collision between incident photons and weakly bound outer electrons of Au atom, in which the energy transfers from photons to electrons cause them to be released from the Au atoms. In the photoelectric mechanism, incident photons are absorbed and energize the electrons present in the K, L or M shells of the Au atom to be released from Au. Once the shells are vacant, they are usually filled up by the outermost electrons which results in the lower energy fluorescence and secondary Auger electrons to be released. These lower energy electrons (LEE) play a critical role in radiosensitization.[307] An ^{111}In-radiolabeled EGF-coated AuNP with a diameter of 14 nm (^{111}In-EGF/AuNP) was developed by Song et al. (2016) and was tested for anti-cancer activity in TNBC (MDA-MB-231) and MCF-7 cell lines through RT. They suggested that the uptake of AuNPs solely depended on the EGF/Au molar ratio. A higher internalization of ^{111}In was observed for MDA-MB-231 cells than MCF-7. The clonogenic assay suggested dose enhancement by ^{111}In-EGF/AuNPs along with decreased survival fraction to MDA-MB-468 compared to non-labeled AuNPs.[308]

Chemical radio enhancement of AuNPs deals with catalysis of a radical reaction by surface activation of AuNPs. The low energy electrons with very little energy (<10 eV) generated after radiation energy is applied weakens H-bonding in DNA and makes DNA more vulnerable to radiation damage. The photoelectric effect of AuNPs also induces catalytic cascade where the energized surface electrons of AuNPs transfer to biological O_2, creating ROS (reactive oxygen species) or free radicals which in turn damage DNA, RNA, mitochondria and cell membranes of cancer cells.[309] According to some studies, small and positively charged AuNPs with a large surface area can lead to chemical enhancement through both DNA damage and radical cascade following superoxide or ROS production.[310]

While physical dose enhancement by lower (kV) energy is used to treat superficial tumors, biological radio-enhancing capability of AuNPs offers deep penetrating treatment with higher energy irradiation (MV).[311] Biological radio enhancing can be induced by ROS production, cell cycle arrest, inhibiting DNA repair or by inducing autophagy and (endoplasmic reticulum) ER stress[312] (Fig. 16). A study with dihydrorhodamine (DHR)-123 radiolabeled PEG-AuNPs by Choi et al. (2019) suggested not only a significant increase (7–14 fold in vitro and 3–6 fold in vivo than control) of ROS in MDA-MB-231 cells with a radiation dose of 6 Gy, but also induced fluorescence imaging of TNBC cells in vivo.[313] In another study, thioglucose tagged AuNPs of 49 nm in size induced more radiation than smaller particles along with radiative cell cycle arrest in the G_2/M phase in MDA-MB-231 cell line in vitro.[314] Various recent studies with a radiosensitizing effect of AuNPs in treatment of BC are tabulated in Table 6.

4.3.3. AuNPs as suitable drug delivery agents. The passive and targeted delivery of chemotherapeutic drugs with improved pharmacokinetics within the breast tumor microenvironment is quite an interesting approach that AuNPs can offer due to their
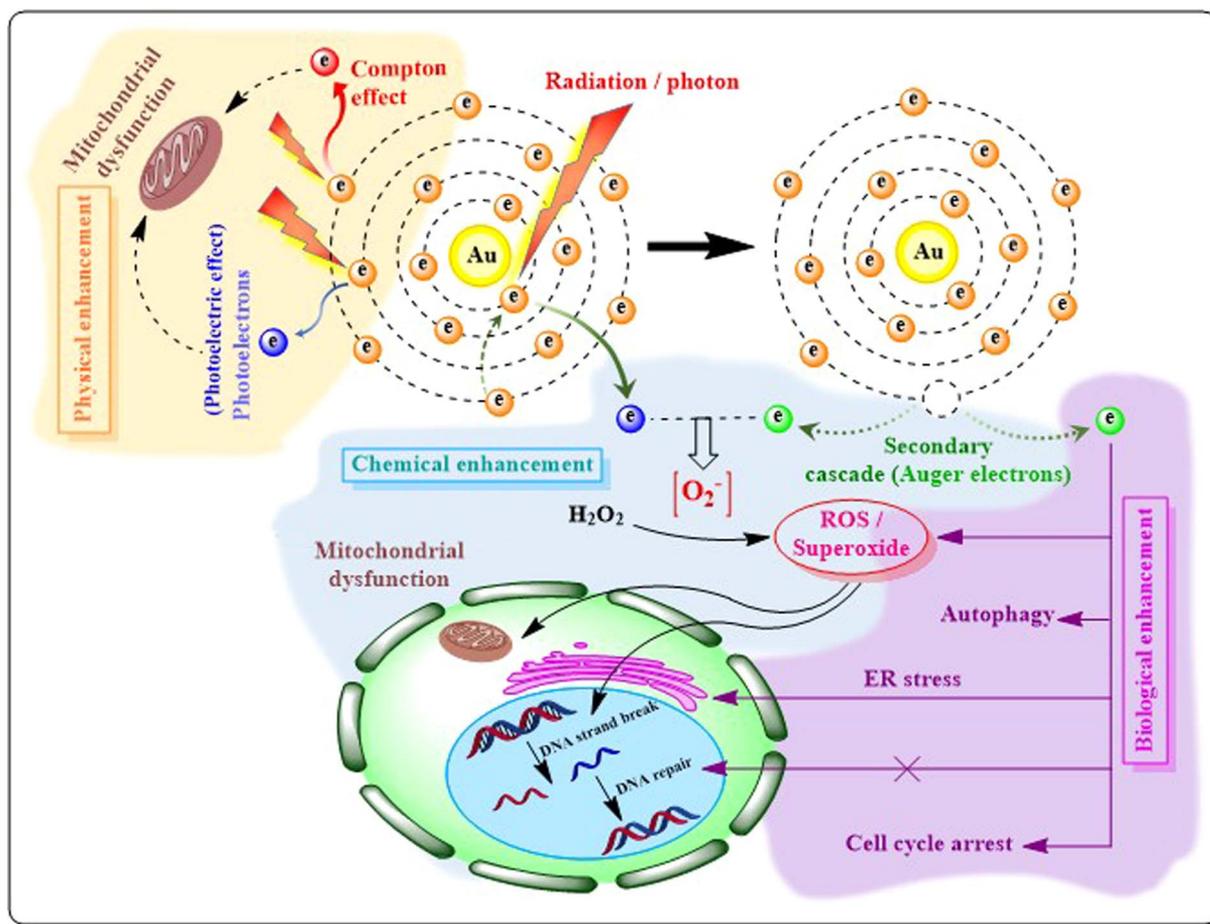
Fig. 16 AuNPs and radiosensitivity: mechanism. Physical method of radio enhancement occurs through the 'Compton effect' and 'photoelectric effect'. The reactive electrons released after radiation exposure led to mitochondrial dysfunction and cell damage. Radiation charging on Au atom also generates auger electrons *via* a secondary cascade mechanism which induces ROS production which subsequently contributes to mitochondrial dysfunction or DNA strand breaks forming the basis of chemical mechanism. The induced ROS levels by auger electrons also indulge in ER stress, autophagy, cell cycle arrest or blocking DNA strand repair thus developing biological mechanism for radio enhancement.

unique surface chemistry, high surface to volume ratio, increased bioavailability and biocompatibility. Different physico-chemical parameters *i.e.* size and shape of NPs, surface charge, drug–nanoparticle interaction, tumor specificity *etc.* influence the delivery and uptake of NP even after targeting is achieved.[10]

Suitable active drug targeting and delivery using AuNPs depend upon the attachment as well as the release of drugs in suitable sites. Covalent attachment, electrostatic attachment, hydrophilic–lipophilic interactions *etc.* offer suitable drug conjugation with AuNPs, whereas the release of the drugs can be achieved using SERS, photothermal release, pH sensitive release, light and radiation mediated release, glutathione mediated release *etc.* Controlled release of drugs from AuNPs can also be achieved by conjugating a time specific release linker between the AuNP surface and drugs.[325–327] Polymers such as poly(acrylic acid) (PAA) or poly(ethylene glycol) (PEG) can be used to coat AuNPs. At acidic pH, the protonation or deprotonation of acidic or basic functional groups within these polymers can trigger changes in their conformation or solubility,

resulting in the disruption of nanoparticle-drug interactions and subsequent drug release. Alternatively, acid/base labile pH-sensitive linkers can be incorporated into the nanoparticle–drug conjugate, where the linker undergoes cleavage or hydrolysis in response to changes in pH, releasing the drug payload. According to the study by Joshi *et al.* (2012), chloroquine loaded AuNPs when incubated with MCF-7 cells, the drug release occurred at the lower pH environment and exhibited concentration dependent cytotoxicity after being taken up by lysosome or endosome in BC cells. In a lower pH tumor microenvironment, approximately 26% of the drug was released after 2 h, which increased to 81% after 48 h, indicating a sustained drug release over time. These levels may be the result of the release of non-specifically bound drugs from the surface of the nanoparticles.[328] Cisplatin release mediated by an endosomal lower pH environment using dumbbell shaped Au–Fe$_3$O$_4$ magnetic nanoparticles in SK-BR-3 cells was reported by Xu and co-researchers.[329] Another example of drug release on SK-BR-3 cells with doxorubicin-loaded biohybrid AuNPs was achieved using SERS. Dox can be released from biohybrid nanoparticle surfaces

Table 6 Recent studies involving radiosensitizing of AuNPs in treatment of BC

Nanoparticle system	Particle size	Cell line/tumor models	Radiation energy	Outcomes	Reference
Citrate, glutathione and aminodextran reduced AuNPs	8.8–21.9 nm	In vitro: MDA-MB-231	6 MV; dose: 4 Gy	Biological radio enhancement observed with accumulation of cyclin B and cyclin D and over-expression of p53. S and G_2/M arrest after irradiation	315
Mercaptosuccinic acid (MSA) coated AuNPs	14 nm	In vitro: MDA-MB-232; in vivo: NCRNU f sp/sp athymic mice	160 kV; dose: 15 Gy	Size-dependent RT enhancement in vitro; RT induced immunogenic cell death (ICD), enhanced macrophage infiltration in vivo	316
Glutamine and folic acid functionalized BSA-AuNPs	12.2 ± 3.1 nm, 12.5 ± 3.5 nm	In vivo: 4T1 breast tumor-bearing female BALB/c mice	6 MV; dose: 6 Gy	Physical dose enhancement with increased cytotoxicity	204
AS1411 aptamer-conjugated AuNPs	10 ± 1.5 nm	In vitro: MCF-7, MDA-MB-231	4 MeV electron beams	Physical dose enhancement (DEF) 1.35 and 1.66 for MCf-7, MDA-MB-231	317
Doxorubicin-loaded chitosan capped AuNPs	18 nm	In vitro: MCF-7	6 MV; dose 0.5, 1, 3 Gy	Physical or chemical enhancement observed for combination of chemo-radiotherapy; necrosis occurred due to DNA DSB even at lowest dose (0.5 Gy)	318
Bleomycin loaded RDG modified AuNPs	10 nm	In vitro: MDA-MB-231	6 MV; dose: 2 Gy	Biological enhancement observed due to combination therapy as p53 binding protein found to cause DSB of DNA. DEF: 1.31	319
^{177}Lu-dendrimer conjugated folate and bombesin modified AuNP	Not mentioned	In vitro: T47D	Dose: 63.16 ± 4.20 Gy	^{177}Lu-DenAuNP-folate-bombesin is about 4 times more lethal than ^{177}Lu-DenAuNP; ^{177}Lu-DenAuNP is more lethal than ^{177}LuCl$_3$	320
DSPE PEGylated Au nanowares (AuNWs) and nanospheres (AuNSs)	AuNW: 3.6 nm (diameter) and 1.3 μm (length); AuNS: 14 nm	In vitro and in vivo: 4T1 and 4T1 xenograft BALB/c mice	5 Gy	Biological enhancement observed for increased hydroxyl radical and superoxide dismutase levels. AuNS showed better radiosensitized cell viability than AuNW	321
PEGylated curcumin modified AuNPs	73.8 ± 6.76 nm	In vitro and in vivo: 4T1 and 4T1 xenograft BALB/c mice	6 MV; dose: 4 Gy	Enhanced ROS generation via chemical radio-enhancement	322
Cisplatin loaded RDG AuNPs	10.04 ± 0.89 nm	In vitro: MDA-MB-231	6 MV; dose: 2 Gy	Biological radio-enhancement observed with DNA DSB and induced p53BP levels	323
MSA coated AuNPs	4 and 14 nm	In vitro: MCF-7	160 kV, 2.5 MV or 10 MV; dose: 4 Gy	Radiation induced inhibition of cell proliferation at 160 kV for 4 nm AuNPs and for 14 nm AuNPs at 2.5 or 10 MV. Biological dose enhancement suggested by DNA DSBs	324

Table 7 AuNPs as drug delivery agents in the treatment of BC

Anticancer drug	AuNP system	Study method	Drug release	Experimental outcomes	Reference
Doxorubicin (Dox)	DOX-conjugated levan-capped AuNPs	In vitro: MCF-7	pH responsive biphasic release. Initial burst release disrupting electrostatic and hydrogen bonding interaction between drugs and particles followed by sustained release disrupting levan-particle strong hydrophobic interaction	Dox-levan linked AuNPs showed better cytotoxicity due to specific targeting	336
	EpCAM Apt-peptosome conjugated AuNRs loaded with Dox	In vitro: MCF-7 and 4T1; in vivo: 4T1 xenograft BALB/c mice	pH responsive sustained, controlled release of DOX	EpCAM-Apt-Pep@AuNR-Dox showed higher cellular uptake with increased cytotoxicity against 4T1	337
Docetaxel (DTX)	Magnetic Au/Fe$_3$O$_4$/PVA-10%DTX nanocomposite	In vitro and in vivo: MCF-7 and xenograft mouse model	Release via NIR irradiation onto nanosystem through temperature sensitive PVA swelling after heating with green light	In vitro apoptosis 75% and in vivo apoptosis 70% achieved with minimal side effect	338
Epirubicin (EPI)	EPI-folic acid-AuNPs complex	In vitro: MCF-7	pH dependent controlled release	200% increased cytotoxicity observed for EPI-FA-AuNPs than free drug	339
Gemcitabine (GEM)	GEM loaded gum acacia (GA) influenced AuNPs	In vitro: MDA-MB-231	Acidic pH mediated drug release	GEM-GA-AuNPs displayed more cytotoxicity than free GEM	223
Letrozole (LTZ)	LTZ loaded GA-AuNPs	In vitro: MCF-7	Acidic pH mediated release without burst effect	Higher and dose dependent cytotoxicity than free LTZ was observed	340
Linalool (LIN)	LIN-AuNPs-modified with CALNN peptide	In vitro: MCF-7	Not reported	LIN-AuNPs-CALNN were remarkably more cytotoxic than LIN or AuNPs alone	341
Methotrexate (MTX)	Gelatin-coated and MTX loaded AuNPs and AuNRs	In vitro: MCF-7	pH mediated size and shape dependent drug release. Drug released more with small sized AuNR	AuNRs exhibited more drug release efficacy and cytotoxicity than AuNPs	342
	99mTc-MTX-AuNPs	In vitro: MCF-7	Acidic environment controlled biphasic drug release; initially from the core shell followed by release from the core	99mTc-MTX-AuNPs showed three times better anticancer activity (IC$_{50}$ = 0.098 mL/100 mL) than MTX alone (IC$_{50}$ = 0.3 mL/100 mL)	343
Paclitaxel (PTX)	PTX-loaded PEG-AuNPs@antiMUC1 system	In vitro: MCF-7 and MDA-MB-231	PTX was physically loaded into the PEG-AuNPs through the non-covalent interactions. Dual NIR/pH-dependent sustained release due to mitigation of electrostatic interaction by coulomb repulsion forces and OH group protonation of the drug and PEG-AuNPs	PTT and targeted drug delivery indicated a synergistic effect	184
Tamoxifen (TMX)	TMX loaded HAS-AuNPs	In vitro: BT-474 and MDA-MB-231	pH responsive biphasic release due to disruption of the disulfide bonds of albumin and the protonation of drug	Effective eradication of tumor cells achieved with targeted NPs	163

Table 7 (Contd.)

Anticancer drug	AuNP system	Study method	Drug release	Experimental outcomes	Reference
Curcumin (CUR)	CUR-loaded FA-functionalized Au-PVP NCs	*In vitro*: MDA-MB-231 and MCF-7; *in vivo*: 4T1 xenograft mice	pH responsive release *via* the protonation of drug	Inhibitory effects on cell migration and high antitumor efficacy	160
Berberine (BB)	BB loaded collagen (Col)-fabricated AuNPs	*In vitro*: HER-2 positive BC	Not defined	AuNPs-Col-BB significantly inhibited cell migration in HER-2 BC *via* inducing MMP-9 expression	344
5-Fluorouracil (5-FU)	5FU-complexed cyclodextrin conjugated AuNPs	*In vitro*: MDA-MB-231 and MCF-7	Not defined	5-FU/cyclodextrin/AuNPs showed enhanced EPR and increased proliferation inhibitory effect	345
Bleomycin (BLM)	BLM-RGD-AuNPs	*In vitro*: MDA-MB-231	pH mediated release	More internalization, higher DNA damage and less survival than free BLM	346
Cisplatin (CPT)	Hyaluronic acid decorated CPT loaded AuNPs	*In vitro*: MCF-7; *in vivo*: MCF-7 xenograft mice	pH dependent release associated with polymer coating disruption by chloride ion, and due to electrophilicity of platinum	Enhanced cytotoxicity with encapsulated cisplatin AuNPs was noticed in comparison to free drug *in vitro* and *in vivo*	347

by intracellular GSH. GSH is the most abundant thiol species in the cell cytoplasm, with a concentration range of 1–10 mM, and has been used as an *in situ* releasing reagent in living cells, owing to its biochemical reducing capability.[330] The thiol group in the GSH has strong affinity to AuNPs and can bind with the AuNPs through covalent coupling. For this reason, amine containing Dox can easily be replaced from AuNP surfaces.

When AuNPs are irradiated with light of a specific wavelength (usually in the near-infrared region), they absorb photons, leading to an increase in temperature at the NP surface. This localized heating triggers the release of the drug payload either by disrupting the surrounding matrix (*e.g.*, polymeric coating) or by inducing a phase transition in thermosensitive drug carriers. Light responsive molecules or photosensitive linkers can be designed to break or cleave in response to specific wavelengths of light, resulting in the release of the drug payload. Higher drug accumulation and increased cytotoxicity was observed when 785 nm NIR laser of 3 mW power was irradiated.[331] NIR laser mediated drug release by Au-nanoshells for the treatment of TNBC was also studied by You *et al.* (2012). NIR laser irradiation triggers local Doxorubicin release at the tumor site because of the photothermal conducting effect of hollow AuNS.[332] Another group explained the involvement of dual NIR/pH dependent sustained release of paclitaxel (PTX) from the PTX-loaded PEG-AuNPs@antiMUC1 system in treatment of BC. PTX was physically loaded into the PEG-AuNPs through the non-covalent interactions between the OH group of PTX and the oxygen of PEG. The authors suggested that at higher pH, the repulsive ionic interactions between the carboxyl groups caused prolonged encapsulation of the PTX onto the AuNPs surface, assisting drug ligands dispersion. However, in acidic pH (pH 5.4), because of Coulomb repulsion forces and protonation of OH group of PTX and PEG-AuNPs, electrostatic interaction was mitigated resulting in an increased PTX release.[223]

Drug loading onto AuNPs can offer a solution for by-passing several barriers *i.e.* the RES system, blood–brain barrier (BBB) and blood tumor barrier.[333] Doxorubicin-loaded TAT (*trans*-activating transcriptional activator)-modified AuNPs were reported to have BBB penetrating ability which was confirmed after accumulation of the drug in brain for the treatment of brain metastatic TNBC (MDA-MB-231/Br). Our study implemented an acid-labile hydrazine bond between Dox and the surface of the gold nanoparticle, which has been shown to cleave in response to an acidic environment such as that found in endosomal compartments (late stage endosome pH 5.5, lysosomes pH 4.8).[334] Development of multi-drug resistance (MDR) tumor cells has become a complex threat for drug development scientists for over a decade. The unique targeting capability of AuNPs ensures suitable drug release in the specific site of action enhancing the chemotherapeutic efficacy even against MDR. Wang *et al.* (2011) developed a nanosystem (Dox-hyd@AuNP) with Dox, PEG-coated AuNP and an acid-labile-linker. The acidic environment of MCF-7/MDR helps in cleaving the linker followed by release of Dox which ultimately resulted in increased cytotoxicity in MDR BC cells.[25]

Though several studies have been performed exploring the area of active drug targeting using different nanosystems, AuNP-based drug targeting to BC cells is relatively limited. Jiang *et al.* (2008) perfectly demonstrated how the size and antibody conjugation greatly affects the uptake and internalization of drug loaded AuNPs in the tumor site. Their group suggested that the smaller particles became dissociated from the cell membrane whereas trastuzumab loaded AuNPs of 40–50 nm diameter reduced the membrane wrapping, thus permitting the AuNPs to enter inside SK-BR-3 cells. They also suggested that the targeting approach is achieved in a larger extent for HER2-conjugated Trastuzumab/AuNPs than non-targeted drug loaded NPs alone with a 2-fold increase in chemotherapeutic efficacy for Trastuzumab, being released by the lowered pH of lysosomal compartments inside the cell.[335] In another study by Garcia Calavia *et al.* (2018), increased ROS production and apoptosis was observed with lactose-phthalocyanine-AuNPs after irradiation. The attached lactose in AuNPs helped in targeting MDA-MB-231 and SK-BR-3 cells and in binding with the galactose binding receptor (galactin-1) present in the surface of BC cells.[196] Similar studies exploring AuNPs as targeted therapeutics in BC management are tabulated in Table 7.

5. Clinically developed nano-gold products: the major challenge for clinical application

Global research impetus on cancer management has crossed many decades but a permanent curative solution still eludes healthcare management in spite of cutting-edge technological breakthroughs in both diagnosis and management of the disease. Curative success to date is limited mostly to the 3rd stage. Research on nano-medicine in cancer control is now the sought after approach because of possibilities of site-specific delivery and evasion of drug resistance. Plenty of nano-formulations are on the market for cancer treatment with a crowded pipeline of such candidates currently undergoing preclinical or clinical investigations. Some obvious hurdles exist in the translation of such products to clinical use like complexity in scaling up, stability issues, cost-effectiveness *etc.* However the Nanotechnology Characterisation Laboratory (NCL) is responsible for analysis of the pre-clinical trial data of various nano-formulations targeted for cancer therapy. The Nanotechnology Characterisation Laboratory (NCL) is a federally funded facility in United States, collectively established by the National Cancer Institute (NCI), the National Institute of Standards and Technology (NIST), the Food and Drug Administration (FDA), and the National Institutes of Health (NIH) in purview of the fast-growing interest in clinical translation of nanotherapeutics/nanodiagnostics/nanotheranostics. NCL supports physicochemical characterization, *in vitro* testing, and *in vivo* studies to assess the safety, efficacy, and pharmacokinetics of nano-scale agents targeted for clinical application. By offering standardized protocols, reference materials, and expertise in nanotechnology characterization, the NCL plays a crucial role in safe and effective translation of nanotechnology-based solutions for diverse clinical applications. To date the NCL has performed different standardisation

Table 8 Nano-gold products in clinical trial for cancer management

Sl. no.	Name of the gold nanoparticle	No. of participants	Stage	Clinical trial identifier	Application	Reference
1	Aurimune CYT-6091	60	Phase I completed (April 2009)	NCT00356980	Advanced solid tumors	333
	Aurimune CYT-6091 (PEGylated colloidal AuNP-bound rhTNFα)	108	Phase I completed (August 2009)	NCT00436410	Adrenocortical carcinoma breast, colorectal, gastrointestinal, kidney, liver, skin, ovarian, pancreatic cancer	
2	Auroshell (AuroLase™)	11	Interventional pilot study completed (August 2014)	NCT00848042	Recurrent tumour and cancers (head & neck)	355
	AuroShell particle infusion	45	Phase I (October 2020)	NCT02680535	Neoplasms of the prostate	356
3	NU-0129 (spherical nucleic acid-AuNPs)	8	Early phase 1 completed (August 19, 2020)	NCT03020017	Gliosarcoma and Recurrent glioblastoma	357
4	Organically functionalized AuNP and carbon nanotubes	1000	Observational completed	NCT01420588	Patients associated with malignant or benign gastric lesions	354
5	CD24-Au nanocomposite	60	Observational completed (February 3, 2021)	NCT04907422	Carcinoma ex pleomorphic adenoma of salivary glands	358
6	Nano swarna bhasma	6	Pilot study completed	DNA_SPN_B001_17 (AYUSH, India)	Breast cancer	352

Table 9 Impact of diverse parameters on AuNPs toxicity

Parameter	System and functionalization	Size	Cell line and animal used	Assay method (for in vitro)	Results obtained	Reference
Particle size	AuNPs without any surface modifiers	1–3 nm, 3–5 nm, 5–7 nm, 7–10 nm	In vitro: mouse melanoma (B16F10) and non-malignant human keratinocyte (HaCaT)	MTT, crystal violet assay, trypan blue exclusion assay	Smaller particles (1–3 nm) produce more toxicity	406
	Mono and tri-sulfonated triphenylphosphine functionalized AuNPs	0.8–15 nm	HeLa, SK-Mel-28, L929, J774A1	MTT assay	NPs with 1.4 nm size showed most toxicity; however, 15 nm AuNPs caused no toxicity	363
	Bare AuNPs	20 and 100 nm	In vitro: human retina microvascular endothelial cells (HRMECs), CTX-TNA2, human retinoblastoma cells, SNUOT-Rb1; in vivo: C57BL/6 mice; dose given iv	MTT assay for in vitro; TUNEL assay for in vivo	No toxicity observed in in vitro analysis. However, 20 nm AuNPs penetrates trough BRB (blood retinal barrier) in vivo	407
	Citrate capped AuNPs	13 ± 1.1 and 45 ± 3.2 nm	In vitro: human dermal fibroblasts (CF-31)	Apoptosis and colony formation assay	Larger particles were taken up in cell by clathrin mediated endocytosis and the smaller ones by phagocytosis	408
	Citrate stabilized AuNPs	10, 30, 60 nm	In vitro: HepG2 and HT-29; in vivo model: Wister rats	LDH assay, Comet assay	Smaller particles damaged DNA via induced ROS and oxidative stress; larger particles got accumulated in liver and spleen though no inflammatory cytokine levels altered in rats	236
Particle shape	Gold-silica nanoshells	Core 55 nm, shell 10 nm	In vitro: SK-BR-3 cells; in vivo: canine TVT cells inoculated female non-obese diabetic CB17-Prkd c SCID/J mice models	Fluorescent viability stain assay	No toxicity observed	409
Surface functionalization	Tea phytochemicals- and gum arabic-stabilized AuNPs	15–45 nm	In vitro: PC-3, MCF-7	MTT assay	Nontoxic	410
	AuNPs coated with PEG and betulin	10 nm, 50 nm	In vitro: HaCaT, 1BR3 cells	MTT assay	PEG coating diminished cytotoxicity in both the non-malignant cell lines	374
	AuNPs coated with citrate, starch, and gum arabic	20 ± 1 nm	In vitro: PC-3, MCF-7, CHO22 cells	MTT, neutral red cell, and LDH assay	Gum arabic-AuNPs most biocompatible and citrate-AuNPs showed toxicity w.r.t. dose and time of exposure	411
	AuNRs coated with CTAB, phosphatidylcholine (PC)	65 ± 5 nm × 11 ± 1 nm	In vitro: HeLa	MTT	Toxicity decreases remarkably for PC-AuNRs than CTAB-AuNRs	412
	Cumin-gum arabic-AuNPs	13 nm	In vitro: human fibroblast cells	MTT assay	No toxicity observed	376

Table 9 (*Contd.*)

Parameter	System and functionalization	Size	Assay method (for *in vitro*)	Cell line and animal used	Results obtained	Reference
Administered dose	Citrate AuNPs	12.5 nm	N/A	*In vivo*: male C57/BL6 mice; ip given	Dose-dependent tissue accumulation without any toxicity	360
Route of administration	Citrate AuNPs	13.5 nm	N/A	*In vivo*: male ICR mice	Oral and ip route causes more toxicity	403
Shape and surface chemistry	Spherical, rod-shaped, prismatic, and cubic AuNPs, citrate, tryptophan, tyrosine and CTAB coated NPs	Varying size	MTT assay	*In vitro*: human prostate cancer cells (PC3)	CTAB-stabilized spherical and prismatic AuNPs produced more toxicity where rod and cube shapes found to be bio-compatible. Uptake increased observed with amino acid coated NPs	391
Size and surface chemistry	BPEI-lipoic acid-PEG coated AuNPs forming biocorona with HSA	40 and 80 nm	AlamarBlue assay	*In vitro*: HUVEC	40 nm BPEI-AuNPs showed most uptake and toxicity. Biocorona formation led to non-toxic nature. HAS tagging increased uptake	413

activity both *in vitro* and *in vivo* for more than 170–180 such drugs.[348,349]

The exclusive optical, electrical and magnetic properties expressed by AuNPs are widely explored for clinical applications in different cancer variants (Table 8). Aurimune (CYT-6091) was the first developed product in this domain and was applied to solid tumour diagnosed patients (NCT00356980 and NCT00436410). CYT-6091, a recombinant human tumour necrosis factor alpha (TNF-α)-functionalized polymer (PEG) coated nano-gold with a size of 30 nm, is another such agent which modulated immune responses to treat cancer. The phase I clinical trial (NCT00356980) of this agent was among the earliest ones in this segment. The observed result revealed a tolerance dose range of 50–600 µg m^{-2} as well as the maximum tolerated dose of 600 µg m^{-2} with no acute side effects.[333]

Auroshell is a silica-gold nanoconjugation product of size ~150 nm which in under clinical trials using photothermal ablation technique in cancer therapy. Auroshell was applied in 22 patients of prostate cancer and provided excellent control with minimal adverse symptoms like itching and burning sensation in epigastrium.[350] Aurolase is the modification of Auroshell therapy which also adds the NIR laser approach for inducing thermal ablation of recurrent head and neck cancers.[351] Khoobchandani *et al.* (2020) in his research investigated a sustainable newer biosafe gold nano-formulation for breast cancer management from preclinical to clinical trials. This product was designed by conjugation of mangiferin with AuNPs with subsequent engineering with siRNA & thiolated PEG and was named "Nano-Swarna-Bhasma".[352] Another spherical nucleic acid-Au-nanoconjugate named NU-0129 (NCT03020017) has completed an early phase I study intended for the treatment of glioblastoma, with minimal toxicity.[353] Another example of AuNP under clinical evaluation is organically functionalized AuNPs and single-walled carbon nanotubes (NCT01420588) which is in observation I stage and targeted for patients with malignant or benign gastric lesions. The nanocomplex exclusively diagnose gastric cancer and distinguishes it from other gastric diseases.[354]

Despite continuous efforts, Au-nano based products' clinical status is limited to early phase I or phase I clinical stages. Compared to other nano-formulations *viz.* liposomes and polymeric nanoparticles, AuNP-based products or formulations or nanodevices failed to enter the late phase clinical stage and they have not been marketed. One of the major limitations contributing to the failure of Au-based nanoformulations include toxicity, which is discussed next at length. Despite using a targeted approach, AuNPs cause significant side-effects to non-malignant tissues due to several factors like size, shape, chemical functionalities, biodistribution alterations *etc.*[355] AuNPs can produce long-term toxicity as they are non-degradable entities. CYT-6091 and NU-0129, phase I cleared AuNP based products, pre-clinically suggested detectable amounts of gold in the liver and tumor cells even after 120 or 174 days of treatment.[359] The pilot study with AuroLase™ in primary or metastatic lung cancer was terminated in 2014.[355]

To develop encouraging and improved results of cancer management using AuNPs, a length of detailed understanding of NP-target interaction and the toxicity parameters are highly required. More pre-clinical studies are needed prior to starting any early stage clinical trials associated with Au-based nano-systems against cancer for successful clinical outcomes.

6. Toxicity issues of AuNPs

The major question in scientific minds while exploring the versatile applications of AuNPs is their toxicity and biosafety especially in the case of clinical applications. Interestingly, gold in bulk form exhibits inertness and biocompatibility most of the time. However, its behavior changes contrastingly when Au is in nano-dimensional form. Scientific reports related to its formulation development to date failed to provide a concrete idea regarding to what extent or at which concentration AuNPs exert toxicity or to what extent the toxicity arises when the effective concentration is applied. Repeated dose administration of AuNPs in animals revealed interesting facts with no prominent signs of toxicity. Firstly, even after increasing the dose, gold concentration in systemic circulation did not increase, although its presence in the different organs increased. Secondly, different studies reported there were no toxicity signs such as life-span, behavioral pattern, body-weight, organ morphology, blood parameters and tissue histo-architecture.[360]

Diverse parameters which influence the toxicity of AuNPs include: (i) dimension, (ii) morphology, (iii) chemical functionalization and coating agents defining their surface chemistry, (iv) type of assay used, (v) incubation conditions related to time of exposure and concentration used and (vi) their interaction with biological materials like proteins, fluids *etc*.[361] However, the complexity enhances when in assessment of toxicity of AuNPs because of the overlapping factors where multi-variants come to play with distinctive roles in contributing the biocompatibility assessments of AuNPs.

6.1. Size dependent AuNPs toxicity

The primary concern related to the toxicity of AuNP is the particle size and shape. Particle size as well as the stabilizing agents used in its synthesis significantly affects agglomeration as well as the sedimentation of AuNPs which in-turn hampers the passage of the AuNPs through the cell membrane. Generally, the smaller particles with a large surface area tend to bio-accumulate more, leading to enhanced toxicity manifestations.[362] Dependency of cytotoxicity on the size of AuNPs has yielded somewhat inconclusive results, as shown in the investigations by Pan *et al.* (2007). Their group synthesized tri-phenylphosphine stabilized AuNPs with particle size ranges from 0.8–15 nm, in which particularly AuNPs with 1.4 nm diameter showed toxicity to different cell lines.[363] These peculiarity in toxicity levels by distinct particles most likely occur due to the well-fitting of AuNPs of a particular size with the major DNA groove. Different *in vivo* studies in rats and mice by De Jong *et al.* (2008), Abdelhalim *et al.* (2013) and Sonavane *et al.*

(2008) confirmed that smaller particles tended to accumulate more in the organs like the liver, lung, spleen, kidney and heart as well as blood, indicating signs of toxicity.[364–366] Irrespective of increased cellular uptake with smaller AuNPs, matching toxicity with size may not produce definite conclusions. Studies by Connor *et al.* (2005) and Murphy *et al.* (2008) suggested that AuNPs 4, 12 or 18 nm in diameter synthesized with different coating agents exhibited no significant toxicity at all in K562 human leukemia cells though the particles were well taken up by the cells as observed in TEM.[367,368] AuNPs of size 3, 5, 50, and 100 nm administered to BALB/C mice i.p. at a dose of 8 mg per kg per week did not exhibit a toxic response however similar AuNPs with 8 to 37 nm diameter produced fatigue, loss of appetite, change of fur color and weight loss, subsequently causing mortality of the majority of the population after three weeks.[369]

6.2. Shape dependent AuNPs toxicity

Different geometries of AuNPs play a critical role in their toxicity presentations. Among the different shapes of AuNPs, some researchers suggest that Au-nanostars with their specific shape provide additional advantages *i.e.* large surface area and high drug load which ultimately reduce their quantity used and thereby reduce toxicity compared to other shapes.[361] However, AuNRs possess two different plasmon responses depending on the longer (longitudinal) and shorter (transverse) axis, hence possessing a different physicochemical property which complexes their cytotoxicity influence.[370] Wang *et al.* (2013) developed naked and PEGylated Au-nanocages, nanorods and nanohexapods and compared their toxicities in the MDA-MB-435 BC cell line. According to the study, AuNRs were found to be most toxic whereas, Au-nanohexapods showed the lowest toxicity in spite of being well taken up by the cells.[237] However, some studies clearly indicate that cellular uptake takes place more rapidly in spherical AuNPs than AuNRs. In this context, Li *et al.* (2015) suggested fastest internalization capability of Au-nanospheres followed by AuNRs, Au-nanocubes and Au-nanodisks.[371] The researcher also suggested that Au-nanostars can definitely compete with Au-nanospheres in case of internalization as they were observed to be readily taken up by the cell membrane. In an *in vivo* study with the murine EMT-6 breast cancer model, Black *et al.* (2014) also confirmed that radioactive [198]Au-doped nanospheres were better taken up by cancer cells than [198]AuNRs and [198]Au-nanocages of a similar size despite their good distribution pattern.[372] AN *in vivo* study using a zebrafish model also confirmed this fact to be related to Au-nanospheres.[373]

6.3. Surface functionalization and surface charge dependent AuNPs toxicity

Surface functionalization is one of the most important factors that governs different properties as well as toxicity of AuNPs. Different ligand functionalization or surface modification facilitates distribution as NP circulation in the bloodstream increases. PEG-coating on the surface of AuNPs not only defends particles against opsonization, but also develops a non-

toxic AuNP delivery platform against healthy cells. Mioc *et al.* (2018) observed no toxicity against HaCaT and IBR-3 non-malignant cells. The author also suggested botulin-modified PEG-coated AuNPs indeed exerted toxicity against human and murine melanoma (A375 and B164A5) cell lines.[374] However, Zhang *et al.* (2011) in their *in vivo* research study showed that the toxicity of PEG-coated AuNPs is somehow perplexing with respect to particle size. The toxicity exerted by 10 nm and 60 nm PEG-AuNPs was higher than that of the 5 nm and 30 nm particles.[375]

Gum arabic coated cumin derived AuNPs of 13 nm size when tested for a viability assay against human fibroblast cells turned out to be non-toxic also after 24 h at a dose of 150 μM.[376] Like PEG, surface modification with chitosan not only exerts excellent biocompatibility but also offers stability in the circulation period as well. The presence of sodium citrate residue in case of citrate capped AuNPs exposed to different cells generally induced toxicity as confirmed by different studies. However, according to Connor *et al.* (2005), AuNPs with varying sizes of 4–18 nm and varying functionalization *i.e.* citrate, glucose, biotin or cysteine or CTAB did not induce toxicity against the K562 leukemia cell line despite its higher internalization.[367] A similar result with no toxicity was observed with citrate modified AuNPs against human dermal fibroblast-fetal cells even at high concentration of 300 μM but they had an impact on their morphology.[377] On the other hand, conjugating phytochemicals with AuNPs has recently attracted the attention of researchers because of their ability to reduce the toxic impact of AuNPs.[378]

The net surface charge carried by NPs is another important aspect that modulates toxicity. NPs with a positive charge on their surface can bind to the negatively charged DNA, specifically targeting the minor and major grooves of DNA *via* electrostatic interaction causing DNA to bend around AuNPs which finally results in strand separation of the organized DNA structure.[379] Damage to the DNA was also observed when the hydrophobic ligands of NPs attached to DNA due to van der Waals interactions. As electrostatic attraction strongly induces cellular uptake, the NPs with a negative charge on the surface can be internalized within the cellular microenvironment specifically in the vacuoles.[380] Goodman *et al.* (2004) showed that the electrostatic interaction between the negative charges carried by cationic AuNPs was responsible for the lysis of the cell membrane which made them toxic as compared to the anionic AuNPs.[381] However, interestingly Schaeublin *et al.* (2011) suggested that both positively and negatively charged AuNPs were equally responsible for inducing oxidative stress *via* altering of mitochondrial membrane potential.[382]

6.4. AuNP interaction with biological proteins

While determining cytotoxicity *in vitro*, the commonly used culture medium bypasses the use of serum or when even used, the media contains a lower amount of serum. For that reason, the cellular viability does not represent the actual toxicity. In case of *in vivo* study, the toxicity represents quite different results as serum and different proteins influence aggregation of particles hampering particle concentration. Interaction between biological proteins and AuNPs alter the surface charge of NPs.

To decrease the high surface energy of NP, after entering the biological system, they adsorb biomolecules especially plasma proteins to form a protein shell called a "protein corona" (PC), which alters the original interfacial physicochemical properties of the NPs. In the circulatory environment, speedy protein corona formation occurs, influencing interactions with blood cells and potentially modulating their behavior *in vivo*[383] [6–10 of protein corona]. The interaction between AuNPs and proteins is driven by various forces including van der Waals forces, hydrophobic and electrostatic interaction, solvation forces, coordination, steric hindrance, and hydrogen bonding.[384] For instance, bovine serum albumin (BSA) interacts with AuNPs, *via* at least 12 strong Au–S bonds, where ubiquitin forms corona with citrate-coated Au NPs mainly *via* short-range hydrogen bonds.[385] Proteins with high abundance initially adsorb onto nanoparticles, but are eventually replaced by high-affinity proteins, forming NP-protein complexes. The protein corona can be categorized as hard, with tightly bound proteins, or soft, with proteins less tightly bound and dynamically exchanging with those in the surrounding media over time.[386]

Various factors, including NP size, hydro/lipophilicity, surface properties, and incubation time, influence the composition of the protein corona, subsequently impacting the biological behavior of the nanomaterials. M. Schäffler *et al.* (2013) used gel electrophoresis and a combination of matrix-assisted laser desorption/ionization and time-of-flight mass spectrometry for quantitative identification of mouse serum proteins adsorbed on 5, 15 and 80 nm phosphine stabilized AuNPs with negative surface charges and reported that smaller nanoparticles exhibit lower protein adsorption due to their higher curvature.[387] Reports by Cheng *et al.* (2015) also confirm that cellular uptake inhibition in phagocytic cells by PC is inversely proportional to the size of AuNPs.[388] Surface modification with hydrophilic PEGs can resist complement protein adsorption, prolonging nanoparticle circulation time by evading uptake by the reticuloendothelial system (RES).[387] Serum proteins interact with the particle surface and facilitate uptake *via* clathrin-mediated endocytosis, which is suggested to be linked to hydrophobicity or dispersibility of AuNPs.[361] These findings underscore the importance of understanding protein corona dynamics in nanoparticle interactions with biological systems for optimizing their biomedical applications.

The interaction between gold nanoparticles (Au NPs) and proteins induces structural changes in both the nanoparticles and the adsorbed proteins, with the protein corona dynamically evolving over time due to continuous adsorption, desorption, and exchange influenced by various factors including protein concentration, surface chemistry of GNPs, and environmental conditions. Understanding how nanoparticle properties affect protein corona composition is crucial, and analytical techniques such as TEM, DLS, UV-Vis-NR spectra, CD spectra, QCM, and NMR, as well as conventional methods like chromatography and electrophoresis are essential for studying NP–protein interactions and characterizing the NP-protein complex. Advanced techniques like synchrotron radiation X-ray near edge

absorption spectroscopy (XANES) provide insights into the bound interface structure of proteins.[389]

The formation of a protein corona can significantly alter the physical characteristics of AuNPs, including size, charge, and morphology and subsequently their bioactivities. Lai *et al.* (2017) demonstrated how proteins from human plasma induce negative surface charge to overall corona formed over 20 nm AuNPs. Around 300 proteins were identified on the coronas, while 99 are commonly found on each Ag and Au-nano-material.[390] A biocorona can render them effectively invisible to the immune system, potentially masking the functionality of functionalized AuNPs. Although many reports convey that PC enhances the nanoparticle cellular localization. Carnovale *et al.* (2019) reported that serum-pre-incubation of AuNPs assisted in minimization of cellular uptake and subsequent toxicity. The same study reported that tyrosine capped AuNPs exhibited different cellular viabilities in diverse media conditions like serum-free (52.2%), serum-pre-incubated (79.9%) and serum-supplemented (106.1%).[391] Moreover, the composition of the biocorona can change over time due to its dynamic nature, making it challenging to predict the behavior of NPs after exposure to a particular host environment.[392] For example, interactions between fibrinogens and poly(acrylic acid)-coated AuNPs can induce protein unfolding, exposing its cryptic peptide which specifically interact with the Mac-1 receptor, leading to inflammation and cytokine release mediated by the NF-κB pathway.[393]

The attachment of opsonins like immunoglobulins and complements, can lead to rapid immune recognition and removal of the corona from the blood by macrophages, eventually leading to loss of its therapeutic effects.[384] Studies suggested rapid AuNP agglomeration and associated toxicities due to an increased hydrodynamic size of formed biocorona complexes.[394] The dynamic interaction of different proteins with the NPs can cover or eliminate the targeting moieties on NP surfaces, and effectively mitigate the recognition of the targeting ligands or functional groups by different targets *in vivo*.[395,396] Also, changes in the protein secondary structure can reveal hydrophobic regions and new epitopes, affecting its native function, including protein fibrillation and enzymatic activity. These alterations are closely linked to potential biological toxicity.[397] Zhifang Ma and his research group reported that the cytotoxicity exposed by AuNP–PC complex depends upon the degradation of PC degradation process. They suggested that HSA corona degrades faster than γ-globulin (HGG), and serum fibrinogen (HSF) corona and AuNP–HSA PC complex exhibit highest cytotoxicity by elevating ROS level, slowing down ATP production and lowering MMP.[398] The research group of Yang *et al.* (2019) showed how conformational transition of HSA from partial β-sheet to α-helix upon AuNP–HSA PC formation led to increased thermal stability of the corona and increased cytotoxic nature of NP–PC complex *via* inducing apoptosis.[399]

However, tuning protein corona to possess beneficial applications like increasing residence time and reduced accumulation in the liver and spleen, ensuring drug delivery targeting also holds considerable appeal. It is widely recognized that AuNPs with an albumin-enriched surface exhibit a strong affinity for tumors because of the transcytosis mediated by albumin, suggesting significant promise for cancer-targeted therapy along with long–circulation properties, better biocompatibility and rapid clearance bypassing efficacy.[400] The detailed impact of protein corona is well reviewed by Liu *et al.*[384] and Wang *et al.*[389]

6.5. Variation in cell line and assay technique

Differences in toxicity with respect to use of different cell lines can be well observed in the study of Patra *et al.* (2007). Citrate capped AuNPs with 13 nm diameter exhibited remarkable anti-proliferative activity in human lung carcinoma cell line A549 while the toxicity vanished when the same dose was applied against the HepG2 human hepatocarcinoma cell line.[401] One of our previous studies with luteolin tagged AuNPs goes in line with the difference in toxicity with respect to variable cell lines as the non-targeted nanosystem produced toxicity against TNBC cells while remained biocompatible with fibroblast cells (NIH-3T3).[26]

While determining cytotoxicity, choosing an appropriate assay method is one of the major tasks to be carried out. There are different assays *i.e.* 3-(4, 5-dimethylthiazolyl-2)-2, 5-diphe-nyltetrazolium bromide (MTT) assay, lactate dehydrogenase (LDH) leakage test, calcein AM assay, colony forming (CFE) assay, 2-(4-iodophenyl)-3-(4-nitrophenyl)-5-(2,4-disulfophenyl)-2*H*-tetrazolium (WST-1) assay, tryptan blue assay *etc.* which are used routinely for cytotoxicity assessments. The conflicting result of toxicity of AuNPs also arises with varying assay methods used in experimental study. An example of the toxicity dependency on the assay method was reported by Coradeghini *et al.* (2013). The group showed that 5 nm AuNPs exerted toxicity after 72 h of treatment at a dose above 50 μM against Balb/3T3 mouse fibroblast cell line when determined through CFE assay while no toxicity was observed applying same sized AuNP, same dose and same cell line in case of cytotoxicity evaluation using tryptan blue assay. Even if the dose was escalated to a higher dose (300 μM) no toxic influence was observed.[402]

Besides the above discussed parameters, nanoparticle dose and concentration as well as administration route greatly affects the toxicity in a definite cell line.[403] While evaluating toxicity relationship, it is better to consider not only LD_{50}, but also ED_{50}. NP concentration in the cells can be measured using two different but related concentration parameters *i.e.* numerical concentration and mass concentration which are expressed as below: $\text{numerical conc.} = \dfrac{6M\text{Mw}}{\pi \rho r^3 10^3}$ and $\text{mass conc.} = \dfrac{M\text{Mw}}{10^3}$ [where M = gold molar conc., Mw = Molar mass in g mol^{-1}, r = radius of NP, ρ = density in g mol^{-1}].[404] Also, the clearance of the nanoparticles after completion of therapeutic action is also a parameter which can raise a question in defining toxicity states. According to Huang *et al.* (2008) the size may contribute to the clearance as they observed the persistence of >10 nm AuNPs in mice up to 6 months although no significant toxicity was observed.[405]

Thus, we can well understand that determining toxicity of AuNPs is a complex task to perform as lots of factors govern the toxic impact of the particle. And it is also highly required to

design a suitable pathway or formula by which the toxicity of NPs can be addressed accurately. In Table 9, we generalize some of the studies with different toxicities of AuNPs as well as their governing attributes.

Development of surface defects during nanomaterial development like constitutional arrangement, disarray, grain margins, and diverse surface topography would modulate its interactions with cellular environment thus influencing toxicity signs.[361] The impact of such deformities in formation and subsequently their effect on toxicity in case of AuNPs could be an area of interest for future investigations.

Conclusions

Gold mediated nanotechnological interventions have revolutionized cancer management by facilitating transport of drug cargo along with particle engineering mediated pin-point selectivity and magnified uptake in cancerous cells. The role of AuNPs has undergone a paradigm shift in the last decade making them the go-to candidate not only for therapy and diagnosis but also as a multifunctional device with theranostic attributes. Breast cancer management often involve single chemotherapeutics or their combination and, in both cases, AuNPs serve as an efficient carrier. The unique properties of gold at the nanoscale, the influence of particle engineering and ease of metamorphosis of AuNPs into potent multifunctional structures, as well as their inertness, biocompatibility, chemical and thermal stability, and resistance to oxidation or corrosion support their superiority over other nanoparticles and have propelled their journey from laboratories to the market. Moreover, the entry of AuNPs into newer avenues like PTT and PDT therapy or their use as contrast agents in X-ray, CT and multi-modal imaging has further prompted clinicians to explore nanodimensional gold in cancer management. As stated in the review, AuNPs in clinical practice has now become a reality. In addition to this fact, a huge pipeline of nano-scale gold products are currently undergoing Phase I, Phase II or Phase III trials and may soon reach the market. This review focuses on unravelling the various synthesis routes and tailoring of gold nanoparticles for their targeted use in breast cancer management.

Immense scientific variations in synthesis procedures of AuNPs have occurred from the route initiated by Frens or Turkevich, which have significantly favoured their pharmacodynamics but the toxicity aspects of nano-scale gold are a major concern in their translation to clinics. Even toxicity assessments of engineered or multifunctional AuNPs pose a complex challenge to nano-toxicologists. However, biocompatibility issues, scale-up obstacles and the development of proper regulatory framework to cater these nano-dimensional products still require brainstorming ideas from all connected scientific professionals to strengthen AuNPs' clinical presence.

Gold nanoparticles enable the combination of chemotherapy, photothermal therapy, and radiotherapy, enhancing efficacy while minimizing side effects. Gold nanoparticles' unique properties circumvent drug resistance mechanisms, prolonging therapy effectiveness. AuNP-based immunotherapies leverage the immune system, improving patient outcomes and long-term survival rates. Selectively heating and destroying cancer cells with laser-activated AuNPs allows precise tumor removal, reducing damage to healthy tissue and improving patient recovery. Future research may focus on optimizing targeting strategies and investigating novel ligands for improved specificity. Additionally, exploring synergies between gold nanoparticles and conventional cancer therapies could enhance efficacy while minimizing side effects. Investigating AuNPs' potential to overcome drug resistance mechanisms may lead to more effective combination therapies. Developing multifunctional AuNPs capable of imaging cancer cells while delivering therapeutic payloads is a promising avenue. Elucidating the mechanisms underlying the immunomodulatory effects of AuNPs and integrating AuNPs with emerging technologies for cancer screening are areas of interest. Last but not least, optimizing the physicochemical properties of AuNPs to enhance biocompatibility and safety, along with long-term studies assessing systemic effects, are crucial for clinical translation.

Conflicts of interest

The authors declare no relevant financial or non-financial conflict of interests.

Acknowledgements

References

1 H. Sung, J. Ferlay, R. L. Siegel, M. Laversanne, I. Soerjomataram, A. Jemal and F. Bray, *Ca-Cancer J. Clin.*, 2021, **71**, 209–249.

2 G. N. Sharma, R. Dave, J. Sanadya, P. Sharma and K. Sharma, *J. Adv. Pharm. Technol. Res.*, 2010, **1**, 109.

3 M. Mahapatra, P. Mohapatra, K. Pakeeraiah, R. K. Bandaru, I. Ahmad, S. Mal, R. Dandela, S. K. Sahoo, H. Patel and S. K. Paidesetty, *Int. J. Biol. Macromol.*, 2023, **249**, 126084.

4 K. W. Powers, M. Palazuelos, B. M. Moudgil and S. M. Roberts, *Nanotoxicology*, 2007, **1**, 42–51.

5 M. E. Davis, Z. Chen and D. M. Shin, *Nat. Rev. Drug Discovery*, 2008, 7, 771–782.

6 K. Pakeeraiah, S. Mal, M. Mahapatra, S. K. Mekap, P. K. Sahu and S. K. Paidesetty, *Int. J. Biol. Macromol.*, 2023, 128402.

7 B. Mekuye and B. Abera, *Nano Sel.*, 2023, 486–501.

8 G. D. Nash, *Calif. Hist.*, 1998, **77**, 276–292.

9 M. Zaimy, N. Saffarzadeh, A. Mohammadi, H. Pourghadamyari, P. Izadi, A. Sarli, L. Moghaddam, S. Paschepari, H. Azizi and S. Torkamandi, *Cancer Gene Ther.*, 2017, **24**, 233–243.

10 M. Yafout, A. Ousaid, Y. Khayati and I. S. El Otmani, *Sci. Afr.*, 2021, **11**, e00685.

11 Á. I. López-Lorente, *Anal. Chim. Acta*, 2021, **1168**, 338474.

12 W. Yang, H. Liang, S. Ma, D. Wang and J. Huang, *Sustainable Mater. Technol.*, 2019, **22**, e00109.

13 M. K. Hameed, J. B. Parambath, M. T. Gul, A. A. Khan, Y. Park, C. Han and A. A. Mohamed, *Appl. Surf. Sci.*, 2022, **583**, 152504.

14 M. Fan, Y. Han, S. Gao, H. Yan, L. Cao, Z. Li, X.-J. Liang and J. Zhang, *Theranostics*, 2020, **10**, 4944.

15 L. Rotimi, M. O. Ojemaye, O. O. Okoh, A. Sadimenko and A. I. Okoh, *Green Chem. Lett. Rev.*, 2019, **12**, 61–68.

16 J. S. Chen, J. Chen, S. Bhattacharjee, Z. Cao, H. Wang, S. D. Swanson, H. Zong, J. R. Baker and S. H. Wang, *J. Nanobiotechnol.*, 2020, **18**, 1–9.

17 K. Shrivas, N. Nirmalkar, S. S. Thakur, R. Kurrey, D. Sinha and R. Shankar, *RSC Adv.*, 2018, **8**, 24328–24337.

18 W. N. Rahman, N. Bishara, T. Ackerly, C. F. He, P. Jackson, C. Wong, R. Davidson and M. Geso, in *Nanomedicine in Cancer*, Jenny Stanford Publishing, 2017, pp. 737–752.

19 S. Chakraborty, S. Mal, A. Halder, S. Das, K. K. Sen, A. Mukherjee and P. Roy, *Part. Sci. Technol.*, 2024, **42**, 145–163.

20 N. Sarfraz and I. Khan, *Chem.–Asian J.*, 2021, **16**, 720–742.

21 V. Ramalingam, *Adv. Colloid Interface Sci.*, 2019, **271**, 101989.

22 S. Murthy, P. Effiong and C. C. Fei, in *Metal Oxide Powder Technologies*, Elsevier, 2020, pp. 233–251.

23 N. R. S. Sibuyi, K. L. Moabelo, A. O. Fadaka, S. Meyer, M. O. Onani, A. M. Madiehe and M. Meyer, *Nanoscale Res. Lett.*, 2021, **16**, 1–27.

24 J. Lee, D. K. Chatterjee, M. H. Lee and S. Krishnan, *Cancer Lett.*, 2014, **347**, 46–53.

25 F. Wang, Y.-C. Wang, S. Dou, M.-H. Xiong, T.-M. Sun and J. Wang, *ACS Nano*, 2011, **5**, 3679–3692.

26 S. Mal, T. Saha, A. Halder, S. K. Paidesetty, S. Das, W. T. Wui, U. Chatterji and P. Roy, *J. Drug Delivery Sci. Technol.*, 2023, **80**, 104148.

27 V. Patsula, L. Kosinová, M. Lovrić, L. Ferhatovic Hamzić, M. Rabyk, R. Konefal, A. Paruzel, M. Šlouf, V. Herynek and S. k. Gajović, *ACS Appl. Mater. Interfaces*, 2016, **8**, 7238–7247.

28 S. Wirunchit, P. Gansa and W. Koetniyom, *Mater. Today: Proc.*, 2021, **47**, 3554–3559.

29 N. Z. A. Naharuddin, A. R. Sadrolhosseini, M. H. A. Bakar, N. Tamchek and M. A. Mahdi, *Opt. Mater. Express*, 2020, **10**, 323–331.

30 M. Pišlová, K. Kolářová, B. Vokatá, A. Brož, P. Ulbrich, L. Bačáková, Z. Kolská and V. Švorčík, *Mater. Sci. Eng. C*, 2020, **115**, 111087.

31 M. Annadhasan, J. Kasthuri and N. Rajendiran, *ChemistrySelect*, 2019, **4**, 6557–6567.

32 M. Gautam, J. O. Kim and C. S. Yong, *J. Pharm. Invest.*, 2021, **51**, 361–375.

33 S. Manivannan and R. Ramaraj, *Chem. Eng. J.*, 2012, **210**, 195–202.

34 Y. He, E. Du, X. Zhou, J. Zhou, Y. He, Y. Ye, J. Wang, B. Tang and X. Wang, *Spectrochim. Acta, Part A*, 2020, **230**, 118031.

35 R. G. Palgrave and I. P. Parkin, *J. Am. Chem. Soc.*, 2006, **128**, 1587–1597.

36 K. X. Lee, K. Shameli, Y. P. Yew, S.-Y. Teow, H. Jahangirian, R. Rafiee-Moghaddam and T. J. Webster, *Int. J. Nanomed.*, 2020, 275–300.

37 A. Rónavári, N. Igaz, D. I. Adamecz, B. Szerencsés, C. Molnar, Z. Kónya, I. Pfeiffer and M. Kiricsi, *Molecules*, 2021, **26**, 844.

38 J. Turkevich, P. C. Stevenson and J. Hillier, *Discuss. Faraday Soc.*, 1951, **11**, 55–75.

39 W. Patungwasa and J. H. Hodak, *Mater. Chem. Phys.*, 2008, **108**, 45–54.

40 G. Frens, *Nature Phys. Sci.*, 1973, **241**, 20–22.

41 K. Zabetakis, W. E. Ghann, S. Kumar and M.-C. Daniel, *Gold Bull.*, 2012, **45**, 203–211.

42 J. Dong, P. Carpinone, G. Pyrgiotakis, P. Demokritou and B. Moudgil, *KONA Powder Part. J.*, 2020, **37**, 2020011.

43 L. M. Liz-Marzán, *Chem. Commun.*, 2013, **49**, 16–18.

44 C. A. Waters, A. J. Mills, K. A. Johnson and D. J. Schiffrin, *Chem. Commun.*, 2003, 540–541.

45 M. Brust, M. Walker, D. Bethell, D. J. Schiffrin and R. Whyman, *J. Chem. Soc. Chem. Commun.*, 1994, 801–802.

46 M. T. Reetz and W. Helbig, *J. Am. Chem. Soc.*, 1994, **116**, 7401–7402.

47 C.-J. Huang, P.-H. Chiu, Y.-H. Wang, K.-L. Chen, J.-J. Linn and C.-F. Yang, *J. Electrochem. Soc.*, 2006, **153**, D193.

48 Z.-C. Xu, C.-M. Shen, C.-W. Xiao, T.-Z. Yang, H.-R. Zhang, J.-Q. Li, H.-L. Li and H.-J. Gao, *Nanotechnology*, 2007, **18**, 115608.

49 N. Li, P. Zhao and D. Astruc, *Angew. Chem., Int. Ed.*, 2014, **53**, 1756–1789.

50 C. Kohout, C. Santi and L. Polito, *Int. J. Mol. Sci.*, 2018, **19**, 3385.

51 B. Prasad, S. I. Stoeva, C. M. Sorensen and K. J. Klabunde, *Chem. Mater.*, 2003, **15**, 935–942.

52 S. J. Amina and B. Guo, *Int. J. Nanomed.*, 2020, 9823–9857.

53 M. S. Punnoose, D. Bijimol and B. Mathew, *Environ. Nanotechnol., Monit. Manage.*, 2021, **16**, 100525.

54 J. Choi, S. Park, Z. Stojanović, H.-S. Han, J. Lee, H. K. Seok, D. Uskoković and K. H. Lee, *Langmuir*, 2013, **29**, 15698–15703.

55 M. J. Firdhouse and P. Lalitha, *Inorg. Chem. Commun.*, 2022, 109800.

56 U. Shedbalkar, R. Singh, S. Wadhwani, S. Gaidhani and B. Chopade, *Adv. Colloid Interface Sci.*, 2014, **209**, 40–48.

57 A. Ahmad, S. Senapati, M. I. Khan, R. Kumar, R. Ramani, V. Srinivas and M. Sastry, *Nanotechnology*, 2003, **14**, 824.

58 S. Mukherjee and C. R. Patra, *Future Sci. OA*, 2017, **3**, FSO203.

59 D. Lahiri, M. Nag, H. I. Sheikh, T. Sarkar, H. A. Edinur, S. Pati and R. R. Ray, *Front. Microbiol.*, 2021, **12**, 636588.

60 C. Kamaraj, S. Karthi, A. D. Reegan, G. Balasubramani, G. Ramkumar, K. Kalaivani, A. A. Zahir, P. Deepak, S. Senthil-Nathan and M. M. Rahman, *Environ. Res.*, 2022, **213**, 113711.

61 S. Pandey, G. Oza, A. Gupta, R. Shah and M. Sharon, *Eur. J. Exp. Biol.*, 2012, **2**, 475–483.

62 M. Ovais, A. T. Khalil, M. Ayaz, I. Ahmad, S. K. Nethi and S. Mukherjee, *Int. J. Mol. Sci.*, 2018, **19**, 4100.

63 R. Sanghi, P. Verma and S. Puri, *Adv. Chem. Eng. Sci.*, 2011, **1**, 154.

64 J. T. Nandhini, D. Ezhilarasan and S. Rajeshkumar, *Environ. Toxicol.*, 2021, **36**, 24–32.

65 R. Shunmugam, S. R. Balusamy, V. Kumar, S. Menon, T. Lakshmi and H. Perumalsamy, *J. King Saud Univ., Sci.*, 2021, **33**, 101260.

66 T. Cherian, D. Maity, R. T. Rajendra Kumar, G. Balasubramani, C. Ragavendran, S. Yalla, R. Mohanraju and W. J. Peijnenburg, *Nanomaterials*, 2022, **12**, 2940.

67 N. Y. Nadaf and S. S. Kanase, *Arabian J. Chem.*, 2019, **12**, 4806–4814.

68 F. Kabiri, S. S. Aghaei, A. A. Pourbabaee, M. Soleimani and T. Komeili Movahhed, *Prep. Biochem. Biotechnol.*, 2023, **53**, 265–278.

69 N. Naimi-Shamel, P. Pourali and S. Dolatabadi, *J. Mycol. Med.*, 2019, **29**, 7–13.

70 M. A. Dheyab, M. N. Owaid, M. A. Rabeea, A. A. Aziz and M. S. Jameel, *Environ. Nanotechnol., Monit. Manage.*, 2020, **14**, 100312.

71 P. Clarance, B. Luvankar, J. Sales, A. Khusro, P. Agastian, J.-C. Tack, M. M. Al Khulaifi, H. A. Al-Shwaiman, A. M. Elgorban and A. Syed, *Saudi J. Biol. Sci.*, 2020, **27**, 706–712.

72 S. Krishnan, P. N. Patel, K. K. Balasubramanian and A. Chadha, *New J. Chem.*, 2021, **45**, 1915–1923.

73 B. Babu, S. Palanisamy, M. Vinosha, R. Anjali, P. Kumar, B. Pandi, M. Tabarsa, S. You and N. M. Prabhu, *Bioprocess Biosyst. Eng.*, 2020, **43**, 2231–2242.

74 M. Vinosha, S. Palanisamy, R. Muthukrishnan, S. Selvam, E. Kannapiran, S. You and N. M. Prabhu, *Process Biochem.*, 2019, **85**, 219–229.

75 N. González-Ballesteros, L. Diego-González, M. Lastra-Valdor, M. Grimaldi, A. Cavazza, F. Bigi, M. C. Rodríguez-Argüelles and R. Simón-Vázquez, *Mar. Drugs*, 2022, **20**, 182.

76 E. Castro-Longoria, A. R. Vilchis-Nestor and M. Avalos-Borja, *Colloids Surf., B*, 2011, **83**, 42–48.

77 K. K. Bharadwaj, B. Rabha, S. Pati, T. Sarkar, B. K. Choudhury, A. Barman, D. Bhattacharjya, A. Srivastava, D. Baishya and H. A. Edinur, *Molecules*, 2021, **26**, 6389.

78 D. A. Lomelí-Rosales, A. Zamudio-Ojeda, O. K. Reyes-Maldonado, M. E. López-Reyes, G. C. Basulto-Padilla, E. J. Lopez-Naranjo, V. M. Zuñiga-Mayo and G. Velázquez-Juárez, *Molecules*, 2022, **27**, 1692.

79 M. Uzma, N. Sunayana, V. B. Raghavendra, C. S. Madhu, R. Shanmuganathan and K. Brindhadevi, *Process Biochem.*, 2020, **92**, 269–276.

80 S. Akhtar, S. Asiri, F. A. Khan, S. Gunday, A. Iqbal, N. Alrushaid, O. Labib, G. Deen and F. Henari, *Arabian J. Chem.*, 2022, **15**, 103594.

81 J. Chen, J. Ding, D. Li, Y. Wang, Y. Wu, X. Yang, A. Chinnathambi, S. H. Salmen and S. A. Alharbi, *Arabian J. Chem.*, 2022, **15**, 103479.

82 M. S. Majoumouo, J. R. Sharma, N. R. Sibuyi, M. B. Tincho, F. F. Boyom and M. Meyer, *Molecules*, 2020, **25**, 4469.

83 S. Ahmed and S. Ikram, *J. Photochem. Photobiol., B*, 2016, **161**, 141–153.

84 J. Santhoshkumar, S. Rajeshkumar and S. V. Kumar, *Biochem. Biophys. Rep.*, 2017, **11**, 46–57.

85 S. Vimalraj, T. Ashokkumar and S. Saravanan, *Biomed. Pharmacother.*, 2018, **105**, 440–448.

86 S. O. Anadozie, O. B. Adewale, N. R. Sibuyi, A. O. Fadaka, C. C. Isitua, H. Davids and S. Roux, *Process Biochem.*, 2023, **128**, 49–57.

87 P. Ahati, T. Xu, L. Chen and H. Fang, *Inorg. Chem. Commun.*, 2022, **143**, 109791.

88 I. S. Saputra, A. H. Saputro, D. O. B. Apriandanu, Y. N. Permana and Y. Yulizar, *Chem. Pap.*, 2022, **76**, 4733–4742.

89 A. A. Dudhane, S. R. Waghmode, L. B. Dama, V. P. Mhaindarkar, A. Sonawane and S. Katariya, *Int. J. Nanosci. Nanotechnol.*, 2019, **15**, 75–82.

90 S. S. Asl, F. Tafvizi and H. Noorbazargan, *Environ. Sci. Pollut. Res.*, 2023, **30**, 20168–20184.

91 M. S. Punnoose and B. Mathew, *Res. Chem. Intermed.*, 2022, **48**, 1025–1044.

92 S. Balasubramanian, S. M. J. Kala and T. L. Pushparaj, *J. Drug Delivery Sci. Technol.*, 2020, **57**, 101620.

93 O. T. Fanoro, S. Parani, R. Maluleke, T. C. Lebepe, J. R. Varghese, V. Mavumengwana and O. S. Oluwafemi, *Antibiotics*, 2021, **10**, 893.

94 I. Fatimah, H. Hidayat, B. H. Nugroho and S. Husein, *S. Afr. J. Chem. Eng.*, 2020, **34**, 97–106.

95 G. Suriyakala, S. Sathiyaraj, R. Babujanarthanam, K. M. Alarjani, D. S. Hussein, R. A. Rasheed and K. Kanimozhi, *J. King Saud Univ., Sci.*, 2022, **34**, 101830.

96 M. A. Alghuthaymi, C. Rajkuberan, T. Santhiya, O. Krejcar, K. Kuča, R. Periakaruppan and S. Prabukumar, *Plants*, 2021, **10**, 2370.

97 F. A. Alhumaydhi, I. Khan, A. Rauf, M. N. Qureshi, A. S. Aljohani, S. A. Khan, A. A. Khalil, M. A. El-Esawi and N. Muhammad, *Green Process. Synth.*, 2021, **10**, 230–245.

98 N. Alikhani, M. Hekmati, B. Karmakar and H. Veisi, *Inorg. Chem. Commun.*, 2022, **139**, 109351.

99 S. O. Anadozie, O. B. Adewale, A. O. Fadaka, O. B. Afolabi and S. Roux, *Biocatal. Agric. Biotechnol.*, 2022, **42**, 102348.

100 S. Bawazeer, I. Khan, A. Rauf, A. S. Aljohani, F. A. Alhumaydhi, A. A. Khalil, M. N. Qureshi, L. Ahmad and S. A. Khan, *Green Process. Synth.*, 2022, **11**, 11–28.

101 C. Pechyen, K. Ponsanti, B. Tangnorawich and N. Ngernyuang, *Toxicol Rep*, 2022, **9**, 1092–1098.

102 C. Pechyen, K. Ponsanti, B. Tangnorawich and N. Ngernyuang, *J. Mater. Res. Technol.*, 2021, **14**, 2982–2991.

103 V. Sekar, M. M. Al-Ansari, J. Narenkumar, L. Al-Humaid, P. Arunkumar and A. Santhanam, *J. King Saud Univ., Sci.*, 2022, **34**, 102197.

104 M. Reyes-Becerril, F. Ruvalcaba, V. Sanchez, M. G. López, J. Silva-Jara, L. Hernandez-Adame and C. Angulo, *Aquacult. Res.*, 2021, **52**, 3391–3402.

105 N. González-Ballesteros, J. Vidal-González and M. C. Rodríguez-Argüelles, *J. Nanostruct. Chem.*, 2021, 1–10.

106 T. ul Haq and R. Ullah, *Int. J. Nanosci.*, 2022, **21**, 2250008.

107 N. S. Al-Radadi, *Arabian J. Chem.*, 2021, **14**, 102956.

108 J. Shilpha, V. Meyappan and N. Sakthivel, *Process Biochem.*, 2022, **122**, 224–237.

109 S. Kandasamy, S. Chinnappan, S. Thangaswamy and S. Balakrishnan, *Mater. Res. Express*, 2020, **6**, 1250c1251.

110 B. A. Varghese, R. V. R. Nair, S. Jude, K. Varma, A. Amalraj and S. Kuttappan, *J. Taiwan Inst. Chem. Eng.*, 2021, **126**, 166–172.

111 O. S. ElMitwalli, O. A. Barakat, R. M. Daoud, S. Akhtar and F. Z. Henari, *J. Nanopart. Res.*, 2020, **22**, 1–9.

112 R. C. Sandulovici, M. Carmen-Marinela, A. Grigoroiu, C. A. Moldovan, M. Savin, V. Ordeanu, S. N. Voicu, D. Cord, G. M. Costache and M. L. Galatanu, *Pharmaceuticals*, 2022, **16**, 48.

113 M. Salandari Rabori, M. Noroozi Karimabad and M. R. Hajizadeh, *World Cancer Res. J.*, 2021, **8**, e2037.

114 S. Mal and D. Pal, *Bioactive Natural Products for Pharmaceutical Applications*, 2021, pp. 715–757.

115 A. Halder, S. Das, D. Ojha, D. Chattopadhyay and A. Mukherjee, *Mater. Sci. Eng. C*, 2018, **89**, 413–421.

116 A. Zuhrotun, D. J. Oktaviani and A. N. Hasanah, *Molecules*, 2023, **28**, 3240.

117 S. Durmazel, A. Uzer, B. Erbil, B. Sayın and R. Apak, *ACS Omega*, 2019, **4**, 7596–7604.

118 P. Kuppusamy, M. M. Yusoff, G. P. Maniam and N. Govindan, *Saudi Pharm. J.*, 2016, **24**, 473–484.

119 N. Gan, C. Wakayama, S. Inubushi, T. Kunihisa, S. Mizumoto, M. Baba, H. Tanino and T. Ooya, *ACS Appl. Bio Mater.*, 2021, **5**, 355–365.

120 M. H. Oueslati, L. B. Tahar and A. H. Harrath, *Arabian J. Chem.*, 2020, **13**, 3112–3122.

121 J. J. Park, S. J. Hwang, Y. S. Kang, J. Jung, S. Park, J. E. Hong, Y. Park and H.-J. Lee, *Arch. Pharmacal Res.*, 2019, **42**, 977–989.

122 Z. Sharifiaghdam, S. M. Amini, F. Dalouchi, A. B. Behrooz and Y. Azizi, *Heliyon*, 2023, **9**(3), e14024.

123 A. J. Jasim, G. M. Sulaiman, H. Ay, S. A. Mohammed, H. A. Mohammed, M. S. Jabir and R. A. Khan, *Nanotechnol. Rev.*, 2022, **11**, 2726–2741.

124 A. Parthiban, V. Sachithanandam, S. Sarangapany, R. Misra, P. Muthukrishnan, T. C. Jeyakumar, R. Purvaja and R. Ramesh, *J. Mol. Struct.*, 2023, **1272**, 134167.

125 S. Kondath, R. Rajaram and R. Anantanarayanan, *Inorg. Nano-Met. Chem.*, 2020, **51**, 601–613.

126 B. S. Inbaraj, L.-H. Hua and B.-H. Chen, *Pharmaceutics*, 2021, **13**, 1871.

127 L. Chen, Y. Huo, Y. X. Han, J. F. Li, H. Ali, I. Batjikh, J. Hurh, J. Y. Pu and D. C. Yang, *Appl. Phys. A*, 2020, **126**, 1–12.

128 V. V. Vodnik, M. Mojić, U. Stamenović, M. Otoničar, V. Ajdžanović, D. Maksimović-Ivanić, S. Mijatović, M. M. Marković, T. Barudžija and B. Filipović, *Mater. Sci. Eng. C*, 2021, **124**, 112078.

129 K. Pearce, V. C. Thipe, R. R. Henkel and K. V. Katti, *J. Drug Delivery Sci. Technol.*, 2023, **80**, 104100.

130 J. d. S. Oliveira and E. J. Guidelli, *Mater. Sci. Eng. C*, 2021, **126**, 112122.

131 A. Gupta, R. Mathur, S. Singh, N. Bag, U. A. Khan, F. J. Ahmad, G. A. Gabr, P. Kesharwani and G. K. Jain, *J. Pharm. Sci.*, 2021, **110**, 888–897.

132 M. K. Hameed, I. M. Ahmady, C. Han and A. A. Mohamed, *Amino Acids*, 2020, **52**, 941–953.

133 S. Zhang, M. Bai, J. Qian and Y. Guo, *Microchem. J.*, 2021, **169**, 106564.

134 B. A. Makwana, D. J. Vyas, K. D. Bhatt and V. K. Jain, *Sens. Actuators, B*, 2017, **240**, 278–287.

135 Z. Huang, X. Zhang, Z. Yao, Y. Han, J. Ye, Y. Zhang, L. Chen, M. Shen and T. Zhou, *Msphere*, 2023, e00549.

136 K. Rajendran, A. Anwar, N. A. Khan, M. R. Shah and R. Siddiqui, *ACS Chem. Neurosci.*, 2019, **10**, 2692–2696.

137 I. Rajendran, T. Ponrasu, R. Rajaram and L. Suguna, *J. Drug Delivery Sci. Technol.*, 2021, **63**, 102478.

138 R. Chen, F. Chen, M. Sun, R. Zhang, S. Wu and C. Meng, *Inorg. Nano-Met. Chem.*, 2022, **52**, 1345–1351.

139 W. I. El-Ghareb, M. M. Swidan, I. T. Ibrahim, A. Abd El-Bary, M. I. Tadros and T. M. Sakr, *Int. J. Pharm.*, 2020, **586**, 119514.

140 T. Ferreira-Gonçalves, M. M. Gaspar, J. M. Coelho, V. Marques, A. S. Viana, L. Ascensão, L. Carvalho, C. M. Rodrigues, H. A. Ferreira and D. Ferreira, *Biomolecules*, 2022, **12**, 71.

141 W. Caseri, *Macromol. Rapid Commun.*, 2000, **21**, 705–722.

142 H. Kang, J. T. Buchman, R. S. Rodriguez, H. L. Ring, J. He, K. C. Bantz and C. L. Haynes, *Chem. Rev.*, 2018, **119**, 664–699.

143 A. Kraynov and T. E. Müller, *Applications of Ionic Liquids in Science and Technology*, 2011, vol. 9, pp. 235–260.

144 S. Levine and G. Dube, *Trans. Faraday Soc.*, 1939, **35**, 1125–1140.

145 A. M. Kalsin, M. Fialkowski, M. Paszewski, S. K. Smoukov, K. J. Bishop and B. A. Grzybowski, *Science*, 2006, **312**, 420–424.

146 R. Javed, M. Zia, S. Naz, S. O. Aisida, N. u. Ain and Q. Ao, *J. Nanobiotechnol.*, 2020, **18**, 1–15.

147 P. Dash and R. W. Scott, *Chem. Commun.*, 2009, 812–814.

148 K.-S. Kim, S. Choi, J.-H. Cha, S.-H. Yeon and H. Lee, *J. Mater. Chem.*, 2006, **16**, 1315–1317.

149 A. Madu, P. Njoku, G. Iwuoha and U. Agbasi, *Int. J. Phys. Sci.*, 2011, **6**, 635–640.

150 L. Vigderman and E. R. Zubarev, *Adv. Drug Delivery Rev.*, 2013, **65**, 663–676.

151 C. Caro, A. Avasthi, J. M. Paez-Muñoz, M. P. Leal and M. L. García-Martín, *Biomater. Sci.*, 2021, **9**, 7984–7995.

152 Z. R. Goddard, M. J. Marín, D. A. Russell and M. Searcey, *Chem. Soc. Rev.*, 2020, **49**, 8774–8789.

153 J. C. Love, L. A. Estroff, J. K. Kriebel, R. G. Nuzzo and G. M. Whitesides, *Chem. Rev.*, 2005, **105**, 1103–1170.

154 H. Li and L. Rothberg, *Proc. Natl. Acad. Sci. U. S. A.*, 2004, **101**, 14036–14039.

155 A. S. Angelatos, K. Katagiri and F. Caruso, *Soft Matter*, 2006, **2**, 18–23.

156 N. Hadjesfandiari and A. Parambath, in *Engineering of Biomaterials for Drug Delivery Systems*, Elsevier, 2018, pp. 345–361.

157 E. C. Dreaden, S. C. Mwakwari, Q. H. Sodji, A. K. Oyelere and M. A. El-Sayed, *Bioconjugate Chem.*, 2009, **20**, 2247–2253.

158 S. Sarkar, S. Konar, P. N. Prasad, S. Rajput, B. P. Kumar, R. R. Rao, A. Pathak, P. B. Fisher and M. Mandal, *Langmuir*, 2017, **33**, 7649–7659.

159 Y. Wang, M. Pasternak, K. Sathiyamoorthy and M. C. Kolios, *Biomed. Opt. Express*, 2021, **12**, 2171–2185.

160 S. Mahalunkar, A. S. Yadav, M. Gorain, V. Pawar, R. Braathen, S. Weiss, B. Bogen, S. W. Gosavi and G. C. Kundu, *Int. J. Nanomed.*, 2019, 8285–8302.

161 M. J. Hostetler, A. C. Templeton and R. W. Murray, *Langmuir*, 1999, **15**, 3782–3789.

162 R. Lévy, N. T. Thanh, R. C. Doty, I. Hussain, R. J. Nichols, D. J. Schiffrin, M. Brust and D. G. Fernig, *J. Am. Chem. Soc.*, 2004, **126**, 10076–10084.

163 O. Akbal Vural, *Int. J. Polym. Mater. Polym. Biomater.*, 2022, **71**, 1437–1448.

164 M.-E. Aubin-Tam, H. Zhou and K. Hamad-Schifferli, *Soft Matter*, 2008, **4**, 554–559.

165 D. Bartczak and A. G. Kanaras, *Langmuir*, 2011, **27**, 10119–10123.

166 L. Raposo, C. Roma-Rodrigues, J. Jesus, L. Martins, A. Pombeiro, P. Baptista and A. Fernandes, *Vet. Comp. Oncol.*, 2017, **15**, 1537–1542.

167 R. Liu, J. Zhao, G. Han, T. Zhao, R. Zhang, B. Liu, Z. Liu, C. Zhang, L. Yang and Z. Zhang, *ACS Appl. Mater. Interfaces*, 2017, **9**, 38222–38229.

168 S. Si and T. K. Mandal, *Langmuir*, 2007, **23**, 190–195.

169 C. Criscitiello, *Breast Care*, 2012, **7**, 262–266.

170 M. K. Yu, J. Park and S. Jon, *Theranostics*, 2012, **2**, 3.

171 S. Puertas, P. Batalla, M. Moros, E. Polo, P. Del Pino, J. M. Guisan, V. Grazu and J. M. de la Fuente, *ACS Nano*, 2011, **5**, 4521–4528.

172 H. Liao and J. H. Hafner, *Chem. Mater.*, 2005, **17**, 4636–4641.

173 C. Loo, L. Hirsch, M.-H. Lee, E. Chang, J. West, N. Halas and R. Drezek, *Opt. Lett.*, 2005, **30**, 1012–1014.

174 Z. Alhalili, J. Shapter, D. Figueroa and B. Sanderson, *Drug Deliv. Lett.*, 2018, **8**, 217–225.

175 G. Obaid, I. Chambrier, M. J. Cook and D. A. Russell, *Photochem. Photobiol. Sci.*, 2015, **14**, 737–747.

176 O. Penon, M. J. Marín, D. A. Russell and L. Pérez-García, *J. Colloid Interface Sci.*, 2017, **496**, 100–110.

177 F. Nicolson, A. Ali, M. F. Kircher and S. Pal, *Adv. Sci.*, 2020, **7**, 2001669.

178 B. Liu, P. Wu, Z. Huang, L. Ma and J. Liu, *J. Am. Chem. Soc.*, 2018, **140**, 4499–4502.

179 W. Zhao, L. Lin and I.-M. Hsing, *Bioconjugate Chem.*, 2009, **20**, 1218–1222.

180 R. Wu, L.-P. Jiang, J.-J. Zhu and J. Liu, *Langmuir*, 2019, **35**, 13461–13468.

181 J. Shin, X. Zhang and J. Liu, *J. Phys. Chem. B*, 2012, **116**, 13396–13402.

182 J. A. Dougan, C. Karlsson, W. E. Smith and D. Graham, *Nucleic Acids Res.*, 2007, **35**, 3668–3675.

183 X. Zhang, B. Liu, N. Dave, M. R. Servos and J. Liu, *Langmuir*, 2012, **28**, 17053–17060.

184 J. Kadkhoda, A. Aghanejad, B. Safari, J. Barar, S. H. Rasta and S. Davaran, *J. Drug Delivery Sci. Technol.*, 2022, **67**, 102954.

185 P. Bayat, K. Abnous, S. Balarastaghi, S. M. Taghdisi, M. Saeedi, R. Yazdian-Robati and M. Mahmoudi, *Nanomed. J.*, 2022, **9**, 164–169.

186 A. Kardani, H. Yaghoobi, A. Alibakhshi and M. Khatami, *J. Cell. Physiol.*, 2020, **235**, 6887–6895.

187 M. V. Liberti and J. W. Locasale, *Trends Biochem. Sci.*, 2016, **41**, 211–218.

188 C. Tzror-Azankot, T. Dreifuss, T.-S. Ben-Gal, A. Jacob, T. Sadan, M. Motiei and R. Popovtzer, *Nanoscale Imaging, Sensing, and Actuation for Biomedical Applications XVI*, March 2019.

189 F. D. Moghaddam, G. Heidari, E. N. Zare, E. Djatoubai, A. C. Paiva-Santos, F. R. Bertani and A. Wu, *Carbohydr. Polym.*, 2022, 120510.

190 R. V. Murthy, P. M. Chaudhary, R. Kikkeri, H. V. Thulasiram, A. Paul and S. Sangabathuni, *Chem. Commun.*, 2015, **51**, 15669–15672.

191 S. Combemale, J.-N. Assam-Evoung, S. Houaidji, R. Bibi and V. Barragan-Montero, *Molecules*, 2014, **19**, 1120–1149.

192 T. Fyrner, T. Ederth, D. Aili, B. Liedberg and P. Konradsson, *Colloids Surf., B*, 2013, **105**, 187–193.

193 F. Compostella, O. Pitirollo, A. Silvestri and L. Polito, *Beilstein J. Org. Chem.*, 2017, **13**, 1008–1021.

194 K. K. Katti, V. Kattumuri, S. Bhaskaran, K. V. Katti and R. Kannan, *Int. J. Green Nanotechnol.*, 2009, **1**, B53–B59.

195 U. K. Mondal and J. J. Barchi Jr, *Front. Chem.*, 2022, **10**, 1002146.

196 P. G. Calavia, I. Chambrier, M. J. Cook, A. H. Haines, R. A. Field and D. A. Russell, *J. Colloid Interface Sci.*, 2018, **512**, 249–259.

197 V. O. Uzonwanne, A. Navabi, J. D. Obayemi, J. Hu, A. A. Salifu, S. Ghahremani, N. Ndahiro, N. Rahbar and W. Soboyejo, *Biomater. Adv.*, 2022, **136**, 212801.

198 P. Maraming, J. Daduang and J. C. Y. Kah, *RSC Adv.*, 2022, **12**, 319–325.

199 S. Law, A. W. Leung and C. Xu, *Artif. Cells, Nanomed., Biotechnol.*, 2020, **48**, 542–559.

200 C. Iodice, A. Cervadoro, A. Palange, J. Key, S. Aryal, M. R. Ramirez, C. Mattu, G. Ciardelli, B. E. O'Neill and P. Decuzzi, *Opt Laser. Eng.*, 2016, **76**, 74–81.

201 E. García-Garrido, M. Cordani and Á. Somoza, *Pharmaceutics*, 2021, **13**, 2067.

202 R. Goyal, C. H. Kapadia, J. R. Melamed, R. S. Riley and E. S. Day, *Cell. Mol. Bioeng.*, 2018, **11**, 383–396.

203 H. Nosrati, M. Salehiabar, J. Charmi, K. Yaray, M. Ghaffarlou, E. Balcioglu and Y. N. Ertas, *ACS Appl. Bio Mater.*, 2023, **6**, 784–792.

204 A. Kefayat, F. Ghahremani, H. Motaghi and M. A. Mehrgardi, *Eur. J. Pharm. Sci.*, 2019, **130**, 225–233.

205 C. Joseph, A. Daniels, S. Singh and M. Singh, *Pharmaceutics*, 2021, **14**, 53.

206 H. Q. Yin, G. Shao, F. Gan and G. Ye, *Nanoscale Res. Lett.*, 2020, **15**, 1–15.

207 R. Liu, H. Guo, Z. Ouyang, Y. Fan, X. Cao, J. Xia, X. Shi and R. Guo, *ACS Appl. Bio Mater.*, 2021, **4**, 1803–1812.

208 B. M. Bavelaar, L. Song, M. R. Jackson, S. Able, O. Tietz, I. Skaripa-Koukelli, P. A. Waghorn, M. R. Gill, R. C. Carlisle and M. Tarsounas, *Mol. Pharm.*, 2021, **18**, 3820–3831.

209 Z. Wu, S. Stangl, A. Hernandez-Schnelzer, F. Wang, M. Hasanzadeh Kafshgari, A. Bashiri Dezfouli and G. Multhoff, *Cancers*, 2023, **15**, 1167.

210 R. K. Samani, M. B. Tavakoli, F. Maghsoudinia, H. Motaghi, S. H. Hejazi and M. A. Mehrgardi, *Eur. J. Pharm. Sci.*, 2020, **153**, 105487.

211 S. Li, S. Bouchy, S. Penninckx, R. Marega, O. Fichera, B. Gallez, O. Feron, P. Martinive, A.-C. Heuskin and C. Michiels, *Nanomedicine*, 2019, **14**, 317–333.

212 A. Kapara, K. A. Findlay Paterson, V. G. Brunton, D. Graham, M. Zagnoni and K. Faulds, *Anal. Chem.*, 2021, **93**, 5862–5871.

213 M. A. Kimm, M. Shevtsov, C. Werner, W. Sievert, W. Zhiyuan, O. Schoppe, B. H. Menze, E. J. Rummeny, R. Proksa and O. Bystrova, *Cancers*, 2020, **12**, 1331.

214 T. S. Rebelo, J. A. Ribeiro, M. G. F. Sales and C. M. Pereira, *Sens. Bio-Sens. Res.*, 2021, **33**, 100445.

215 C. Zhang, F. Zhang, M. Han, X. Wang, J. Du, H. Zhang and W. Li, *Sci. Rep.*, 2020, **10**, 22015.

216 Y. Wu, Y. He, M. Han, D. Zhao, B. Liu, K. Yuan, H. Sun, H.-M. Meng and Z. Li, *CCS Chem.*, 2022, 1–13.

217 A. Graczyk, R. Pawlowska and A. Chworos, *Bioconjugate Chem.*, 2021, **32**, 1667–1674.

218 K. Chakraborty, A. Biswas, S. Mishra, A. M. Mallick, A. Tripathi, S. Jan and R. Sinha Roy, *ACS Appl. Bio Mater.*, 2023, **6**, 458–472.

219 M. Shahidi, O. Abazari, P. Dayati, A. Bakhshi, A. Rasti, F. Haghiralsadat, S. M. Naghib and D. Tofighi, *Nanotechnol. Rev.*, 2022, **11**, 2875–2890.

220 X. Dai, X. Zhao, Y. Liu, B. Chen, X. Ding, N. Zhao and F. J. Xu, *Small*, 2021, **17**, 2006004.

221 T. N. Aslan, E. Aşık, N. T. Güray and M. Volkan, *JBIC, J. Biol. Inorg. Chem.*, 2020, **25**, 1139–1152.

222 A. S. Doghish, A. H. Hashem, A. M. Shehabeldine, A.-A. M. Sallam, G. S. El-Sayyad and S. S. Salem, *J. Drug Delivery Sci. Technol.*, 2022, **77**, 103874.

223 L. Devi, R. Gupta, S. K. Jain, S. Singh and P. Kesharwani, *J. Drug Delivery Sci. Technol.*, 2020, **56**, 101565.

224 B. F. Craciun, L. Clima, D.-I. Bostiog, M. Silion, M. Calin, D. Peptanariu and M. Pinteala, *Biomater. Adv.*, 2023, **144**, 213201.

225 E. D. Abdolahinia, S. Nadri, R. Rahbarghazi, J. Barar, A. Aghanejad and Y. Omidi, *Life Sci.*, 2019, **231**, 116545.

226 A. G. Al-Dulimi, A. Z. Al-Saffar, G. M. Sulaiman, K. A. Khalil, K. S. Khashan, H. S. Al-Shmgani and E. M. Ahmed, *J. Mater. Res. Technol.*, 2020, **9**, 15394–15411.

227 G. Vivo-Llorca, Á. Morellá-Aucejo, A. García-Fernández, P. Díez, A. Llopis-Lorente, M. Orzáez and R. Martínez-Máñez, *Int. J. Nanomed.*, 2022, 409–422.

228 S. S. Kelkar and T. M. Reineke, *Bioconjugate Chem.*, 2011, **22**, 1879–1903.

229 R. Vinhas, M. Cordeiro, F. F. Carlos, S. Mendo, A. R. Fernandes, S. Figueiredo and P. V. Baptista, *Nanobiosensors Dis. Diagnosis*, 2015, 11–23.

230 J. Peng, Q. Yang, K. Shi, Y. Xiao, X. Wei and Z. Qian, *Adv. Drug Delivery Rev.*, 2019, **143**, 37–67.

231 J. Choi and S. Y. Kim, *J. Ind. Eng. Chem.*, 2020, **85**, 66–74.

232 J. Song, J. Zhou and H. Duan, *J. Am. Chem. Soc.*, 2012, **134**, 13458–13469.

233 N. Khlebtsov and L. Dykman, *Chem. Soc. Rev.*, 2011, **40**, 1647–1671.

234 Y. Zhang, A. T. Liu, Y. R. Cornejo, D. Van Haute and J. M. Berlin, *PLoS One*, 2020, **15**, e0234916.

235 J. Cancino-Bernardi, V. Marangoni, J. Besson, M. Cancino, M. Natali and V. Zucolotto, *Chemosphere*, 2018, **213**, 41–52.

236 C. Lopez-Chaves, J. Soto-Alvaredo, M. Montes-Bayon, J. Bettmer, J. Llopis and C. Sanchez-Gonzalez, *Nanomed. Nanotechnol. Biol. Med.*, 2018, **14**, 1–12.

237 Y. Wang, K. C. Black, H. Luehmann, W. Li, Y. Zhang, X. Cai, D. Wan, S.-Y. Liu, M. Li and P. Kim, *ACS Nano*, 2013, **7**, 2068–2077.

238 T. Dubaj, K. Kozics, M. Sramkova, A. Manova, N. G. Bastús, O. H. Moriones, Y. Kohl, M. Dusinska, E. Rundén-Pran and V. F. Puntes, *Nanomaterials*, 2022, **12**, 511.

239 P. Natarajan and J. M. Tomich, *Arch. Biochem. Biophys.*, 2020, **694**, 108592.

240 M. Witkowska, E. Florek and R. Mrówczyński, *Int. J. Mol. Sci.*, 2022, **23**, 15343.

241 J. Xie, S. Lee and X. Chen, *Adv. Drug Delivery Rev.*, 2010, **62**, 1064–1079.

242 A. Vasil'kov, A. Voronova, T. Batsalova, D. Moten, A. Naumkin, E. Shtykova, V. Volkov, I. Teneva and B. Dzhambazov, *Materials*, 2023, **16**, 3238.

243 J. Guo, K. Rahme, Y. He, L.-L. Li, J. D. Holmes and C. M. O'Driscoll, *Int. J. Nanomed.*, 2017, 6131–6152.

244 S. S. Khandker, M. S. Shakil and M. S. Hossen, *Curr. Drug Metab.*, 2020, **21**, 579–598.

245 S. Gori, S. Rimondini, V. De Angelis, M. Colozza, G. Bisagni, G. Moretti, A. Sidoni, C. Basurto, C. Aristei and P. Anastasi, *Oncologist*, 2007, **12**, 766–773.

246 X. Li, C. Yang, H. Wan, G. Zhang, J. Feng, L. Zhang, X. Chen, D. Zhong, L. Lou and W. Tao, *Eur. J. Pharm. Sci.*, 2017, **110**, 51–61.

247 Y. Wu, Y. Feng and X. Li, *J. Colloid Interface Sci.*, 2022, **611**, 287–293.

248 P. Yaşar, G. Ayaz, S. D. User, G. Güpür and M. Muyan, *Reprod. Med. Biol.*, 2017, **16**, 4–20.

249 R. Ahirwar and P. Nahar, *Anal. Bioanal. Chem.*, 2016, **408**, 327–332.

250 Z. Baretta, S. Mocellin, E. Goldin, O. I. Olopade and D. Huo, *Medicine*, 2016, **95**, e4975.

251 J.-H. Oh and J.-S. Lee, *Anal. Chem.*, 2011, **83**, 7364–7370.

252 R. Singh and Y.-Y. Mo, *Cancer Biol. Ther.*, 2013, **14**, 201–212.

253 F. Hakimian, H. Ghourchian, A. S. Hashemi, M. R. Arastoo and M. Behnam Rad, *Sci. Rep.*, 2018, **8**, 2943.

254 M. J. Duffy, C. Duggan, R. Keane, A. D. Hill, E. McDermott, J. Crown and N. O'Higgins, *Clin. Chem.*, 2004, **50**, 559–563.

255 J. Peng, Y. Lai, Y. Chen, J. Xu, L. Sun and J. Weng, *Small*, 2017, **13**, 1603589.

256 E. Wolfson, S. Solomon, E. Schmukler, Y. Goldshmit and R. Pinkas-Kramarski, *Cell Death Dis.*, 2018, **9**, 47.

257 M. Keshtkar, D. Shahbazi-Gahrouei, S. M. Khoshfetrat, M. A. Mehrgardi and M. Aghaei, *J. Med. Signals Sens.*, 2016, **6**, 243.

258 P. F. Rostamabadi and E. Heydari-Bafrooei, *Microchim. Acta*, 2019, **186**, 1–9.

259 S. Sharma, J. Zapatero-Rodríguez, R. Saxena, R. O'Kennedy and S. Srivastava, *Biosens. Bioelectron.*, 2018, **106**, 78–85.

260 Y. Bai, H. Li, J. Xu, Y. Huang, X. Zhang, J. Weng, Z. Li and L. Sun, *Biosens. Bioelectron.*, 2020, **166**, 112424.

261 J.-H. Choi, J. Lim, M. Shin, S.-H. Paek and J.-W. Choi, *Nano Lett.*, 2020, **21**, 693–699.

262 Q. Zhang, Y. Tian, Z. Liang, Z. Wang, S. Xu and Q. Ma, *Anal. Chem.*, 2021, **93**, 3308–3314.

263 C. Wang, W. Wang, Y. Xu, X. Zhao, S. Li, Q. Qian and X. Mi, *Nanomaterials*, 2022, **12**, 666.

264 M. Hasanzadeh, E. Solhi, M. Jafari, A. Mokhtarzadeh, J. Soleymani, A. Jouyban and S. Mahboob, *Int. J. Biol. Macromol.*, 2018, **120**, 2493–2508.

265 Y. Bao, K. Han, Z. Ding, Y. Li, T. Li, M. Guan and G. Li, *Spectrochim. Acta, Part A*, 2021, **253**, 119562.

266 H. Zhao, T. Liu, L. Cui, Y. Li, F. Yang and X. Zhang, *Sens. Actuators, B*, 2021, **345**, 130332.

267 K. Kuntamung, J. Jakmunee and K. Ounnunkad, *J. Mater. Chem. B*, 2021, **9**, 6576–6585.

268 P. Ranjan, M. Abubakar Sadique, S. Yadav and R. Khan, *ACS Appl. Mater. Interfaces*, 2022, **14**, 20802–20812.

269 J. Zhao, Y. Tang, Y. Cao, T. Chen, X. Chen, X. Mao, Y. Yin and G. Chen, *Electrochim. Acta*, 2018, **283**, 1072–1078.

270 V. Maggi, F. Bianchini, E. Portioli, S. Peppicelli, M. Lulli, D. Bani, R. Del Sole, F. Zanardi, A. Sartori and R. Fiammengo, *Chem. –Eur. J.*, 2018, **24**, 12093–12100.

271 W.-J. Lee, K.-J. Kim, M. K. Hossain, H.-Y. Cho and J.-W. Choi, *Biochip J.*, 2022, **16**, 33–40.

272 C. Pothipor, J. Jakmunee, S. Bamrungsap and K. Ounnunkad, *Analyst*, 2021, **146**, 4000–4009.

273 L. Farzin, M. Shamsipur, L. Samandari and S. Sheibani, *Microchim. Acta*, 2018, **185**, 1–9.

274 F. Shafiei, R. S. Saberi and M. A. Mehrgardi, *Bioelectrochemistry*, 2021, **140**, 107807.

275 J. Zhao, D. Huo, X. Geng, J. Bao, J. Hou, Z. Shui, H. Yang, Y. Qi, Y. Hu and M. Yang, *Sens. Actuators, B*, 2021, **332**, 129480.

276 R. A. Sperling, P. R. Gil, F. Zhang, M. Zanella and W. J. Parak, *Chem. Soc. Rev.*, 2008, **37**, 1896–1908.

277 K. Kneipp, H. Kneipp and J. Kneipp, *Acc. Chem. Res.*, 2006, **39**, 443–450.

278 Y. Luo, Y. Xiao, D. Onidas, L. Iannazzo, M. Ethève-Quelquejeu, A. Lamouri, N. Félidj, S. Mahouche-Chergui, T. Brulé and N. Gagey-Eilstein, *Chem. Commun.*, 2020, **56**, 6822–6825.

279 C. Vericat, M. Vela, G. Benitez, P. Carro and R. Salvarezza, *Chem. Soc. Rev.*, 2010, **39**, 1805–1834.

280 M. Li, J. Wu, M. Ma, Z. Feng, Z. Mi, P. Rong and D. Liu, *Nanotheranostics*, 2019, **3**, 113.

281 J. Zhu, J. Zhou, J. Guo, W. Cai, B. Liu, Z. Wang and Z. Sun, *Chem. Cent. J.*, 2013, **7**, 1–5.

282 W. Lu, S. R. Arumugam, D. Senapati, A. K. Singh, T. Arbneshi, S. A. Khan, H. Yu and P. C. Ray, *ACS Nano*, 2010, **4**, 1739–1749.

283 N. Gao, Q. Wang, J. Tang, S. Yao, H. Li, X. Yue, J. Fu, F. Zhong, T. Wang and J. Wang, *Anal. Bioanal. Chem.*, 2021, **413**, 4775–4784.

284 W. Cai, T. Gao, H. Hong and J. Sun, *Nanotechnol., Sci. Appl.*, 2008, 17–32.

285 N. Lewinski, V. Colvin and R. Drezek, *Small*, 2008, **4**, 26–49.

286 X. Huang, P. K. Jain, I. H. El-Sayed and M. A. El-Sayed, *Laser Med. Sci.*, 2008, **23**, 217–228.

287 S. Link and M. A. El-Sayed, *Int. Rev. Phys. Chem*, 2000, **19**, 409–453.

288 V. P. Zharov, E. N. Galitovskaya, C. Johnson and T. Kelly, *Lasers Surg. Med.*, 2005, **37**, 219–226.

289 C. Loo, A. Lowery, N. Halas, J. West and R. Drezek, *Nano Lett.*, 2005, **5**, 709–711.

290 S. N. Mohammed, A. M. Mohammed and K. F. Al-Rawi, *Steroids*, 2022, **186**, 109091.

291 L. Yang, Y.-T. Tseng, G. Suo, L. Chen, J. Yu, W.-J. Chiu, C.-C. Huang and C.-H. Lin, *ACS Appl. Mater. Interfaces*, 2015, **7**, 5097–5106.

292 M. Zhang, H. S. Kim, T. Jin and W. K. Moon, *J. Photochem. Photobiol., B*, 2017, **170**, 58–64.

293 H. Chen, X. Wang, L. Sutrisno, T. Zeng, N. Kawazoe, Y. Yang and G. Chen, *Front. Bioeng. Biotechnol.*, 2020, **8**, 589905.

294 M. R. Ali, H. A. Farghali, Y. Wu, I. El-Sayed, A. H. Osman, S. A. Selim and M. A. El-Sayed, *Cancers*, 2019, **11**, 851.

295 A. S. Abdoon, E. A. Al-Ashkar, O. M. Kandil, A. M. Shaban, H. M. Khaled, M. A. El Sayed, M. M. El Shaer, A. H. Shaalan, W. H. Eisa and A. A. G. Eldin, *Nanomed. Nanotechnol. Biol. Med.*, 2016, **12**, 2291–2297.

296 A. H. Faid, S. A. Shouman, N. A. Thabet, Y. A. Badr and M. A. Sliem, *J. Pharmaceut. Innovat.*, 2023, **18**, 144–148.

297 H.-C. Lin, K.-F. Hsu, C.-L. Lai, T.-C. Wu, H.-F. Chen and C.-H. Lai, *Molecules*, 2020, **25**, 1853.

298 Z. Poursalehi, R. Salehi, N. Samadi, S. H. Rasta, B. Mansoori and H. Majdi, *Photodiagnosis Photodyn. Ther.*, 2019, **28**, 25–37.

299 A. Pakravan, M. Azizi, F. Rahimi, F. Bani, F. Mahmoudzadeh, R. Salehi and M. Mahkam, *Cancer Nanotechnol.*, 2021, **12**, 1–26.

300 L. C. Kennedy, L. R. Bickford, N. A. Lewinski, A. J. Coughlin, Y. Hu, E. S. Day, J. L. West and R. A. Drezek, *Small*, 2011, **7**, 169–183.

301 H. Xia, Y. Gao, L. Yin, X. Cheng, A. Wang, M. Zhao, J. Ding and H. Shi, *ChemBioChem*, 2019, **20**, 667–671.

302 P. P. Pillai, B. Kowalczyk, K. Kandere-Grzybowska, M. Borkowska and B. A. Grzybowski, *Angew. Chem., Int. Ed.*, 2016, **55**, 8610–8614.

303 S. Kang, S. H. Bhang, S. Hwang, J.-K. Yoon, J. Song, H.-K. Jang, S. Kim and B.-S. Kim, *ACS Nano*, 2015, **9**, 9678–9690.

304 T. Bian, L. Shang, H. Yu, M. T. Perez, L. Z. Wu, C. H. Tung, Z. Nie, Z. Tang and T. Zhang, *Adv. Mater.*, 2014, **26**, 5613–5618.

305 S.-R. Kim and E.-H. Kim, *Int. J. Radiat. Biol.*, 2018, **94**, 8–16.

306 Y. Dou, Y. Guo, X. Li, X. Li, S. Wang, L. Wang, G. Lv, X. Zhang, H. Wang and X. Gong, *ACS Nano*, 2016, **10**, 2536–2548.

307 N. M. Dimitriou, G. Tsekenis, E. C. Balanikas, A. Pavlopoulou, M. Mitsiogianni, T. Mantso, G. Pashos, A. G. Boudouvis, I. N. Lykakis and G. Tsigaridas, *Pharmacol. Ther.*, 2017, **178**, 1–17.

308 L. Song, N. Falzone and K. A. Vallis, *Int. J. Radiat. Biol.*, 2016, **92**, 716–723.

309 X. Yao, C. Huang, X. Chen, Y. Zheng and L. Sanche, *J. Biomed. Nanotechnol.*, 2015, **11**, 478–485.

310 M. Misawa and J. Takahashi, *Nanomed. Nanotechnol. Biol. Med.*, 2011, **7**, 604–614.

311 Y. Lin, S. J. McMahon, M. Scarpelli, H. Paganetti and J. Schuemann, *Phys. Med. Biol.*, 2014, **59**, 7675.

312 S. Rosa, C. Connolly, G. Schettino, K. T. Butterworth and K. M. Prise, *Cancer Nanotechnol.*, 2017, **8**, 1–25.

313 J. Choi, K. O. Jung, E. E. Graves and G. Pratx, *Nanotechnology*, 2018, **29**, 504001.

314 C. Wang, Y. Jiang, X. Li and L. Hu, *Breast Cancer*, 2015, **22**, 413–420.

315 N. Hanžić, A. Horvat, J. Bibić, K. Unfried, T. Jurkin, G. Dražić, I. Marijanović, N. Slade and M. Gotić, *Mater. Sci. Eng. C*, 2018, **91**, 486–495.

316 B. Janic, S. L. Brown, R. Neff, F. Liu, G. Mao, Y. Chen, L. Jackson, I. J. Chetty, B. Movsas and N. Wen, *Cancer Biol. Ther.*, 2021, **22**, 124–135.

317 S. S. Mehrnia, B. Hashemi, S. J. Mowla, M. Nikkhah and A. Arbabi, *Radiat. Oncol.*, 2021, **16**, 1–12.

318 M. M. Fathy, F. S. Mohamed, N. Elbialy and W. M. Elshemey, *Phys. Med.*, 2018, **48**, 76–83.

319 C. Yang, K. Bromma, D. Ciano-Oliveira, G. Zafarana, M. van Prooijen and D. B. Chithrani, *Cancer Nanotechnol.*, 2018, **9**, 1–14.

320 H. Mendoza-Nava, G. Ferro-Flores, F. d. M. Ramírez, B. Ocampo-García, C. Santos-Cuevas, L. Aranda-Lara, E. Azorín-Vega, E. Morales-Avila and K. Isaac-Olivé, *J. Nanomater.*, 2016, **2016**, 1039258.

321 L. Bai, F. Jiang, R. Wang, C. Lee, H. Wang, W. Zhang, W. Jiang, D. Li, B. Ji and Z. Li, *J. Nanobiotechnol.*, 2020, **18**, 1–10.

322 H. Nosrati, F. Seidi, A. Hosseinmirzaei, N. Mousazadeh, A. Mohammadi, M. Ghaffarlou, H. Danafar, J. Conde and A. Sharafi, *Adv. Healthcare Mater.*, 2022, **11**, 2102321.

323 C. Yang, K. Bromma, W. Sung, J. Schuemann and D. Chithrani, *Cancers*, 2018, **10**, 150.

324 B. Janic, F. Liu, K. Bobbitt, S. Brown, I. Chetty, G. Mao, B. Movsas and N. Wen, *J. Nanomed. Nanotechnol.*, 2018, **9**, 1–13.

325 X. Yang, X. Liu, Z. Liu, F. Pu, J. Ren and X. Qu, *Adv. Mater.*, 2012, **24**, 2890–2895.

326 P. Shi, K. Qu, J. Wang, M. Li, J. Ren and X. Qu, *Chem. Commun.*, 2012, **48**, 7640–7642.

327 R. Hong, G. Han, J. M. Fernández, B.-j. Kim, N. S. Forbes and V. M. Rotello, *J. Am. Chem. Soc.*, 2006, **128**, 1078–1079.

328 P. Joshi, S. Chakraborti, J. E. Ramirez-Vick, Z. Ansari, V. Shanker, P. Chakrabarti and S. P. Singh, *Colloids Surf., B*, 2012, **95**, 195–200.

329 C. Xu, B. Wang and S. Sun, *J. Am. Chem. Soc.*, 2009, **131**, 4216–4217.

330 K. Ock, W. I. Jeon, E. O. Ganbold, M. Kim, J. Park, J. H. Seo, K. Cho, S.-W. Joo and S. Y. Lee, *Anal. Chem.*, 2012, **84**, 2172–2178.

331 M. K. Hossain, H.-Y. Cho, K.-J. Kim and J.-W. Choi, *Biosens. Bioelectron.*, 2015, **71**, 300–305.

332 J. You, R. Zhang, G. Zhang, M. Zhong, Y. Liu, C. S. Van Pelt, D. Liang, W. Wei, A. K. Sood and C. Li, *J. Contr. Release*, 2012, **158**, 319–328.

333 S. K. Libutti, G. F. Paciotti, A. A. Byrnes, H. R. Alexander Jr, W. E. Gannon, M. Walker, G. D. Seidel, N. Yuldasheva and L. Tamarkin, *Clin. Cancer Res.*, 2010, **16**, 6139–6149.

334 R. A. Morshed, M. E. Muroski, Q. Dai, M. L. Wegscheid, B. Auffinger, D. Yu, Y. Han, L. Zhang, M. Wu and Y. Cheng, *Mol. Pharm.*, 2016, **13**, 1843–1854.

335 W. Jiang, B. Y. Kim, J. T. Rutka and W. C. Chan, *Nat. Nanotechnol.*, 2008, **3**, 145–150.

336 O. Akturk, *Int. J. Biol. Macromol.*, 2022, **196**, 72–85.

337 M. Hasannia, K. Abnous, S. M. Taghdisi, S. Nekooei, M. Ramezani and M. Alibolandi, *J. Nanobiotechnol.*, 2022, **20**, 1–27.

338 R. Taheri-Ledari, W. Zhang, M. Radmanesh, S. S. Mirmohammadi, A. Maleki, N. Cathcart and V. Kitaev, *Small*, 2020, **16**, 2002733.

339 C. S. Kumar, A. Mahesh, M. G. Antoniraj, S. Vaidevi and K. Ruckmani, *RSC Adv.*, 2016, **6**, 26874–26882.

340 H. M. Aldawsari, S. Singh, N. A. Alhakamy, R. B. Bakhaidar, A. A. Halwani and S. M. Badr-Eldin, *Pharmaceutics*, 2021, **13**, 1554.

341 M. S. Jabir, A. A. Taha, U. I. Sahib, Z. J. Taqi, A. M. Al-Shammari and A. S. Salman, *Mater. Sci. Eng. C*, 2019, **94**, 949–964.

342 B. Khodashenas, M. Ardjmand, A. Rad and M. Esfahani, *Mater. Today Chem.*, 2021, **20**, 100474.

343 D. El-Safoury, A. B. Ibrahim, D. El-Setouhy, O. Khowessah, M. Motaleb and T. M. Sakr, *J. Pharm. Sci.*, 2021, **110**, 2955–2965.

344 C.-F. Chiu, R.-H. Fu, S.-h. Hsu, Y.-H. Yu, S.-F. Yang, T. C.-Y. Tsao, K.-B. Chang, C.-A. Yeh, C.-M. Tang and S.-C. Huang, *Cancers*, 2021, **13**, 5317.

345 J. R. Lakkakula, R. W. M. Krause, D. Divakaran, S. Barage and R. Srivastava, *J. Mol. Liq.*, 2021, **341**, 117262.

346 C. Yang, J. Uertz and D. B. Chithrani, *Nanomaterials*, 2016, **6**, 48.

347 O. Gotov, G. Battogtokh, D. Shin and Y. T. Ko, *J. Ind. Eng. Chem.*, 2018, **65**, 236–243.

348 J. E. Bonevich, *Nanotechnology Characterization Laboratory*, National Cancer Institute, Frederick, MD 21702, (301) 846-6939, 2010.

349 P. Kumari, B. Ghosh and S. Biswas, *J. Drug Target.*, 2016, **24**, 179–191.

350 J. M. Stern, V. V. Kibanov Solomonov, E. Sazykina, J. A. Schwartz, S. C. Gad and G. P. Goodrich, *Int. J. Toxicol.*, 2016, **35**, 38–46.

351 J. A. Schwartz, A. M. Shetty, R. E. Price, R. J. Stafford, J. C. Wang, R. K. Uthamanthil, K. Pham, R. J. McNichols, C. L. Coleman and J. D. Payne, *Cancer Res.*, 2009, **69**, 1659–1667.

352 M. Khoobchandani, K. K. Katti, A. R. Karikachery, V. C. Thipe, D. Srisrimal, D. K. Dhurvas Mohandoss, R. D. Darshakumar, C. M. Joshi and K. V. Katti, *Int. J. Nanomed.*, 2020, 181–197.

353 P. Kumthekar, C. H. Ko, T. Paunesku, K. Dixit, A. M. Sonabend, O. Bloch, M. Tate, M. Schwartz, L. Zuckerman and R. Lezon, *Sci. Transl. Med.*, 2021, **13**, eabb3945.

354 Z. Xu, Y. Broza, R. Ionsecu, U. Tisch, L. Ding, H. Liu, Q. Song, Y. Pan, F. Xiong and K. Gu, *Br. J. Cancer*, 2013, **108**, 941–950.

355 Y. Yang, X. Zheng, L. Chen, X. Gong, H. Yang, X. Duan and Y. Zhu, *Int. J. Nanomed.*, 2022, 2041–2067.

356 J. S. Jue, S. Coons, G. Hautvast, S. F. Thompson, J. Geraats, L. Richstone, M. J. Schwartz and A. R. Rastinehad, *J. Endourol.*, 2022, **36**, 369–372.

357 P. Kumthekar, A. Rademaker, C. Ko, K. Dixit, M. A. Schwartz, A. M. Sonabend, L. Sharp, R. V. Lukas, R. Stupp and C. Horbinski, *J. Clin. Oncol.*, 2019, **37**, 3012.

358 A. F. Farag and N. F. Hassabou, *Nanomed. Nanotechnol. Biol. Med.*, 2022, **46**, 102598.

359 L. Yao, D. Bojic and M. Liu, *J. Pharmaceut. Biomed. Anal.*, 2023, **13**, 960–967.

360 C. Lasagna-Reeves, D. Gonzalez-Romero, M. Barria, I. Olmedo, A. Clos, V. S. Ramanujam, A. Urayama, L. Vergara, M. J. Kogan and C. Soto, *Biochem. Biophys. Res. Commun.*, 2010, **393**, 649–655.

361 I. Fratoddi, I. Venditti, C. Cametti and M. V. Russo, *Nano Res.*, 2015, **8**, 1771–1799.

362 M. C. Senut, Y. Zhang, F. Liu, A. Sen, D. M. Ruden and G. Mao, *Small*, 2016, **12**, 631–646.

363 Y. Pan, S. Neuss, A. Leifert, M. Fischler, F. Wen, U. Simon, G. Schmid, W. Brandau and W. Jahnen-Dechent, *Small*, 2007, **3**, 1941–1949.

364 W. H. De Jong, W. I. Hagens, P. Krystek, M. C. Burger, A. J. Sips and R. E. Geertsma, *Biomaterials*, 2008, **29**, 1912–1919.

365 M. A. K. Abdelhalim and S. A. A. Moussa, *Saudi J. Biol. Sci.*, 2013, **20**, 177–181.

366 G. Sonavane, K. Tomoda and K. Makino, *Colloids Surf., B*, 2008, **66**, 274–280.

367 E. E. Connor, J. Mwamuka, A. Gole, C. J. Murphy and M. D. Wyatt, *Small*, 2005, **1**, 325–327.

368 C. J. Murphy, A. M. Gole, J. W. Stone, P. N. Sisco, A. M. Alkilany, E. C. Goldsmith and S. C. Baxter, *Acc. Chem. Res.*, 2008, **41**, 1721–1730.

369 Y.-S. Chen, Y.-C. Hung, I. Liau and G. S. Huang, *Nanoscale Res. Lett.*, 2009, **4**, 858–864.

370 J. Pérez-Juste, I. Pastoriza-Santos, L. M. Liz-Marzán and P. Mulvaney, *Coord. Chem. Rev.*, 2005, **249**, 1870–1901.

371 Y. Li, M. Kröger and W. K. Liu, *Nanoscale*, 2015, **7**, 16631–16646.

372 K. C. Black, Y. Wang, H. P. Luehmann, X. Cai, W. Xing, B. Pang, Y. Zhao, C. S. Cutler, L. V. Wang and Y. Liu, *ACS Nano*, 2014, **8**, 4385–4394.

373 Z. Wang, D. Xie, H. Liu, Z. Bao and Y. Wang, *RSC Adv.*, 2016, **6**, 33009–33013.

374 M. Mioc, I. Z. Pavel, R. Ghiulai, D. E. Coricovac, C. Farcaș, C.-V. Mihali, C. Oprean, V. Serafim, R. A. Popovici and C. A. Dehelean, *Front. Pharmacol*, 2018, **9**, 429.

375 X.-D. Zhang, D. Wu, X. Shen, P.-X. Liu, N. Yang, B. Zhao, H. Zhang, Y.-M. Sun, L.-A. Zhang and F.-Y. Fan, *Int. J. Nanomed.*, 2011, 2071–2081.

376 K. Katti, N. Chanda, R. Shukla, A. Zambre, T. Suibramanian, R. R. Kulkarni, R. Kannan and K. V. Katti, *Int. J. Green Nanotechnol.*, 2009, **1**, B39–B52.

377 Y. Qu and X. Lü, *Biomed. Mater.*, 2009, **4**, 025007.

378 P. Roy, S. Sur, S. Das and W. T. Wui, *Breast Cancer*, 2022, **29**, 761–777.

379 J. G. Railsback, A. Singh, R. C. Pearce, T. E. McKnight, R. Collazo, Z. Sitar, Y. G. Yingling and A. V. Melechko, *Adv. Mater.*, 2012, **24**, 4261–4265.

380 A. S. Poulos, D. Constantin, P. Davidson, M. Impéror-Clerc, B. Pansu and S. Rouzière, *Europhys. Lett.*, 2012, **100**, 18002.

381 C. M. Goodman, C. D. McCusker, T. Yilmaz and V. M. Rotello, *Bioconjugate Chem.*, 2004, **15**, 897–900.

382 N. M. Schaeublin, L. K. Braydich-Stolle, A. M. Schrand, J. M. Miller, J. Hutchison, J. J. Schlager and S. M. Hussain, *Nanoscale*, 2011, **3**, 410–420.

383 C. Ge, J. Tian, Y. Zhao, C. Chen, R. Zhou and Z. Chai, *Arch. Toxicol.*, 2015, **89**, 519–539.

384 J. Liu and Q. Peng, *Acta Biomater.*, 2017, **55**, 13–27.

385 L. Wang, J. Li, J. Pan, X. Jiang, Y. Ji, Y. Li, Y. Qu, Y. Zhao, X. Wu and C. Chen, *J. Am. Chem. Soc.*, 2013, **135**, 17359–17368.

386 S. Milani, F. Baldelli Bombelli, A. S. Pitek, K. A. Dawson and J. Radler, *ACS Nano*, 2012, **6**, 2532–2541.

387 M. Schäffler, M. Semmler-Behnke, H. Sarioglu, S. Takenaka, A. Wenk, C. Schleh, S. M. Hauck, B. D. Johnston and W. G. Kreyling, *Nanotechnology*, 2013, **24**, 265103.

388 X. Cheng, X. Tian, A. Wu, J. Li, J. Tian, Y. Chong, Z. Chai, Y. Zhao, C. Chen and C. Ge, *ACS Appl. Mater. Interfaces*, 2015, **7**, 20568–20575.

389 P. Wang, X. Wang, L. Wang, X. Hou, W. Liu and C. Chen, *Sci. Technol. Adv. Mater.*, 2015, **16**, 034610.

390 W. Lai, Q. Wang, L. Li, Z. Hu, J. Chen and Q. Fang, *Colloids Surf., B*, 2017, **152**, 317–325.

391 C. Carnovale, G. Bryant, R. Shukla and V. Bansal, *ACS Omega*, 2019, **4**, 242–256.

392 K. E. Woods, Y. R. Perera, M. B. Davidson, C. A. Wilks, D. K. Yadav and N. C. Fitzkee, *J. Phys. Chem. C*, 2016, **120**, 27944–27953.

393 Z. J. Deng, M. Liang, M. Monteiro, I. Toth and R. F. Minchin, *Nat. Nanotechnol.*, 2011, **6**, 39–44.

394 K. Saha, M. Rahimi, M. Yazdani, S. T. Kim, D. F. Moyano, S. Hou, R. Das, R. Mout, F. Rezaee and M. Mahmoudi, *ACS Nano*, 2016, **10**, 4421–4430.

395 A. Salvati, A. S. Pitek, M. P. Monopoli, K. Prapainop, F. B. Bombelli, D. R. Hristov, P. M. Kelly, C. Åberg, E. Mahon and K. A. Dawson, *Nat. Nanotechnol.*, 2013, **8**, 137–143.

396 V. Mirshafiee, M. Mahmoudi, K. Lou, J. Cheng and M. L. Kraft, *Chem. Commun.*, 2013, **49**, 2557–2559.

397 A. A. Shemetov, I. Nabiev and A. Sukhanova, *ACS Nano*, 2012, **6**, 4585–4602.

398 Z. Ma, J. Bai and X. Jiang, *ACS Appl. Mater. Interfaces*, 2015, **7**, 17614–17622.

399 H. Yang, M. Wang, Y. Zhang, F. Li, S. Yu, L. Zhu, Y. Guo, L. Yang and S. Yang, *RSC Adv.*, 2019, **9**, 4435–4444.

400 A. O. Elzoghby, W. M. Samy and N. A. Elgindy, *J. Contr. Release*, 2012, **157**, 168–182.

401 H. K. Patra, S. Banerjee, U. Chaudhuri, P. Lahiri and A. K. Dasgupta, *Nanomed. Nanotechnol. Biol. Med.*, 2007, **3**, 111–119.

402 R. Coradeghini, S. Gioria, C. P. García, P. Nativo, F. Franchini, D. Gilliland, J. Ponti and F. Rossi, *Toxicol. Lett.*, 2013, **217**, 205–216.

403 X.-D. Zhang, H.-Y. Wu, D. Wu, Y.-Y. Wang, J.-H. Chang, Z.-B. Zhai, A.-M. Meng, P.-X. Liu, L.-A. Zhang and F.-Y. Fan, *Int. J. Nanomed.*, 2010, 771–781.

404 I. Fratoddi, I. Venditti, C. Cametti and M. V. Russo, *Toxicol. Res.*, 2015, **4**, 796–800.

405 X.-L. Huang, B. Zhang, L. Ren, S.-F. Ye, L.-P. Sun, Q.-Q. Zhang, M.-C. Tan and G.-M. Chow, *J. Mater. Sci.: Mater. Med.*, 2008, **19**, 2581–2588.

406 P.-H. Lu, H.-J. Li, H.-H. Chang, N.-L. Wu and C.-F. Hung, *J. Nanopart. Res.*, 2017, **19**, 1–12.

407 J. H. Kim, J. H. Kim, K.-W. Kim, M. H. Kim and Y. S. Yu, *Nanotechnology*, 2009, **20**, 505101.

408 T. Mironava, M. Hadjiargyrou, M. Simon, V. Jurukovski and M. H. Rafailovich, *Nanotoxicology*, 2010, **4**, 120–137.

409 L. R. Hirsch, R. J. Stafford, J. Bankson, S. R. Sershen, B. Rivera, R. Price, J. D. Hazle, N. J. Halas and J. L. West, *Proc. Natl. Acad. Sci. U. S. A.*, 2003, **100**, 13549–13554.

410 S. K. Nune, N. Chanda, R. Shukla, K. Katti, R. R. Kulkarni, S. Thilakavathy, S. Mekapothula, R. Kannan and K. V. Katti, *J. Mater. Chem.*, 2009, **19**, 2912–2920.

411 S. Vijayakumar and S. Ganesan, *J. Nanomater.*, 2012, **2012**, 14.

412 H. Takahashi, Y. Niidome, T. Niidome, K. Kaneko, H. Kawasaki and S. Yamada, *Langmuir*, 2006, **22**, 2–5.

413 P. Chandran, J. E. Riviere and N. A. Monteiro-Riviere, *Nanotoxicology*, 2017, **11**, 507–519.